# The ICP : fundamental properties

Stoffels-Adamowicz, E.

*Award date:*
1991

# THE ICP:

## I. Fundamental properties

E. Stoffels

# THE ICP: I. FUNDEMENTAL PROPERTIES

M.Sc. work of E. Stoffels

August 1991

Supervisors: F.H.A.G. Fey and J.A.M. van der Mullen.

Group leader: prof. D.C. Schram.

I would like to thank everybody who helped me during last half year. Especially Frank and Joost for the extremely pleasant cooperation and most important Winfred with whom I did all the work.

## SUMMARY

In this work a study of fundamental properties of an Inductively Coupled Plasma is presented. The macroscopic parameters, as temperatures and drift velocity of the plasma are determined by means of the power interruption technique. The deviations of the plasma from equilibrium are discussed.

Further the power interruption technique is used to study the energy transfer processes as well as recombination mechanisms. Some phenomena following the power interruption are explained in terms of the local energy balance. The influence of additives to the plasma ($H_2$, $H_2O$) on the fundamental plasma processes is discussed.

The absorption technique, which appears to be a simple and good tool to study the deviations from equilibrium, is presented.

Finally, we present a model for propagation of disturbances in the energy balance through the plasma. Such disturbances have been found experimentally both during the power interruption and in the steady state.

# CONTENTS

Summary

Contents

**Chapter I, Introduction** 1

**Chapter II, Fundamental properties of the ICP** 3
II.1 Characteristics 3
II.2 Balances 6
II.3 Close-to-LTE concept 10

**Chapter III, The power interruption experiment** 11
III.1 Introduction 11
III.2 Experimental setup 11
III.3 Global results and theory 13

**Chapter IV, Macroscopic characterization of the ICP** 18
IV.1 Introduction 18
IV.2 Temperatures in the ICP 18
IV.2.1 The power interruption method 18
IV.2.2 "Passive spectroscopy" for temperature determination 24
IV.3 Drift velocity of the plasma 26
IV.3.1 A relation with heavy particles temperature 26
IV.3.2 Measurements of the drift velocity 28

**Chapter V, Microscopic characterization of the ICP** 32
V.1 Introduction 32
V.2 Time constants 32
V.3 The energy transfer 34
V.3.1 The kinetics of the cooling jump 37
V.3.2 The relation between electron temperature and density 41
V.3.3 Radial depence of the heating jump 49
V.4 Electron density decay 49
V.4.1 Three body recombination 50
V.4.2 Outward diffusion of electrons 52
V.4.3 Other mechanisms 53
V.4.4 Experimental data 54
V.5 The influence of hydrogen and water 57

**Chapter VI, Absorption measurements** 64
VI.1 Introduction 64
VI.2 The principle of the method 64
VI.2.1 Theory 64
VI.2.2 Description of the method and results 68

**Chapter VII, The delayed response** 74
VII.1 Introduction 74
VII.2 The propagation of fluctuations in the ICP 74
VII.3 Experimantal data 81
VII.4 Spontaneous disturbances 95
VII.5 Conclusion 95

**Chapter VIII, Conclusions and recommendations** 96
VIII.1 Conclusions 96
VIII.2 Recommendations 96

**Chapter IX, References** 97

# I. INTRODUCTION

The Inductively Coupled Plasma (ICP) can briefly be described as a plasma within a load coil where it acts as the secondary winding of a transformer. The absence of electrodes makes it suitable for many applications, especially when high purity is demanded. Another important feature is that the ICP can be maintained in the presence of a streaming gas, the main applications, spectrochemical analysis and material engineering are based on this property. Nevertheless the ICP is also used in a closed configuration as a light source [BEN.90].

In this work we confine ourselves to the spectrochemical side of the ICP, where it serves as a source of various excited and ionized elements. The elements, which are called analytes, are introduced in the plasma in gas form or as salts dissolved in nebulized water or other solvents or as solid particulates produced by laser ablation. The analysis is performed by optical emission spectroscopy (OES) or by a mass spectrometer (MS).

The aim of the plasma physics group at the Eindhoven University of Technology is to find a better understanding of the physical plasma processes in the ICP. On one hand this might help to lower the detection limits and on the other hand it serves as an example of low temperature plasmas in general. In order to understand the plasma behavior one must study the complex interaction between elementary balances and the impact they have on the populations of excited states as well as purely dynamic properties of the plasma, as energy in- and outflow, particle velocities, etc. The combination of all these effects gives a full image of the plasma. The complexity of this image and majority of problems to be worked out challenge a profound study to clarify this area. This study, as always in physics, is most fruitful if experiments are combined with theoretical effort. In this work, which was done in close cooperation with Mr. W.W. Stoffels, some 'old' [STO.90, FEY.90, FEY.91/1] experimental observations are studied. Moreover, several new experiments are designed and performed. A theoretical analysis of the experimental results leads to a new physical insight into the dynamic processes governing the plasma as a whole.

The Chapter II deals with a general description of the fundamental ICP properties. The most important problems (like deviations from equilibrium), encountered by spectroscopists are mentioned and the elementary processes are treated. In the Chapter III the power interruption experiment is presented. The general results and possibilities of this technique are discussed. It appears to bring a huge amount of information about nearly all plasma properties. Further we continue with the detailed analysis of phenomena following the power interruption. This technique is very powerful in studying both elementary balances and dynamic processes in the plasma. The details on elementary balances can be found in [STO.91/3]. Chapter IV is devoted to the determination of temperature and drift velocity of the plasma. In Chapter V the time scales of the plasma processes, like energy transfer on the particle scale and particle density changes are discussed. A proposed model allows to explain many of the phenomena following the power interruption, observed in [FEY.91/1]. The influence of

additives to the plasma on these processes is presented and discussed. Further, in Chapter VI we present a first successful application of the absorption measurements in our ICP. It extends our possibilities beyond the ordinary Optical Emission. This technique, in combination with the power interruption experiment, gives a very valuable information about the deviations from equilibrium in the plasma. Finally, in Chapter VII, the origin of a wave like disturbance, observed in the plasma is clarified. We propose a simple method to study such disturbances. The theory is supported with a vast amount of experimental data.

# II. FUNDAMENTAL PROPERTIES OF THE ICP

## II.1 CHARACTERISTICS

An ICP is an example of a low temperature atmospheric plasma. The ICP is sustained within a quartz tube (torch), through which a gas (in most cases argon) is flowing. A schematic picture of an ICP torch is shown in Fig. II.1. The argon flow consists of three parts:

- The outer or main flow $\Phi$, which supplies the argon for the plasma. It also protects the outer cylinder against overheating.
- The intermediate flow $\Phi_i$. This flow can be used to lift the plasma from the inner cylinders.
- The central flow $\Phi_c$. It is used for analyte injection into the plasma. The analytes are various chemical elements, which are spectroscopically analyzed in the ICP. Typically their salts are dissolved in water, which is afterwards nebulized and carried into the plasma by the central flow.

Further in the text the flow conditions will be denoted as x/y/z l/min. These numbers refer to the main, intermediate and central flow, respectively.

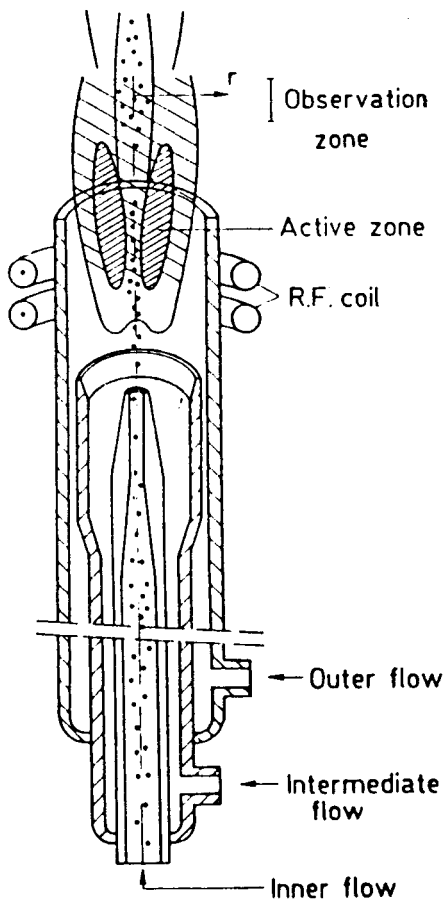


Fig. II.1. The ICP.

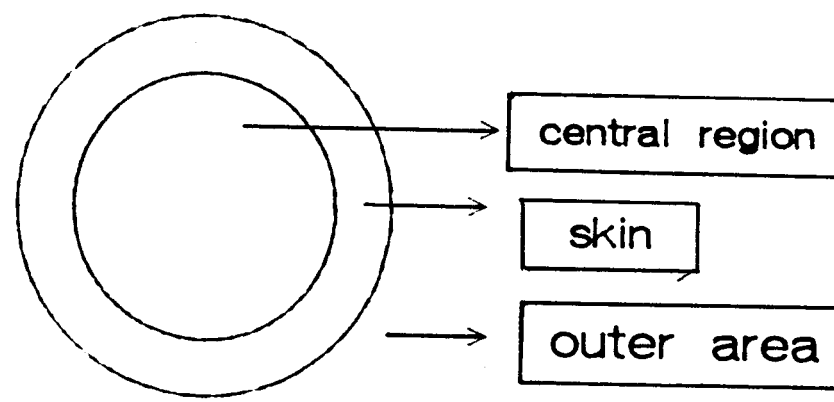


Fig. II.2. Cross section of the plasma, showing the central region, the skin and the outer region.

The plasma is heated by a high frequency electromagnetic field, generated by a R.F. load coil. The charged particles in the plasma are accelerated by this field and thus they gain energy. Because the electron mass is small in comparison with masses of ions, most of the field energy is absorbed by the electrons. They pass their energy to the heavy particles (ions and atoms) by collisions. The heavy particles in turn lose energy to the surroundings by convection and by radiation. The chain of energy transfer can be schematically presented as:

$$\text{RF generator} \longrightarrow \{e\} \longrightarrow \{h\} \longrightarrow \text{surroundings} \qquad \text{II.1}$$

This mechanism implies that steady state the electron temperature ($T_e$) is higher than the heavy particle temperature ($T_h$). A typical value of $T_e$ in the active zone is around 1 eV, $T_h$ is typically 30% lower.

The plasma is roughly axially symmetric and in a cross section (Fig. II.2) different areas can be distinguished due to the flows and the EM field.

a) In the central region the central flow is injected and there exists a channel of fast moving argon in which water droplets are carried on. The diameter of the water droplets is in the order of 10 $\mu$m [STO.91/3].

b) More outward there is the skin. Here most of the energy is coupled into the plasma. It is the hottest area of the ICP from which most of the radiation is emitted. We shall refer to it as to the "active zone" of the plasma.

c) Outside the skin there is a transition area between the plasma and the surrounding cold argon flow. In this region there are large gradients of temperature and densities. Diffusion and radiation escape are dominant processes.

The cross section in Fig. II.2 is typical only for the region between and close to the load coils. Further above the load coils (10 - 20 mm) the active zone gradually disappears [NOW.89]. However, in this work this part of the plasma will not be treated.

In Fig. II.3a a laterally measured intensity profile of an argon line is shown and in Fig. II.3b the radial profile belonging to it. The radial profile is calculated with a symmetrizing Abel inversion procedure described in [SAN.91]. The three regions described above are clearly visible. In the middle there is hardly any intensity. This displays the major problem one encounters in analyzing the plasma center. Furthermore Fig. II.3a shows that there is an asymmetry between the two sides of the plasma. This is due to the coil geometry. If water is introduced into the plasma the asymmetry increases even to about 30% (see Fig. II.4a, 4b). These features in combination with large gradients make Abel inversions very difficult and the results are not always reliable. In this report the lateral measurements as well as Abel inverted data are presented. As the light intensity in maximal in the skin and decreases sharply to the center or to the sides, it is expected that the lateral measurements gives a good representation of the actual plasma behavior in the skin. Only when we aim to study some regions close to the center, the Abel inversion becomes indispensable.

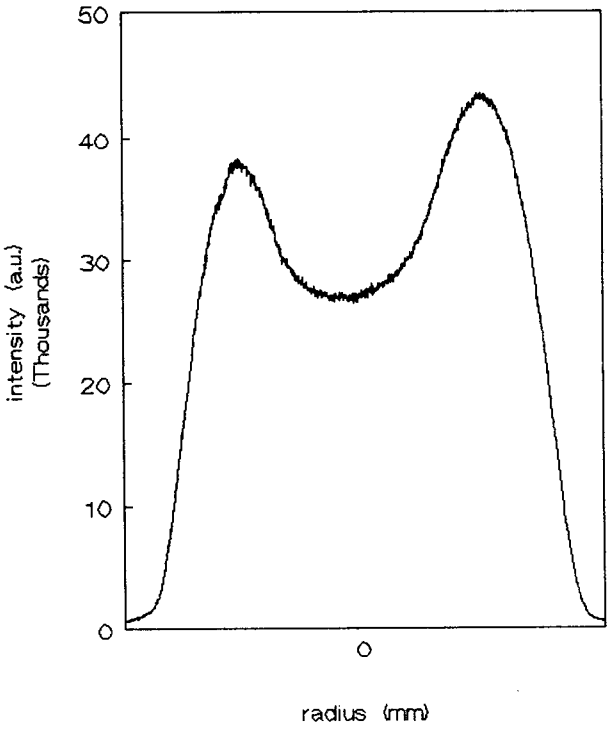


Fig. II.3a. Lateral intensity profile of Ar 6s.
5 mm above the load coil, flows 12/0/0.7 l/min,
no water injection.

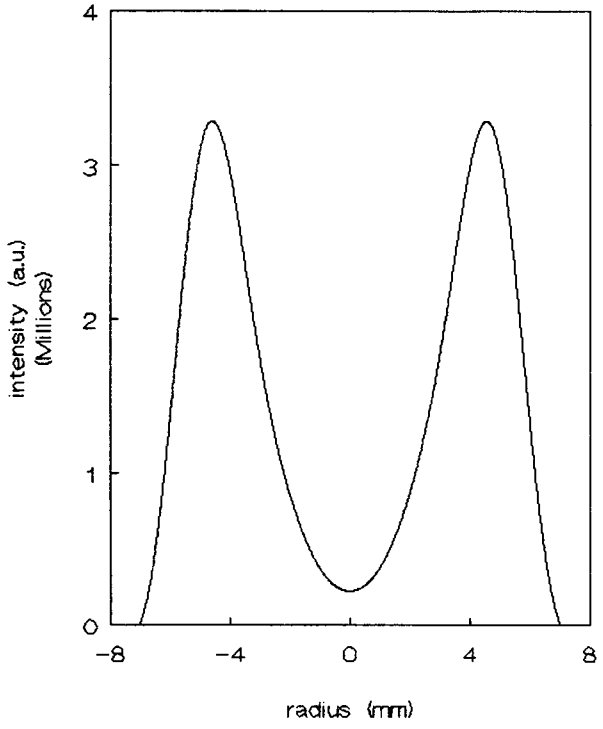


Fig. II.3b. Symmetrized Abel inverted profile of Fig. II.3a
(the Abel inversion of Van der Sanden [SAN.91] has been used).

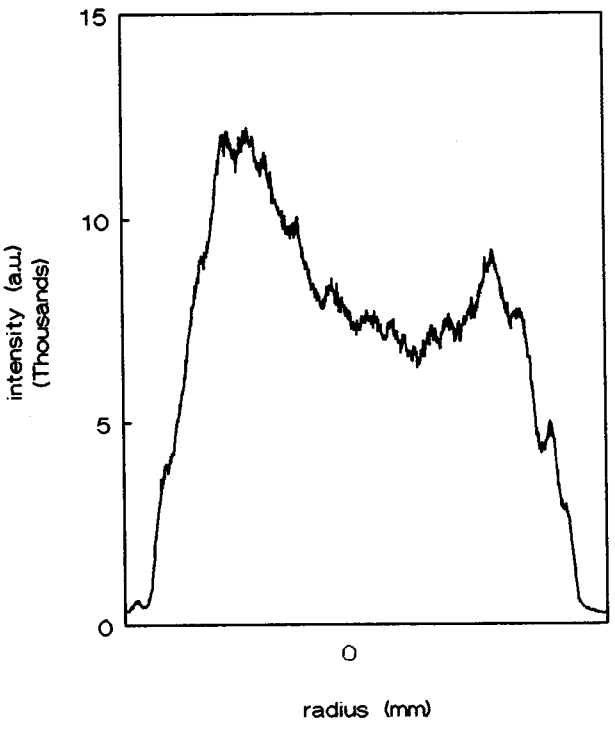


Fig. II.4a. Lateral intensity profile of Ar 6s
with water injection.

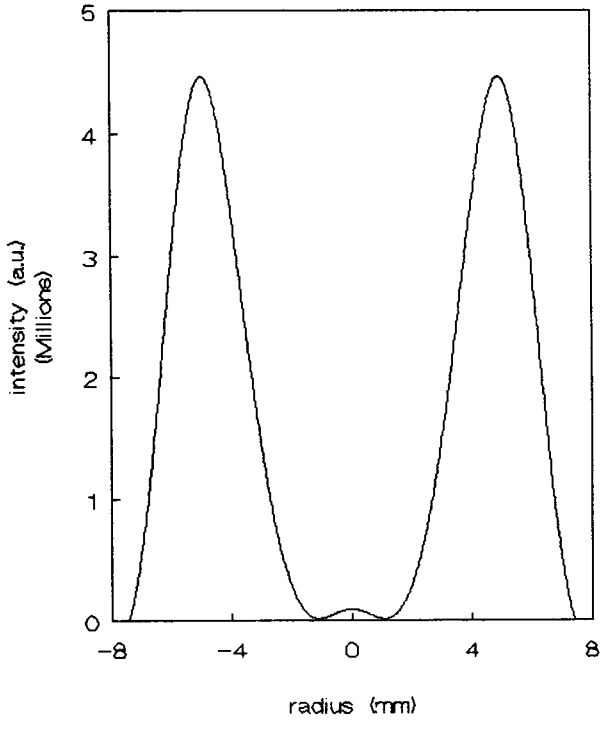


Fig. II.4b. Symmetrized Abel inverted profile of Fig. II.4a.

## II.2 BALANCES

In this section we shall list the elementary balances, responsible for the (de)population of excited states of species in the ICP. These processes determine the shape of the Atomic State Distribution Function (ASDF), i.e. the population of the excited states. The knowledge of ASDF is important for analytical chemists, as it gives an explicit relation between the excited state density (measured in Optical Emission) with the total analyte density in the plasma.

Further the processes leading to deviation of the plasma from equilibrium will be discussed. Some of them are due to the fact that some of the elementary processes listed below do not completely equilibrate.

The atomic (molecular) states of the species present in the ICP are populated in the following processes:

**1. Collisional processes:**

a) ionization/recombination of a species A in electronic state p:

$$A(p) + e + \Delta E \Longleftrightarrow A^+ + e + e$$

b) excitation/deexcitation between two electronic states p and q:

$$A(p) + e + \Delta E \Longleftrightarrow A(q) + e$$

Generally the excitation and ionization could be also performed by heavy particles collisions. However, a considerably high ionization degree of the ICP causes the plasma to be completely electron collision dominated.

c) charge transfer (CT) between species $A^+$ in a state p and B in a state q:

$$A^+(p) + B(q) \Longleftrightarrow A(p') + B^+(q')$$

d) excitation transfer (ET) between species A and B:

$$A(p) + B(q) \Longleftrightarrow A(p') + B(q')$$

e) vibrational and rotational (de)excitation (only for molecular species).

**2. Radiative processes:**

a) radiative ionization/recombination:

$$A(p) + h\nu \Longleftrightarrow A^+ + e$$

b) spontaneous emission/radiation capture:

$$A(q) \Longleftrightarrow A(p) + h\nu$$

The collisional processes can be divided in two groups: the processes dominated by electron or heavy particle collisions. In the ICP the processes 1 a) and b) are completely electron collision dominated and in 1 c) and d) only heavy particles are involved. Since the excitation of rotational and vibrational levels of molecules requires a large momentum of the exciting particle, the process 1 e) is also heavy particle collision dominated.

Generally in the ICP conditions the collisional processes are more important than the radiative ones. For example, at atmospheric pressure the main recombination mechanism from the ion to an excited state of Ar is three body, 1 a) (see also § V), while the radiative recombination to excited states (which gives the continuum radiation) is not really important for the ion depopulation.

If the ionization/recombination is balanced, a following relation between the particle densities (the Saha equation) is valid [MUL.86, MUL.90]:

$$\eta^s(p) = \eta_e \, \eta_+ \, (h^2/2\pi m_e kT_e)^{3/2} \exp\,(E_{ion}(p)/kT_e) \qquad \text{II.2}$$

with:

$\eta^s(p)$ density of particles occupying a state p,

$\eta(p) \equiv n(p)/g(p)$, where

n(p) density of a level p,

g(p) statistical weight of a level p,

$\eta_e$, $\eta_+$ state densities of electrons and ions ( $g_e = 2$ ),

$E_{ion}(p)$ ionization energy of a level p.

For argon $g_+ = 6$. Consequently the populations of two atomic (molecular) states p and q are related by the Boltzmann distribution:

$$\eta^b(p) = \eta^b(q) \exp\,(E_{pq}/kT_e), \qquad \text{II.3}$$

where $E_{pq} = E_{ion}(p) - E_{ion}(q)$.

The existence of Local Thermal Equilibrium requires that all the processes described above are balanced by their backward processes. Then the state densities are ruled by (II.2) and (II.3). For LTE it is also required that $T_e = T_h$. However, when $T_e$ and $T_h$ are decoupled it is still possible that the populations of excited states are ruled by (II.2), dependent on $T_e$ solely. Generally, in a real case there are several sources of deviation from (II.2):

**a) Particle flows:**

The equilibrium relation (II.2) describes a system in which particles are neither produced nor destroyed. This is not a necessary condition for the steady state, which requires only that the rate of production (in some process) must equal the rate of destruction (not necessarily in the reverse process). In the ICP the elements are continuously introduced in their ground state, while the electron density stays constant. This means that there is a net flow through the atomic systems. In the active (ionizing) zone electrons are produced and continuously removed by diffusion (convection) to the cold surrounding, where they recombine. In this case the populations of atomic states will show systematic deviations from Saha. In the active zone the ionization is faster than recombination, so the Elementary Mass Action Law [MUL.86, MUL.90] requires that the densities of atomic states exceeds its equilibrium value (II.2) (the case of ionizing plasma). We can define overpopulation of a level p with respect to (II.2) by:

$$b(p) = n(p)/n^S(p) \qquad \text{II.4}$$

In the ionizing system $b(p) > 1$ and for high excited states ($p \to \infty$) $b(p) \to 1$ [MUL.86, STO.91/3] (see Fig. II.5). Consequently for a recombining system, in which recombination is faster than ionization $b(p) < 1$ and $b(p) \to 1$ for $p \to \infty$ (Fig. II.6). It is justified by the fact that if the electron density is high enough, the collisional processes in the top of an atomic system (and coupling with the ion) are very fast, while radiative losses become of no importance [MUL.86, MUL.90, STO.91/3]. If indeed $b(p) \approx 1$ for high p the top of the atomic system will be coupled to the ion according to (II.2). It allows to use the equilibrium relation for high excited states of atoms in a non equilibrium plasma. A question that arises immediately is how large the deviations from (II.2) are for a particular argon level. The scheme of energy levels for argon is shown in Fig. II.7. It can be easily seen that the collisional excitation of the ground state is very inefficient, due to the large energy gap. In order to provide a significant ionization flow (i.e. comparable to the destructive diffusion flows) the overpopulation of the argon ground state must be in the order of $10^2$ - $10^3$. The deviations for higher excited states will be treated in § IV and VI.

**b) Radiation escape:**

Another factor which decides about the deviation from Saha is radiation escape. The ICP is practically optically thin. Only the resonant argon transitions (4s - 3p, 3d - 3p) are completely reabsorbed and some of Ar 4p - 4s transitions are partially reabsorbed. The radiation escape causes deviations from Saha, which are not so dramatic for argon, but very crucial for heavily radiating analytes [STO.91/3].

**c) Heavy particle collisions:**

The processes like CT and ET are dominated by heavy particle collisions and therefore $T_h$ dependent. Since in the ICP $T_h \neq T_e$, charge and excitation transfer will be decoupled from the electron collisional processes. It is shown in [STO.91/3] that for some elements (like Mg) the

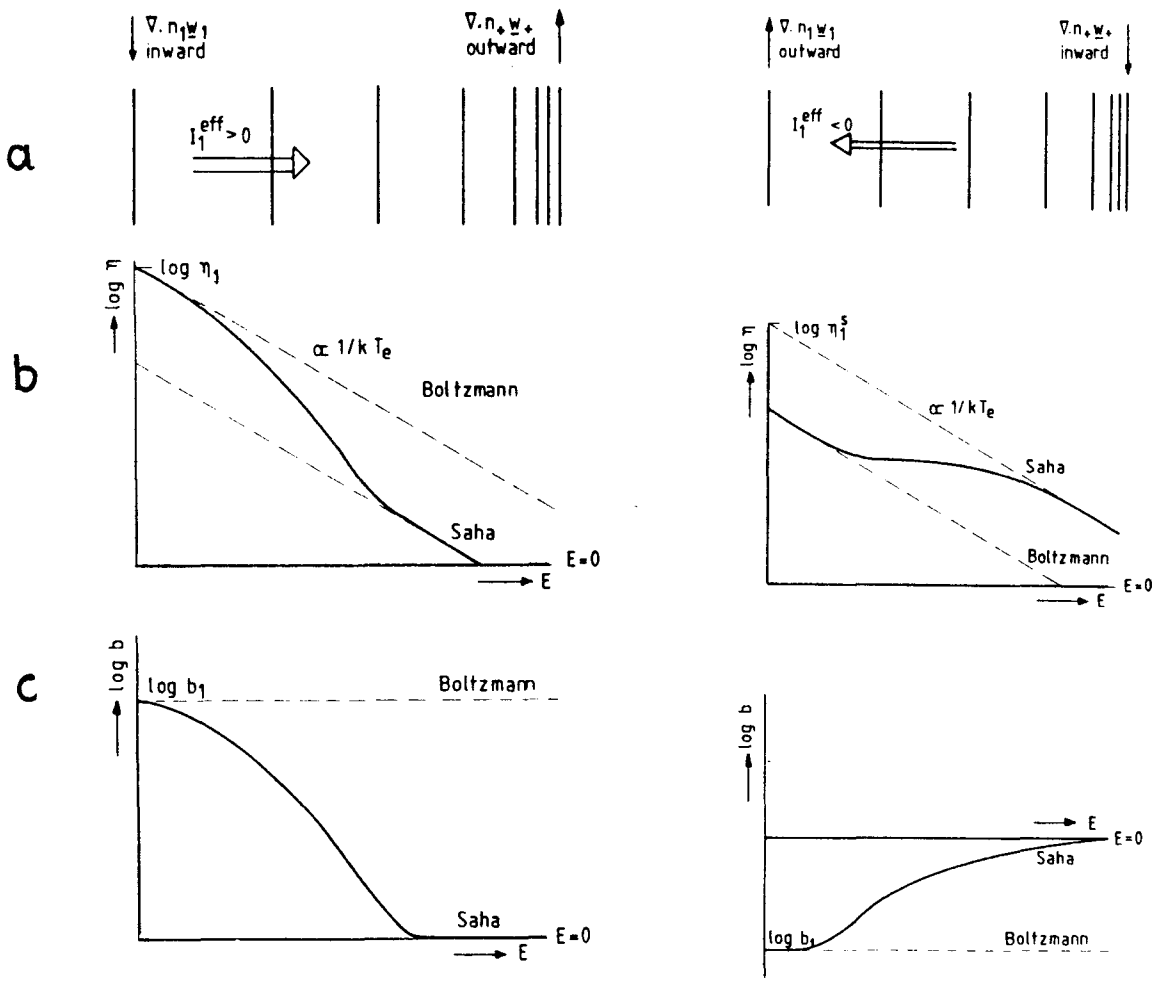


Fig. II.5. An ionizing system (left). a) Inward transport of ground state atoms and outward transport of ions, supported by a flow in the excitation space. b) ASDF of an ionizing system. The lower dotted line indicates the Saha equilibrium density. The actual density, denoted by a full line, is higher. The largest overpopulation is found for the ground state whereas high excited states are close to Saha equilibrium (c).

Fig. II.6. A recombining system (right) with inward transport of charged particles. The upper dotted line in b) indicates the Saha equilibrium density. The actual density, denoted by a full line, is below. The largest underpopulation is found for the ground state whereas high excited states are close to Saha (c).

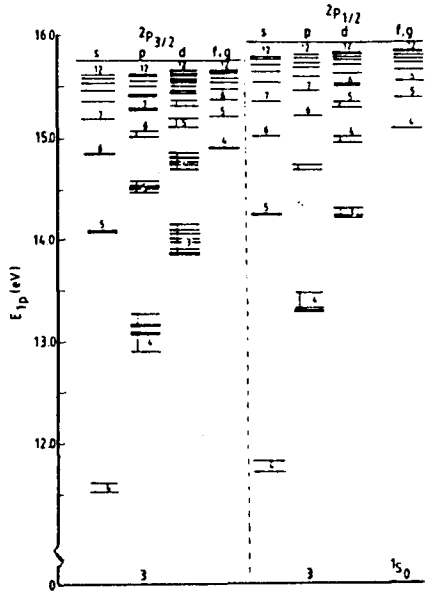

Fig. II.7. The scheme of energy levels of argon.

deviations of the CT sensitive levels from Saha due to CT are significant.

If at least some of the excited state densities satisfy (II.2) it is possible to measure their densities and determine $T_e$ and $n_e$. This has caused many problems in the past, which has not been completely resolved. Therefore we shall give some historical remarks about the development of the temperature notion (see [FEY.91/1]).

## II.3 CLOSE-TO-LTE CONCEPT

One of the aims of plasma physicists is to determine the plasma parameters, like electron density and temperature. Some time ago this lead to the introduction of many temperatures with various adjectives. Thus there was a distinction between the translation temperatures as electron-, ion- and heavy particle temperature and temperatures describing ratios of intensities as ionization-, excitation-, rotational and vibrational temperatures. Most popular was the 2 line or 2-$\lambda$ temperature $T_{2\lambda}$ which was easy to determine by comparing two relative intensities. However, it turned out that this quantity was ambiguous and very treacherous [SIJ.90]. Almost any pair of lines introduced a $T_{2\lambda}$ with an uncertainty of typically 20%. So at that time the conclusion was that the ICP had to be far from LTE. On the other hand there was a suspicion, because the Griem criterion predicted that the plasma could not be far from LTE in this $n_e$ range [GRI.63].

Partly due to the plasma physics group of the University of Eindhoven this paradox was solved. The answer was: abandon the 2-$\lambda$ temperature as a thermodynamic property and replace the relative measurements by the absolute measurement of one argon line [RAA.83]. The combination of the obtained excited state density with the ground state density (obtained from the pressure) gives the electron density $n_e$ and a temperature close to $T_e$. This procedure reduces the plasma indeterminacy drastically and it turns out that the main part is **close** to rather than **far** from LTE.

Other groups also started to characterize the plasma by $n_e$ values. The work of Caughlin and Blades in particular, based on spatially resolved measurements of H$\beta$ broadening [CAU.84, CAU.85] gave good results. In the Eindhoven group, Nowak [MUL.88, NOW.88, NOW.89] compared the $n_e$ values obtained from absolute densities of excited Ar states (see eq.(II.2)) with those of the spatially resolved H$\beta$ broadening technique. The measurements of Nowak gave a new insight into the ICP. It has been found that some regions in the plasma are indeed close to LTE. However, the plasma conditions at this time were different than at present (e.g. the power input was lower). Therefore the conclusions from the work of Nowak are not very well applicable in our conditions.

In this work we shall revise the close-to-LTE concept. In § IV it will appear that the ionization in the active zone of the ICP causes substantial deviations from Saha. Moreover, the active zone stretches pretty far above the load coils. This makes us doubt in the results of temperature determination obtained using spectroscopical methods and creates a need of application of other techniques.

# III. THE POWER INTERRUPTION EXPERIMENT

## III.1 INTRODUCTION

"Passive spectroscopy", based on absolute measurements of line emission intensities in the ICP has been already performed for a long time. In recent years the "active spectroscopy" for the ICP has been developed and implemented. The active spectroscopy is based on disturbing the plasma, in our case switching the power supply off for a short period and observing the plasma responses by monitoring time resolved line intensities. The power interruption technique was introduced by Gurevich for arcs [GUR.63] and used for the ICP [BYD.88, FAR.85, OLE.87]. It has been shown that a vast amount of information can be obtained using this technique [FEY.91/1].

This report will show that our 100 MHz Philips ICP is very suitable for such an power interruption experiment. The short power interruptions (20-100 $\mu$s), the high duty cycle of the measuring system (almost 100%) and the optimum repetition frequency of the interruptions (40 Hz) are essential.

## III.2 EXPERIMENTAL SETUP

For the experiments an RF-generator developed by Philips operating at 100 MHz has been used. The RF-coil consists of two windings with a diameter of 35 mm and a height of 15 mm. The plasma torch consists of three concentric quartz tubes and is a standard torch developed by Philips [BOU.82]. The outlet of the intermediate tube is placed 5 mm below the coil. The argon flows under standard conditions are 12 l/min outer flow, 0 l/min intermediate flow and 0.7 l/min inner flow and the power input is 0.8 kW. Introduction of analyte is done by nebulizing a water solution in the central flow by means of a cross flow nebulizer; under standard conditions the analyte injection rate is 1.4 ml/h.

A scheme of the experimental setup is shown in Fig. III.1. The switching of the generator is performed by providing a pulse circuit inside the generator with block pulses at TTL level. The off period of the generator can be varied from 20 to 100 $\mu$s. The timing diagram of the measurement is shown in Fig. III.2. We measured, using a pick-up coil, that the decay time of the EM-field at the switching off (to 10 % of the stationary value) is 3 $\mu$s, while the rise time (to 90 % of the stationary value) is 1.5 $\mu$s.

Plasma radiation is focused (1:0.78 image) on the entrance slit of a B&M BM100 monochromator with a grating of 1200 gr/mm and a length of 1 m. The wavelength selected light is led to an EMI 9698 QB photomultiplier, operating at a voltage of 1400 V. After being amplified 50 times by an Phillips variable gain amplifier model 777, which has a rise time of 1.8 ns, the anode signal is discriminated by a Phillips discriminator model 715. The pulses from the discriminator can

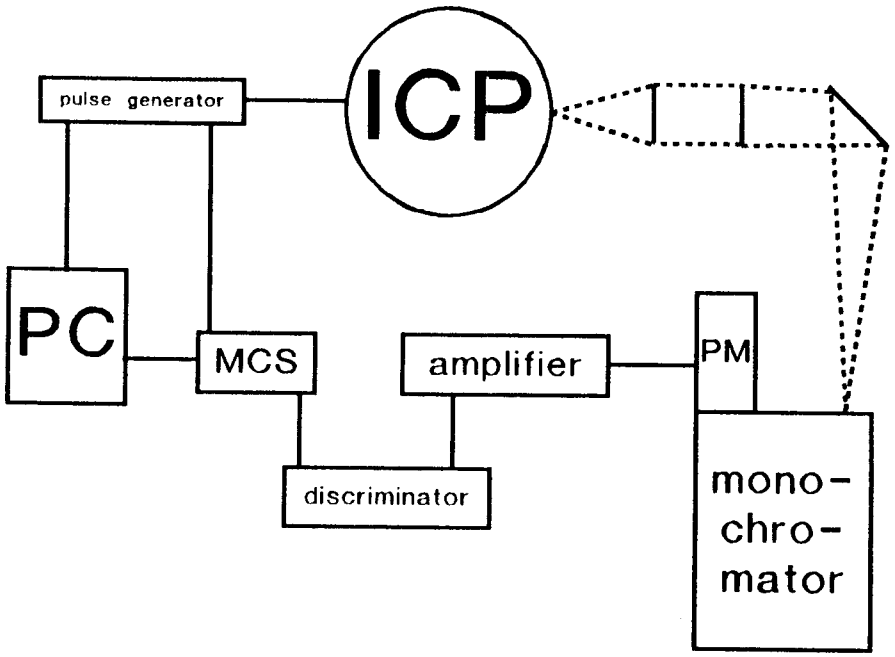


Fig. III.1. A scheme of the experimental setup. PM - photomultiplier, MCS - multi channel scaler.

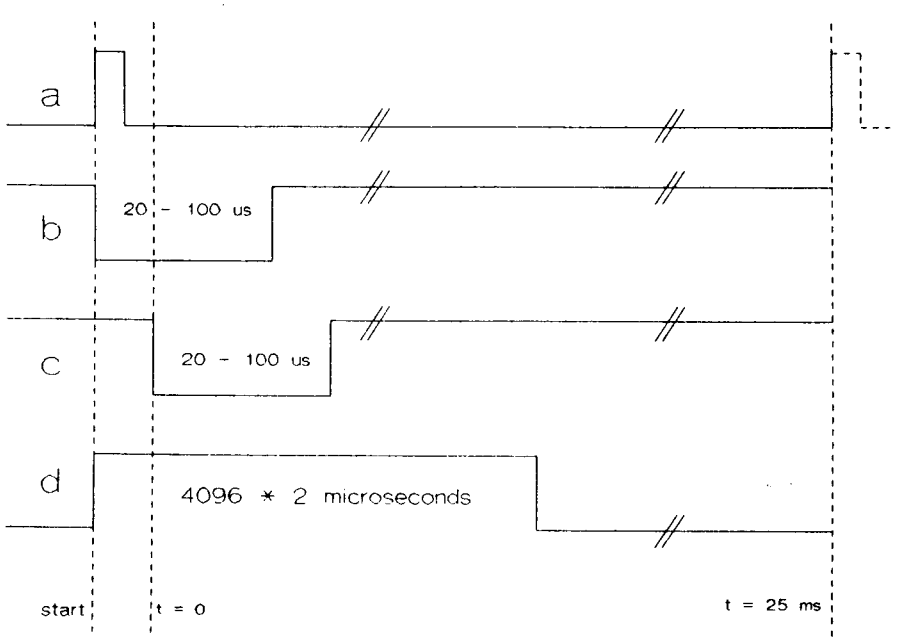


Fig. III.2. The timing diagram. (a) Start pulse of the computer. It triggers (b) the pulse generator, which (c) causes the temporary power interruption the RF generator after a delay of 30 $\mu$s and (d) triggers the MCS which starts counting during 4096*2 $\mu$s. This cycle is generally repeated about 4000 times (number of repetitions) with a repetition frequency of 40 Hz.

be counted as a function of time by a EG&G Ortec ACE-MCS Multi Channel Scaler (MCS), which has 4096 counters of 24 bits. By using this MCS we can observe about 8 ms continuously with a total resolution of 2 $\mu$s, which is determined by the minimum counter resolution of the MCS.

### III.3 GLOBAL RESULTS AND THEORY

The chain of energy transfer in the ICP has been discussed in § II. Here we shall concentrate on the influence of sudden interruption of the RF power on the particular links of this chain.

A) Interrupting the generator gives the following sequence of so called **instantaneous** events:

1) **Cooling:** when the energy flow into the plasma is interrupted, the plasma changes from an ionizing state to a recombinating state. The electrons pass their energy surplus to the heavy particles until $T_e = T_h$ is reached, with an evaluated time constant $\tau_e \simeq 1$ $\mu$s ([BYD.88, MIL.90]). As it will appear, the experimental time constant is larger than 1 $\mu$s.

2) **Recombination:** during the time the generator is off, ions recombine and the electron density decreases. The time constant $\tau_n$ is typically $10^{-4}$ - $10^{-3}$ s [BYD.88].

3) **Heating:** immediately after the switching on of the power the opposite of cooling occurs with $\tau \simeq \tau_e$ , restoring $T_e > T_h$. Temporarily $T_e$ increases above its steady state value.

4) **Ionization:** $n_e$ increases slowly with $\tau \simeq \tau_n$ towards the steady state value.

B) Furthermore the temporary interruption of the energy supply to the plasma causes a macroscopic disturbance. This disturbance is created in the expansion zone (underneath the load coil). It travels through the plasma and is observed in higher regions as a **delayed event:**

5) **The perturbation arrival:** a wave package of typically $\tau_w$ = 5 ms is observed. The time of arrival depends on the spatial position of the observed plasma part.

All these events cause responses of the plasma emission. The study of instantaneous events gives insight into local microscopic processes. However, it should be taken care of that the following conditions are fulfilled:

i) The plasma should be in steady state at the start of the power interruption. This means that mixing of the instantaneous events (1 - 4) and the delayed event (5) of the previous interruption must be avoided. This puts an upper limit to the repetition frequency of the power interruption. We have found it to be 40 Hz.

ii) The off period $\Delta t$ should be smaller than the characteristic transport time, the time needed to transport essential different plasma parts to the observation location. We can write this condition as: $w \Delta t << \Lambda$, where w is the bulk velocity and $\Lambda$ the gradient length of the plasma (the characteristic length on which the plasma conditions change by a factor of e).

For the interpretation of instantaneous responses of line intensities we distinguish between two major production/destruction balances governing the population of excited states: the Saha balance and the Boltzmann balance (see § II). The two other balances, which have influence on

some levels, like the Charge Transfer balance and the Excitation Transfer balance are treated in [STO.91/3].

I. The electron controlled **Saha Balance (S)** of ionization and recombination. The number density of state p, dominated by the Saha balance is given by

$$\eta^S(p) = \eta_+ \eta_e \{h^3/(2\pi m_e kT_e)^{3/2}\} \exp ( E_{ion}(p)/kT_e) \qquad \text{III.1}$$

II. The electron controlled **Boltzmann balance (B)** of excitation from and deexcitation to the ground state. The density of a state p is:

$$\eta^b(p) = \eta(1) \exp ( - E_{1p}/kT_e) \qquad \text{III.2}$$

Note that the effect of a change in $T_e$ on the population of a state governed by the Boltzmann balance will be opposite to the effect on a state governed by the Saha balance.

It is the charm of the power interruption technique that the investigation of the responses of various levels gives insight into the state and hierarchy of the balances in the undisturbed plasma.

Since the elementary balances consist of fast processes with relaxation times smaller than $10^{-8}$ s, we assume that they equilibrate constantly during the relaxation of the electron temperature ($\tau_e \simeq 10^{-6}$ s) and density ($\tau_n \simeq 10^{-4}$ - $10^{-3}$ s).

From eqs. (III.1) and (III.2) it follows that the response to a change in electron temperature ( at cooling and heating ) of a state controlled by the Saha balance differs from the response of a state which is ruled by the Boltzmann balance. Let $\gamma$ be the ratio of the initial electron temperature $T_e$ to the final electron temperature $T_e^*$ ($\gamma = T_e/T_e^*$). The responses of a Saha state and a Boltzmann dominated state to the cooling will be [MIL.90, FEY.91/1]:

$$\ln \frac{\eta^S(p)^*}{\eta^S(p)} = \frac{\gamma - 1}{kT_e} E_{ion}(p) + \frac{3}{2} \ln \gamma \qquad \text{Saha} \qquad \text{III.3}$$

$$\ln \frac{\eta^b(p)^*}{\eta^b(p)} = - \frac{\gamma - 1}{kT_e} E_{1p} \qquad \text{Boltzmann} \qquad \text{III.4}$$

where $\eta_p$ denotes the density at the initial $T_e$ and $\eta_p^*$ the density at the final $T_e^*$. It is assumed that $n_a$, $n_e$ and $n_+$ are constant during $\tau_e$, as $\tau_e << \tau_n$. It will be discussed further in § IV. For $n_a$ one should be careful with this assumption (see [STO.91/3]).

These different responses can be used to investigate by which balance a state is populated. In general situations more than one balance will control the population of a state, so the response to changes of the electron temperature will be a combination of all balances involved. Nevertheless we use the expression "Saha like" response if a line intensity increases when the power input to the plasma is interrupted and "Boltzmann like" response if the intensity decreases, whether or not these

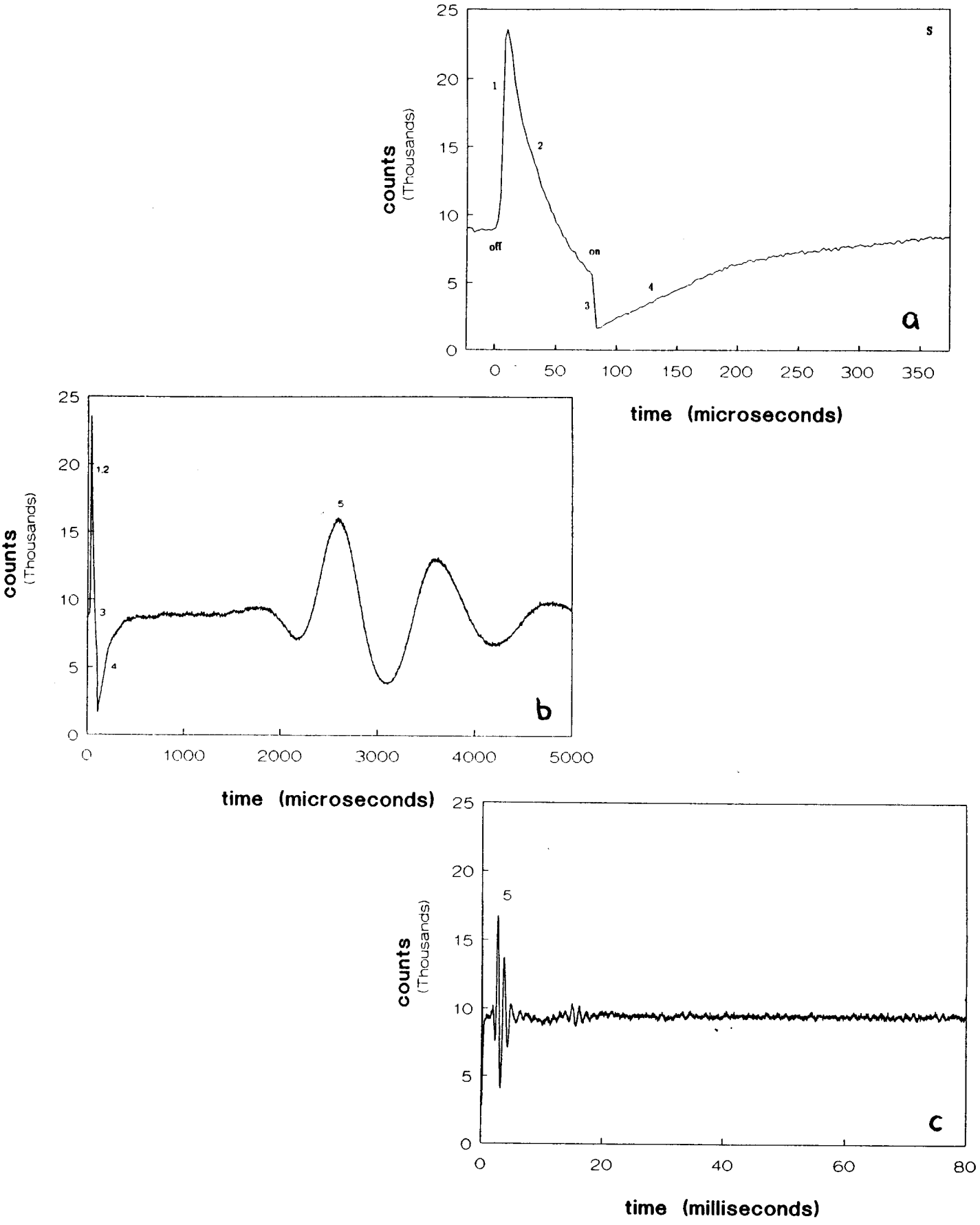


Fig. III.3. Responses of the Ar(6d) level at 3 mm ALC and r = 6 mm over (a) 400 $\mu$s, (b) 5000 $\mu$s and (c) 80 ms. The "Saha like" response to instantaneous events, like electron cooling (1) followed by decay due to recombination (2) and the electron heating (3) followed by ionization (4) are visible. Delayed effects (5) occur after 1.8 ms and 20 ms.

balances actually govern the response.

For general information about the time dependent behavior of the plasma and the quality of our experimental method we present the temporal behavior of the Ar 6d - 4p line at $\lambda$ = 549.59 nm for which the plasma is assumed to be optically thin. The plasma is operated at standard conditions with water injection and the lateral measurement has been taken 3 mm above the load coil (ALC) and 6 mm from the center. Fig. III.3a shows the response during the first 400 $\mu$s. The upward jump is due to electron cooling, the decay during the off-period is due to decay of electron density and the downward jump is due to electron heating. The cooling and heating jumps take about 8 $\mu$s, so the time resolution of the MCS (2 $\mu$s) is sufficient. The upward jump at cooling and the downward jump at heating are typical for a level dominated by the Saha balance (III.1). This instantaneous Saha like response of the 6d level leads to the conclusion that the Saha balance is important for this level. Figs. III.3b and 3c show the response during respectively 5 ms and 80 ms. After about 1.8 ms a package of disturbances with a width of about 5 ms arrives at this plasma location. A second one with the same time structure, but with lower amplitude, arrives after 20 ms. These delayed events labelled with (5) are of completely different nature than the instantaneous events labelled with (1 - 4). The delayed events are discussed in § VII. From this measurement we can conclude that there will nowhere be an overlap from different pulsing periods provided that the repetition frequency of the interruption is less than 43 Hz. The selected frequency of 40 Hz is much higher than the 0.5 Hz used in [BYD.89, MIL.89]. When much higher frequencies are used to pulse or modulate the energy input, like 1 kHz modulation, the overlap of the disturbances is so large that a straightforward interpretation becomes impossible.

Apart from the argon levels we also study the responses of other elements. It has been found that levels of H, O and $N_2$ respond similarly to Ar, i.e. "Saha-like". Metals and some molecular bands (OH) respond in a completely different way. Fig. III.4 shows the response of Mg I (3p3s), the first excited level in the Mg I system at 5 mm ALC and r = 3 mm. Similar response is observed as well for the lowest excited states of Na, Ca, Cu, Al, Cd and Fe in their atomic and ionic systems. We see a downward intensity jump at the cooling, a constant intensity during the off-period and large upward jump at heating, after which the steady state intensity is restored.

This behavior can be explained by a model which takes the evaporation processes of the droplets in which these elements are introduced into account. This model is fully described in [STO.91/3].

Finally, the response of continuum (free - bound) radiation is different from the ones described above (Fig. III.5). The $T_e$ dependence of the continuum changes with the wavelength. Generally, at the cooling the continuum intensity either stays constant or decreases. Since free - bound recombination radiation is $n_e n_+$ dependent it always decreases during the off-period. The responses of continuum are treated in [STO.91/3].

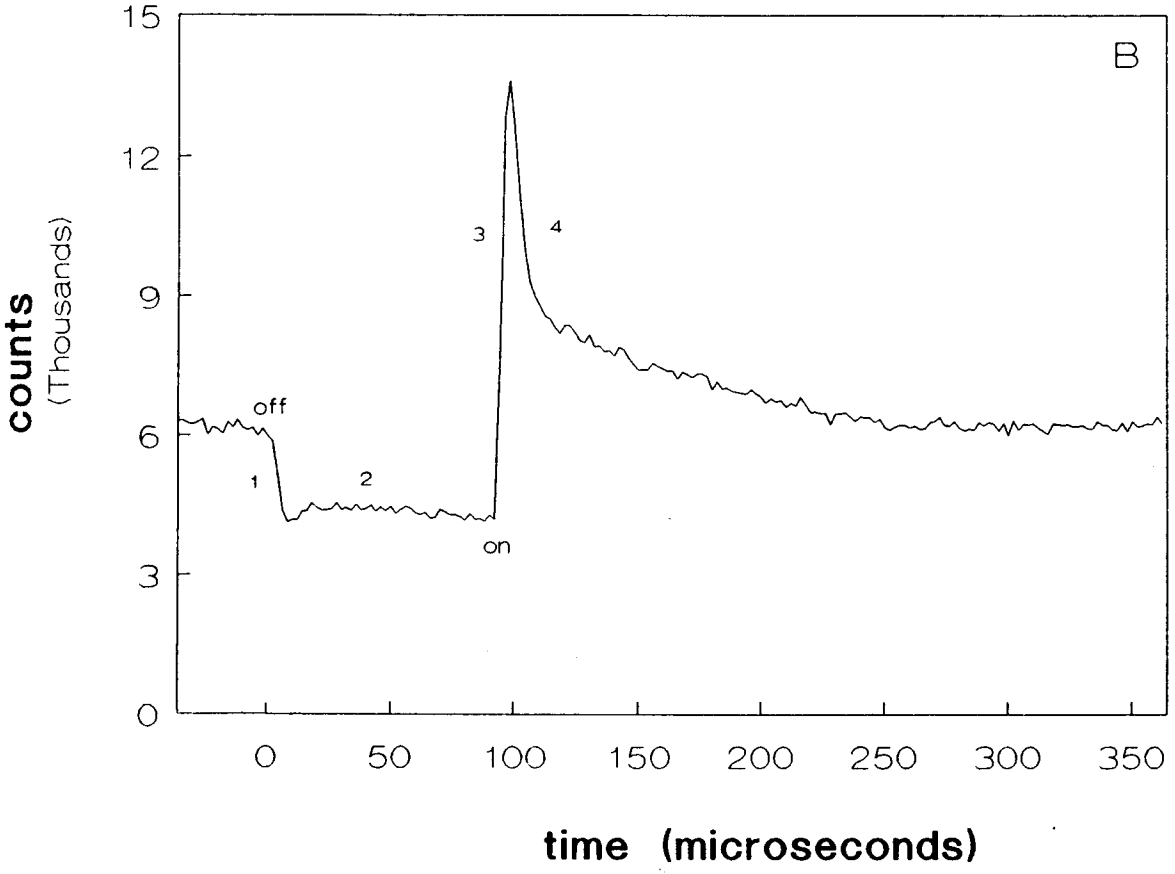


Fig III.4. A response of the Mg I (3p3s) level at 5 mm ALC and r = 3 mm over 400 $\mu$s. Note the Boltzmann dominated instantaneous response with a downward jump at cooling, constant intensity during the off-period and upward jump at heating.

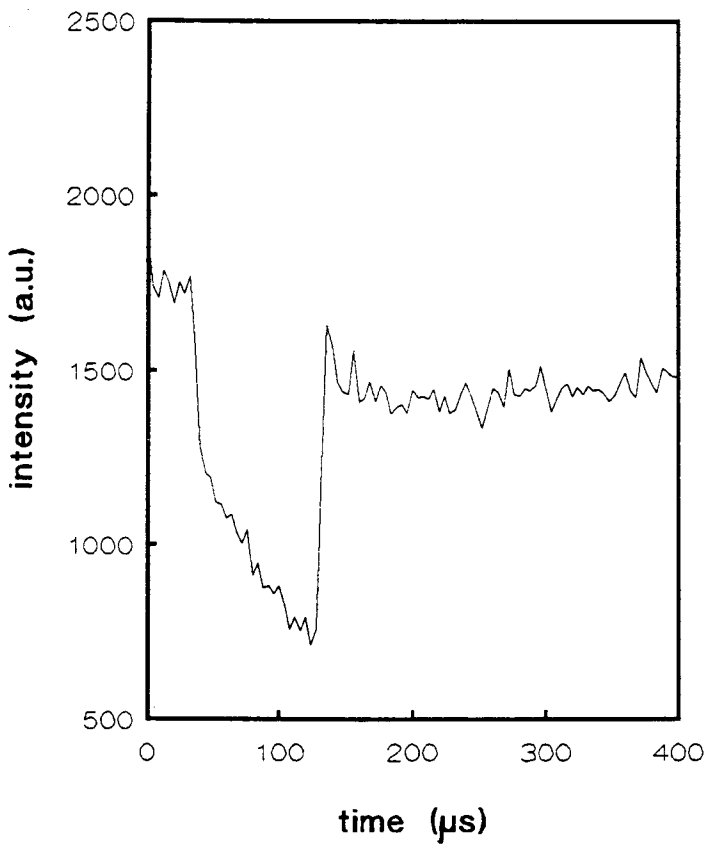


Fig. III.5. A response of continuum at $\lambda$ = 300 nm. Note the downward jump at cooling and the decay during the off-period.

# IV. MACROSCOPIC CHARACTERIZATION OF THE ICP

## IV.1 INTRODUCTION

In this chapter some important macroscopic parameters characterizing the ICP will be studied. One of the most important plasma parameters is the temperature. It has been indicated in § II that in the ICP there are essentially two systems: electrons with temperature $T_e$ and heavy particles with temperature $T_h < T_e$. Due to the inefficient energy transfer between these systems it is possible to sustain $T_e > T_h$ in the steady state. The decoupling of electrons and heavy particles is a non equilibrium feature and it might create a problem in the interpretation of the plasma. It has been shown, however, that the usual way of determining temperature using line emission intensities can be still used to obtain information about the electron temperature (§ II). The extra problem is the determination of the heavy particle temperature. Here we present the power interruption experiment as a method to determine this missing parameter.

The power interruption experiment described in § III gives a deep insight into the plasma processes. As these processes are fairly understood, some information about plasma properties can be obtained. It will be shown that by following the responses of various atomic levels of argon one can obtain information about electron and heavy particle temperatures. This method, however, has a important limitation. The temperatures determined this way do not represent real electron and heavy particle temperatures in case of absence of the Saha equilibrium.

In this chapter the reliability of the power interruption experiment as a method of $T_e$ and $T_h$ determination will be discussed. We shall compare the results of the power interruption experiment with $T_e$ measured using another technique. For $T_e$ determination the alternative technique is "passive spectroscopy" (see § II). We refer to some new results obtained this way.

The power interruption experiment provides information about another important macroscopic plasma parameter, which is the drift velocity of the plasma. In § III it has been shown that the power interruption is always followed by a macroscopic delayed response travelling through the plasma. The velocity of this response is compared with the plasma velocity determined another way. It appears that the disturbance propagates with the velocity close to the plasma drift velocity.

## IV.2 TEMPERATURES IN THE ICP

### IV.2.1. The power interruption method.

In § III the instantaneous responses of the line emission to the power interruption were treated in terms of elementary balances. It has been shown that for a level coupled to the ion ground state by a Saha balance the ratio of densities after and before switching off the generator

(cooling jump) is given by:

$$\ln \{n^*(p)/n(p)\} = \ln(n_e^*/n_e) + \ln(n_+^*/n_+) + 3/2 \ln \gamma + E_{ion}(p)\,(\gamma - 1)/kT_e \qquad \text{IV.1}$$

When the Saha equilibrium is present in the plasma the above formula gives a possibility of determining $\gamma$ and $T_e$ from experimentally found cooling jumps for several excited atomic states of argon.

According to (IV.1) the cooling jumps of the excited states of argon should depend linearly on ionization energy $E_{ion}$ of these excited states:

$$\ln \{ n^*(p)/n(p) \} = a_0 + a_1 E_{ion}(p) \qquad \text{IV.2}$$

In order to be able to determine the temperatures it is not sufficient to know $a_0$ and $a_1$, as $a_0$ contains density jumps which have to be determined. In § III it has been said that during the time the generator is switched off the electron density does not change significantly, so the first term drops out. Still, the second term in (IV.1) needs some more comment.

It is known that in the argon system there are two subsystems with different total angular momentum quantum numbers, J = 1/2 and J = 3/2. The ionization energy of the system with J = 1/2 is 0.17 eV higher that in the other system. If the number of particles in both systems does not change when the generator is switched off, the cooling jumps should split into two groups, lying on two different lines:

$$\ln \{ n^*(p)/n(p) \} = a_0 + a_1 (E_{ion}(p) + 0.17 \text{ eV}) \qquad (J = 1/2)$$

$$\ln \{ n^*(p)/n(p) \} = a_0 + a_1 E_{ion}(p) \qquad (J = 3/2)$$

where $E_{ion}$ is calculated with respect to the 3/2 system. However, it is not clear that both ion densities have to stay constant. On the contrary, the energy difference between them is so small that they will be most likely Boltzmann coupled:

$$\eta_+ (J = 1/2) = \eta_+ (J = 3/2) \exp (- 0.17/kT_e) \qquad \text{IV.3}$$

Using (IV.3) we can find a relation between the jumps of two ion densities:

$$\ln(\eta_+^*/\eta_+)\,(J = 1/2) = \ln \eta_+^*/\eta_+ \,(J = 3/2) - 0.17\,(\gamma - 1)/kT_e \qquad \text{IV.4}$$

Introducing (IV.4) into (IV.1) we can find a formula for the cooling jump:

$$\ln \{ n^*(p)/n(p) \} = \ln(n_+^*/n_+) \, (J = 3/2) + 3/2 \ln \gamma + E_{ion}(p) \, (\gamma - 1)/kT_e \qquad \text{IV.5}$$

for J = 1/2 which is exactly the same as this for J = 3/2. From this it follows that the cooling jumps of levels in both systems will lie on the same line. This fact will be verified experimentally. The last step is the determination of $n_+^*/n_+$. Using (IV.4) and the fact that:

$$n_e = n_+ (J = 1/2) + n_+ (J = 3/2) = \text{const}$$

we find:

$$n_+ (J = 3/2) = \frac{g(J=3/2)/g(J=1/2) \; \exp(0.17/kT_e)}{1 + g(J=3/2)/g(J=1/2) \; \exp(0.17/kT_e)} \, n_e$$

In principle one should introduce the density jump calculated from the above formula into (IV.5). In this case $a_0$, the free term in (IV.5) will be an implicit function of $T_e$ and $T_h$. However, if we substitute g(J = 3/2) = 4, g(J = 1/2) = 2 and calculate $\ln(n_+^*/n_+)$ for typical temperatures $T_e$ = 0.8 eV, $T_h$ = 0.6 eV we see that it is in the order of 0.01, which is about 2% of the term 3/2 ln $\gamma$. Therefore we do not introduce a large error if we assume $\ln(n_+^*/n_+) = 0$.

Having shown that the density jumps due to the fact that argon has two subsystems do not influence the cooling jumps we can determine the temperatures. First it has to be verified whether the logarithms of experimental cooling jumps are increasing linearly with ionization energy (i.e. according to (IV.2)). If so, we can introduce the simplifications discussed above and find the following expressions for $\gamma$ and $T_e$:

$$\gamma = \exp(2/3 \, a_0) \qquad \text{IV.6a}$$

$$T_e = (\gamma - 1)/a_1 \qquad \text{IV.6b}$$

Using this method, however, one should be aware of several sources of error. One of them is just a purely experimental error. It follows from the expressions (IV.6a) and (IV.6b) that if the uncertainty in $a_0$ is $\Delta a_0$ the error in $\gamma$ will be:

$$\Delta\gamma/\gamma = 2/3 \, a_0^{-1} \, \Delta a_0/a_0$$

Typically $a_0 \simeq 0.4$, so the error in $\gamma$ is not substantially larger than error in $a_0$. However, if we calculate an error in $T_e$ only due to error in $\gamma$:

$$\Delta T_e/T_e = \gamma/(\gamma - 1) \, \Delta\gamma/\gamma$$

we see that the error amplifies. For a typical $\gamma = 1.3 \pm 0.1$ ($\Delta\gamma/\gamma \simeq 8\%$) we obtain $\Delta T_e/T_e \simeq 33\%$. From this simple calculation we can conclude that only the value of $\gamma$ determined using the power interruption technique should be trusted. While discussing the values of $T_e$ one should be aware of the cumulation of experimental scatter and therefore be skeptical towards the obtained data.

A dangerous systematic error of this method is due to deviations from Saha equilibrium. Having in mind that most of the measurements are performed in the ionizing part of the plasma (skin) we will try to predict the kind of error we commit using (IV.1) for the ionizing plasma.

When the power supply is switched off there is no energy flow into the plasma, so the electrons are not created anymore. Consequently the plasma switches from ionizing to recombining state. Somewhere between these states there is a point in which the plasma is neither ionizing nor recombining. In this point the Saha equilibrium is reached. It is plausible to assume that the plasma passes this very point of equilibrium just after $T_e$ has dropped to $T_h$, but before $n_e$ started to decrease. The line intensities reach their maximum at this point. Therefore we do not commit a substantial error by assuming that just after the switching the generator off the excited states of argon are populated according to Saha equation for $T_e = T_h$ and $n_e$ the same as that in the steady state. Therefore the cooling jumps of argon will provide information about the deviations from Saha in the steady state. In Fig. IV.1 we present the Atomic State Distribution Function for an element in an ionizing plasma (see § II). We see from Fig. IV.1 that if for given $T_e$ and $T_h$ the steady state ASDF is overpopulated with respect to Saha, the jumps will increase less with ionization energy than what is expected from (IV.1). The jumps of the levels with low $E_{ion}$ will remain almost the same. As a result $a_0$ practically does not change, but the slope $a_1$ becomes substantially smaller. If one uses (IV.6a) and (IV.6b) to determine $\gamma$ and $T_e$ it becomes clear that the ionizing plasma does not cause a large error in $\gamma$. The accuracy of the result depends on how far the highest measured excited states are from the ionization limit. $T_e$ determined this way is much larger than in reality and therefore the method does not give reliable results.

Having briefly described the errors and limitations of this method we can concentrate on the experimental results. In order to introduce the least possible deviation from Saha one has to choose carefully the place in the plasma, in which the responses will be observed. As said in § II, the plasma is far from being homogeneous. Most of the electrons are created in the skin, between, just above and just below the load coils. One can expect that in these regions the deviations from Saha are large. High above the load coils the plasma is recombining, which also introduces and error in (IV.1). Moreover, high above the load coils there is hardly any energy input, so $T_e \approx T_h$. Therefore a "golden mean" must be found: a place which is not too close and not too far from the coils. All the measurements presented below are performed 5 mm Above the Load Coil (ALC). In principle one has to take into account the radial inhomogeneity of the plasma (see § II, profiles). Therefore several lateral scans across the plasma have been performed and further the lateral data have been Abel inverted using the procedure described in [BRA.90]. However, one can imagine that most of the emission comes from the skin. Therefore the difference between lateral and Abel inverted data from

Fig. IV.1. ASDF of an element in an ionizing plasma. The Saha lines for two temperatures are indicated. As the temperature decreases the densities increase. However, for lower excited states the jumps are not as large as theyshould be according to Saha.

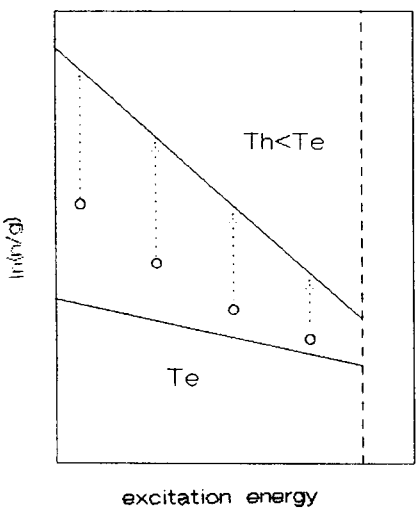


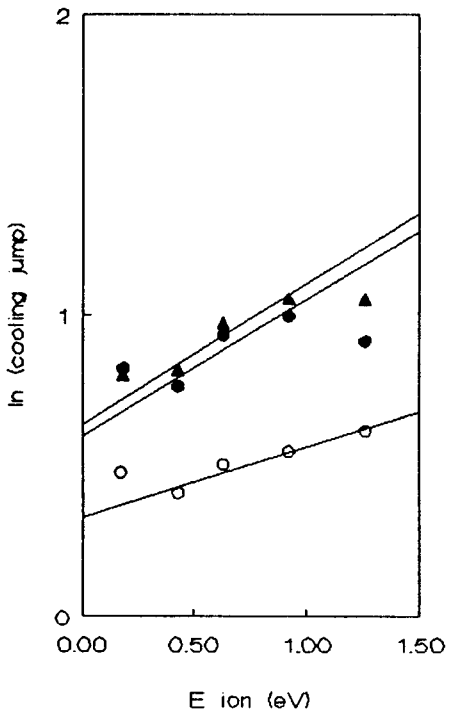


Fig. IV.2. The cooling jumps of Ar, a comparison of lateral and Abel inverted data.
▲ lateral scan at r = 6.5 mm, $\gamma$ = 1.53, $T_e$ = 1.14 eV
● Abel inverted lat. data at r = 6.5 mm, $\gamma$ = 1.49, $T_e$ = 1.08 eV
o Abel inverted lat. data at r = 4 mm, $\gamma$ = 1.25, $T_e$ = 1.06 eV.
Conditions: dry plasma, flows: 12/0/0.7 l/min, power input: V = 3 kV, I = 0.4 A, 5 mm ALC.

the skin will be small. On the other hand Abel inversion has one doubtless advantage: it gives the radially resolved information, which is lost when an ordinary lateral scan is analyzed.

Here we present the data originating from lateral scans for the following argon lines:

| | | |
|---|---|---|
| 5p - 4s | $\lambda$ = 420.1 nm | $E_{ion}$(5p) = 1.260 eV |
| 6s - 4p | $\lambda$ = 703.0 nm | $E_{ion}$(6s) = 0.921 eV |
| 5d - 4p | $\lambda$ = 603.2 nm | $E_{ion}$(5d) = 0.629 eV |
| 6d - 4p | $\lambda$ = 549.7 nm | $E_{ion}$(6d) = 0.428 eV |
| 9d - 4p | $\lambda$ = 495.7 nm | $E_{ion}$(9d) = 0.183 eV |

In Fig. IV.2 the cooling jumps at r = 6.5 mm from the center of the plasma are plotted as a function of ionization energy. We can see that the difference between lateral and Abel inverted data is not substantial. There is a far more serious problem, which is data scatter. We see that the points are not really collinear. 5p and 9d are the most deviating ones. The error in the cooling jump of 5p can be still explained by its relatively large ionization energy. If we look at the overpopulation distribution (Fig. IV.1) we can expect that the deviation of 5p from Saha is still substantial. The error for 9d can not be explained by departure from Saha due to ionizing system. It seems though to be well reproducible. It might be due to some process (de)populating selectively 9d (e.g. some molecular

reaction).

The value of $\gamma$ obtained from the above data is about 1.5. In Fig. IV.2 we have also shown the cooling jumps at r = 4 mm, which give $\gamma$ = 1.25. Though these values suffer from large experimental error, they can give an idea about the energy incoupling into the plasma. In Fig. IV.3 the radially resolved responses are shown. It is clear that the cooling jumps increase with increasing distance from the center of the plasma. It can be observed for all the responses of all measured lines. This indicates that $\gamma$ increases with increasing radius. This effect is due to shielding of the EM

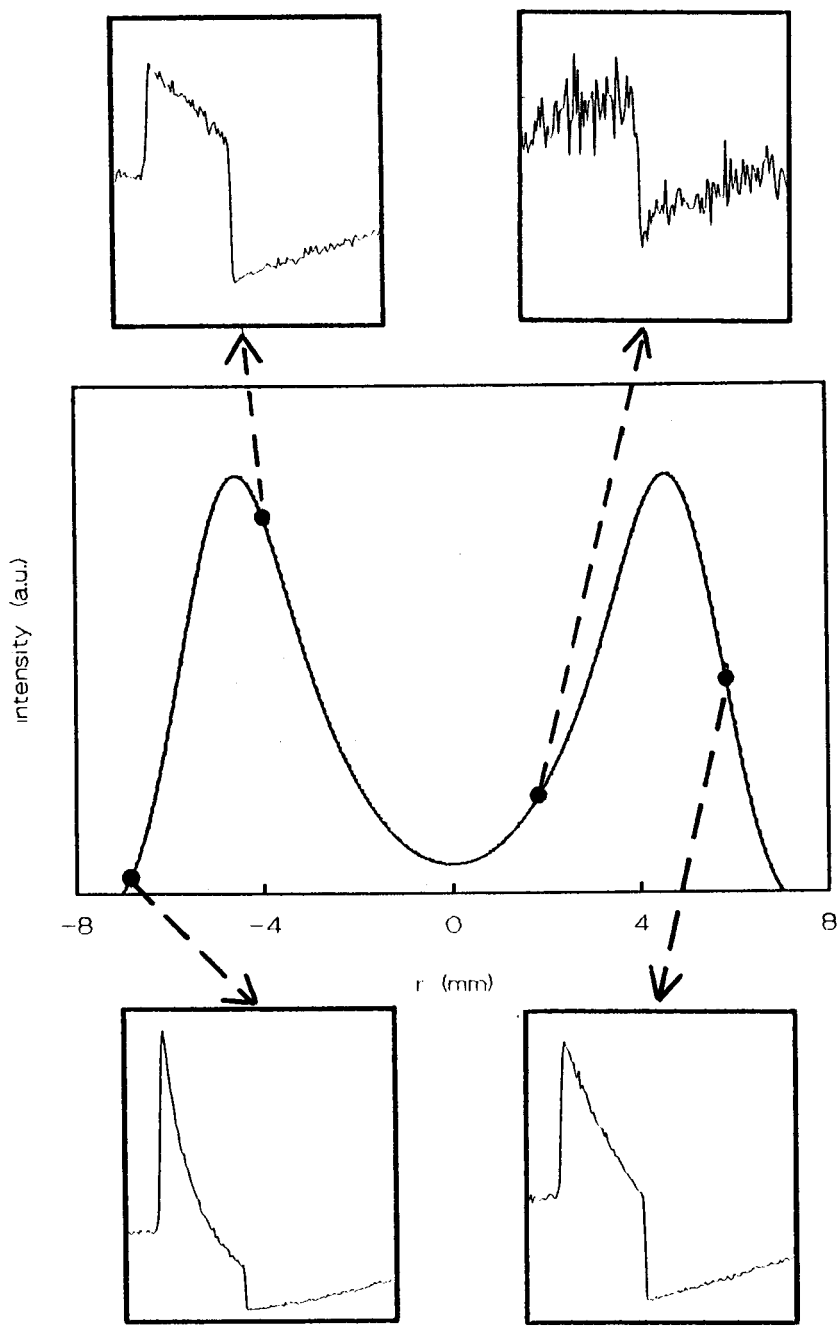


Fig. IV.3. The Abel inverted instantaneous responses at several places in the plasma (as indicated on the enclosed plasma profile).

field of the coils in the plasma. In the center of the plasma there is hardly any energy input from the field and consequently $T_e \approx T_h$. This problem will be treated in detail in § V. Here we shall concentrate on a region in the plasma where $\gamma$ = 1.3 (r = 4 - 5 mm). In fact, the measurements in the more outer regions should be avoided, as the results are probably strongly influenced by outwards diffusion flows due to large $n_e$ and $T_e$ gradients. For a fixed place in the middle of the skin $\gamma$ does not differ by more than 0.1 for different measurements, so the reproducibility is acceptable.

From the results presented above we see that the scatter in experimental data is quite substantial. In order to be able to determine $\gamma$ more accurately more points are needed. As the lateral scans and Abel inversions are extremely time consuming, further we shall present data obtained in only one place (5 mm ALC, at r = 4 mm). We are aware, though, that this procedure provides $\gamma$ averaged over r = 4 - 6 mm, i.e. the region from which we collect the majority of the emission (see § II, profiles).

In Fig. IV.4 we present the cooling jumps for many argon levels, in pure argon plasma. It can be seen that most of the points are fairly collinear. The temperatures determined from this set of data are: $\gamma$ = 1.31, $T_e$ = 0.72 eV. In Fig. IV.5 we show the results of measurements in the same conditions, only with water injection, give $\gamma$ = 1.37, $T_e$ = 1.23 eV. However, one cannot take it as a proof that $T_e$ is higher when water is injected into the plasma. Latter data for both situations show that this is a normal experimental scatter. The conclusion is rather negative: this method does not give reproducible $T_e$ and therefore it should be used only for the determination of $\gamma$. Moreover, the value of $T_e$ can be substantially influenced by the deviations from Saha. As most of the latter measurements bring a relatively high $T_e$, we have to realize that even at 5 mm ALC the plasma is still ionizing.

### IV.2.2 "Passive spectroscopy" for temperature determination.

The values of $T_e$ and $T_h$ obtained from the power interruption technique are rather dubious. For sure some reference data is needed. Therefore we present $T_e$ and $T_h$ determined using "passive spectroscopy" (in the steady state). The temperature determined from intensities of atomic lines should equal $T_e$. However, if the plasma is ionizing the error of this method is large. From Fig. IV.1 it follows that the slope of steady state ASDF in ionizing plasma is larger than it should be if the densities obeyed the Saha equation. Therefore the temperature determined this way is lower then in reality (oppositely to the result of power interruption method). The measurements were performed 5 mm ALC, at r = 4 mm [FEY.91/3]. The obtained "electron temperature" is 0.3 eV. It is clear that it cannot represent the real $T_e$. This ridiculously low value confirms that the deviations from Saha in this region of the plasma are very large. Thus the accurate determination of $T_e$ in the ICP remains an open question.

The steady state ASDF of argon does not bring any information about $T_h$. However, $T_h$ can be also determined by means of "passive spectroscopy". We only have to find a species in the

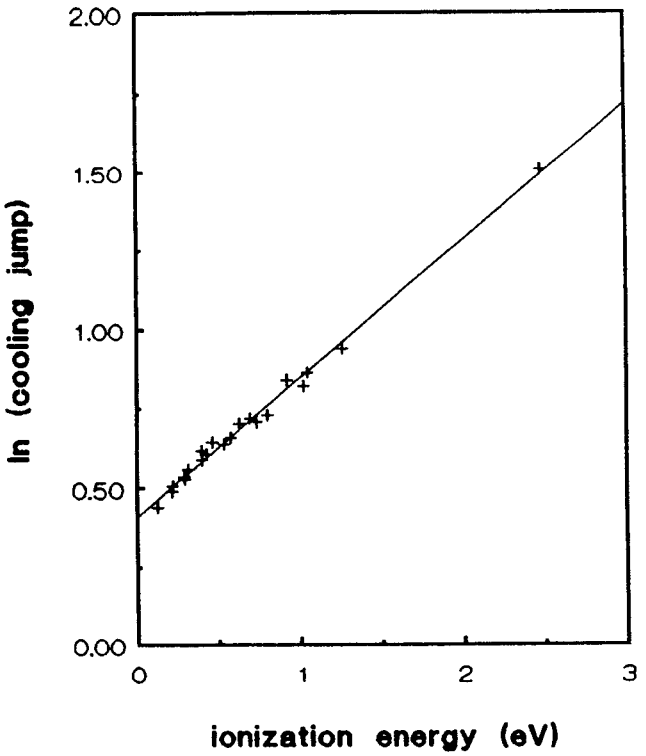


Fig. IV.4. Cooling jumps of Ar levels. Conditions: as in Fig. IV.2, r = 4 mm. The parameters determined from this data are: $\gamma$ = 1.31, $T_e$ = 0.72 eV.

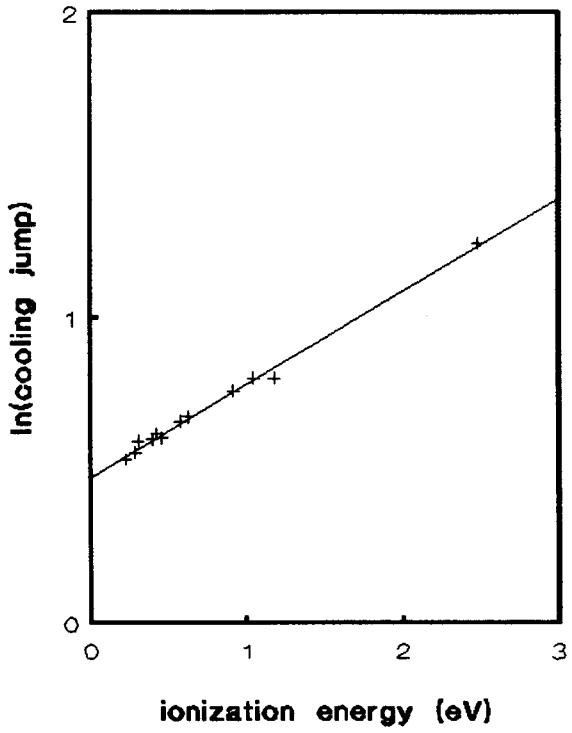


Fig. IV.5. Cooling jumps of Ar levels. Conditions are like in Fig. IV.4., but water is introduced into the plasma.
The determined parameters are: $\gamma$ = 1.37, $T_e$ = 1.23 eV.

plasma, whose excited states are populated by collisions with heavy particles. If such a species exists, its excited states will be ruled by $T_h$ dependent Boltzmann equation.

Molecular nitrogen, abundantly present in the outer parts of the plasma, seems to be a good candidate for a species which energy levels are $T_h$ dominated. In Fig. IV.6 a part of the $N_2$ spectrum is shown. We see rotational structure of a (0,0) band belonging to the second positive system $C^3\Pi_u$ - $B^3\Pi_g$. The excitation of rotational levels is likely to be performed by heavy particles solely, since momentum of electrons is too small to influence rotational motion of a (heavy) molecule. Moreover, the distance between rotational energy levels is very small, much smaller than $kT_h$. Therefore these energy levels (at least the lower ones) are likely to be in Boltzmann equilibrium, with $T = T_h$. Here we do not present the actual procedure leading to determination of $T_h$. We only suggest that Fig. IV.6 be used for determination of $T_h$ in future.

All the spectroscopical methods described above are in principle not suited for temperature determination in a system like ICP. Their validity strongly depends on the presence of equilibrium. We have shown, that the error in determined electron temperature due to ionizing plasma is very large. Data obtained using two different spectroscopical techniques differ by a factor of 4.

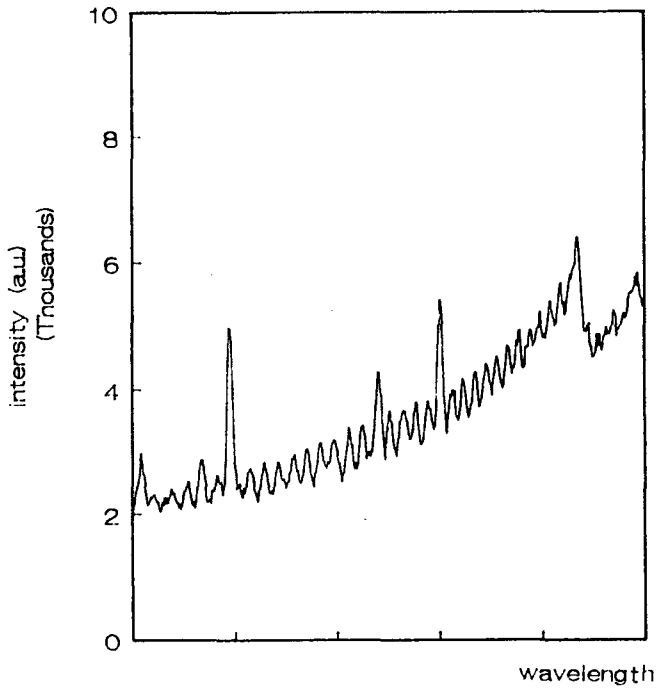


Fig. IV.6. A part of the $N_2$ spectrum (second positive system, $C^3\Pi_u$ - $B^3\Pi_g$, (0,0) band at $\lambda$ = 337 nm). The rotational structure of this band is well visible. The full scale is 5 nm.

Perhaps there are places in the ICP where the deviations from Saha are smaller (e.g. higher above the load coils). In these places a usage of "passive spectroscopy" would be justified. However, the method of power interruption, which is more elegant and brings more information would fail in those places due to $T_e \approx T_h$. It is recommended that another diagnostics, free from equilibrium assumptions, be introduced.

## IV.3 DRIFT VELOCITY OF THE PLASMA

### IV.3.1. A relation with heavy particles temperature

An important parameter, closely related to the heavy particles temperature is the drift velocity of the plasma. We have already presented a method of determination of $T_h$. These method, however, is based on the assumption of Saha equilibrium for atomic argon states. The validity of this assumption is very problematic. We should also not forget about large experimental errors, uncertainty of used transition probabilities, etc. Therefore it is necessary to have another method, free from the equilibrium assumption. The method which we present now gives only an evaluation of $T_h$.

In order to give such an evaluation of the gas temperature, we have to consider the following macroscopic energy balance: the energy supplied by the EM field is absorbed by electrons and transmitted to heavy particles. Let us assume that the volume in which the plasma is confined is large enough, so outwards radial fluxes can be neglected. If we moreover neglect excitation and radiative losses we can simply write that all the EM power is used to heat the volume in which the plasma is confined. This gives:

$$P = 5/2\ p\ (w - w_0)\ A$$

where P is the power, p - pressure, w - drift velocity of the plasma, $w_0$ - velocity of the cold gas below the coils, A - cross section of the heated volume. The power input is about 800 W. The radius we take must be large enough, e.g. 9 mm (the inner radius of the torch). It is known that the plasma cannot extend that far. Therefore the plasma volume is overestimated. It is needed in order to be able to neglect the radial losses by heat conduction. If the volume is large enough we can state that all the energy remains in this volume. The pressure is assumed to be atmospheric. Therefore:

$$w - w_0 = \frac{2\ P}{5\ p\ A} = \frac{2 \cdot 800}{5 \cdot 10^5 \cdot 2.5 \cdot 10^{-4}} \approx 11\ m/s$$

The velocity $w_0$ can be found from the flow (12 l/min) divided over the cross section (r = 9 mm). Thus $w_0$ = 0.85 m/s. The experimentally determined w is surprisingly close to this roughly estimated one. In order to relate w to $T_h$ we have to consider the steady state continuity equation for the bulk of gas: $\nabla \cdot (\rho\ \mathbf{w}) = 0$, where $\rho$ is the gas density. Therefore $\rho\ \mathbf{w} = p / kT_h\ \mathbf{w}$ = const. The drift velocity has practically only the axial component, which is about 12 m/s. Finally we can write:

$$\frac{w_0}{T_{h0}} = \frac{w}{T_h}$$

where index 0 refers to the cold gas. The velocity of the cold gas below the load coils is 0.85 m/s. The temperature of the cold gas is 300 K. Therefore the heavy particles temperature in the plasma can be estimated to be 4000 K. We should remember, however, that the temperature and velocity we have evaluated are averaged over the considered volume. Remembering, that the temperature is decreases substantially with radius at r = 6 - 9 mm from the center, we expect that in the skin $T_h$ is much higher. The real drift velocity close to the center is probably also higher.

### IV.3.2 Measurements of the drift velocity

Below we present two techniques of determination of the actual drift velocity of the plasma [FEY.91/2].

It has appeared that the power interruption experiment provides a good method to measure w. The responses of line emission to the power interruption have been described in § III. The delayed response has been mentioned. If the measurements of line emission are performed at different heights in the plasma it appears that the time of arrival of the delayed response is not constant. In Fig. IV.7a the time of arrival of the two maxima of the response is plotted as a function of the height above the load coil (z) (as shown in Fig. IV.7b). The dependence is linear: $t = a_0 + a_1 z$. The slope $a_1$ is related to the (constant) velocity with which the disturbance propagates. Knowing $a_0$ and velocity we can trace back a place in the plasma where the disturbance is created. Typically this place is about 2 - 5 mm below the load coils (the expansion zone). The origin and properties of this disturbance are discussed in detail in § VII. Here we only note that its propagation velocity is close to the drift velocity of the plasma, estimated before. In § VII it is made plausible, that such a disturbance is frozen in the gas flow, i.e. it propagates exactly with the drift velocity of the plasma.

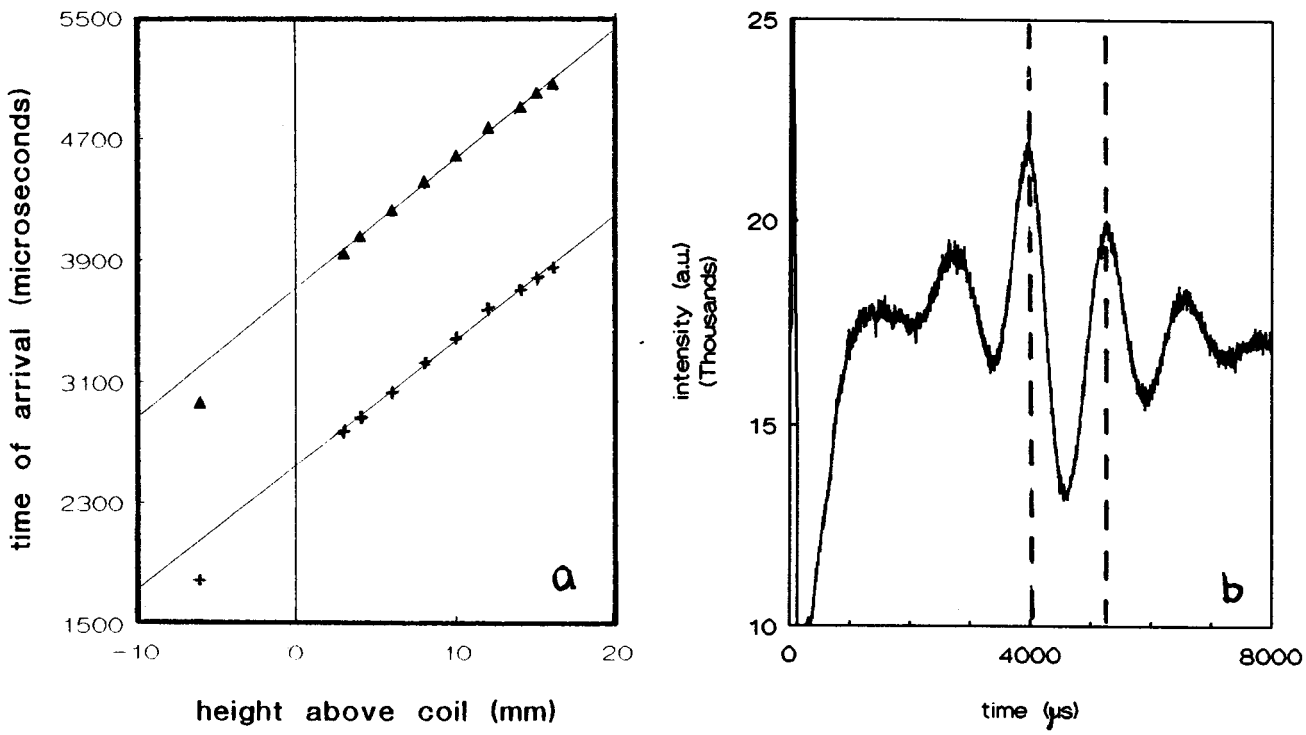


Fig. IV.7. Time of arrival of the delayed response as a function of the heigth above the coil is shown (a).

- ✚ first maximum,
- ♠ second maximum,

as indicated in (b).

If so, the power interruption experiment provides a very accurate method of determination of v. The value determined from Fig. IV.7 is:

$$w = 12.1 \pm 0.1 \text{ m/s}$$

The good accuracy of this method is due to good reproducibility in time of arrival of the disturbance.

It is necessary, however, to compare the above result with a value of v obtained using another method. Such an alternative technique is described in [FEY.91/2]. It is also based on disturbing the plasma and monitoring the responses of line intensities. In this case the disturbance is created by injection of small gas pulses. The introduced gas is hydrogen or neon. A typical response of an argon 6d line to the Ne injection is shown in Fig. IV.8. The decrease in intensity is due to arrival of neon, so the local density of a monitored Ar decreases. In Fig. IV.9 the H$\alpha$ emission line as a function of time after the injection of a hydrogen pulse is shown. The time of arrival is defined as the time for which the response is at half of its minimal (maximal) height. If the time of arrival is measured as a function of the height in the plasma the velocity with which it travels through the plasma can be found. The results are shown in Fig. IV.10. If the gas pulse is small enough, so it does not substantially cool all the plasma, its velocity is equal to the drift velocity of the plasma. As can be seen from Fig. IV.10, the data contain much more scatter than data obtained from the power interruption experiment. Therefore the precision of this method is worse. The resulting values of w are:

for Ne pulse: $w = 15 \pm 1$ m/s

for $H_2$ pulse: $w = 10 \pm 1$ m/s

The discrepancy in the two results, obtained using the same method, is probably not just accidental. A possible explanation of this difference can be the following: when the neon pulse is injected, temporarily an overpressure is created. The amount of supplied gas is larger than in the steady state. Therefore the injected gas will stay colder, until the heat conduction and diffusion smear it out. When the hydrogen is injected the same effect occurs. However, in this case the line intensity of the injected element is monitored. In order to be able to see the emission, the injected cold gas has to be heated and partially ionized. In § IV the time constant of ionization of argon is discussed. It is shown to be a rather slow and inefficient process, with time constant $10^{-2}$ - $10^{-3}$ s. It can be expected that the ionization rate for hydrogen is not much faster, especially as the temperature of the pulse is lower than the steady state ICP temperature. The ionization time constant is comparable with the time in which the pulse travels through the plasma ($10^{-3}$ s). This will influence the reaction of H$\alpha$ emission to the $H_2$ pulse. It can be expected that when the argon line emission is monitored, the results will be the same as these for Ne injection. Therefore in order to obtain representative results the same element (Ar) must be monitored for both Ne and $H_2$ pulses. Another fact supporting

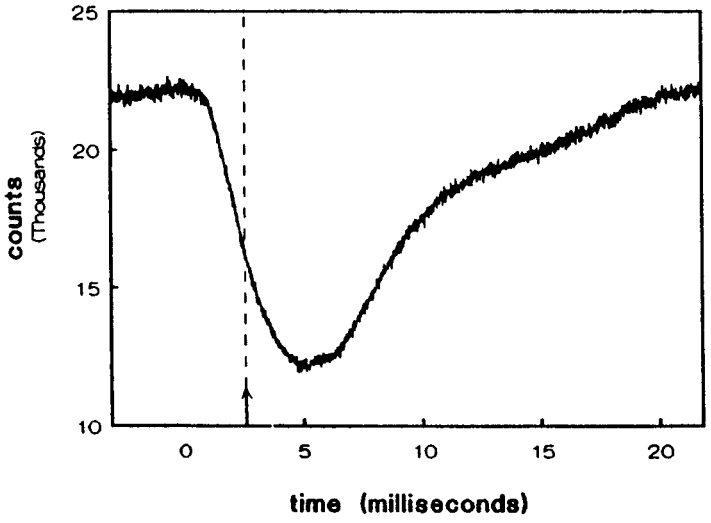


Fig. IV.8. A response of Ar 6d line to a Ne pulse injecti

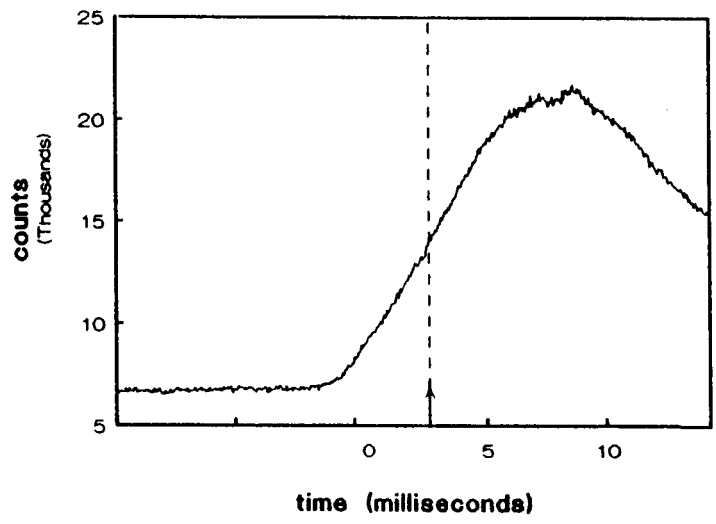


Fig. IV.9. A response of H$\alpha$ line to a $H_2$ pulse injection.

Fig. IV.10. Determination of velocity from the time of arrival of gas pulses:
- o Ne pulse: v = 15 ± 1 m/s
- Δ $H_2$ pulse: v = 10 ± 1 m/s

Time of arrival of the delayed response (+) is shown for comparison.

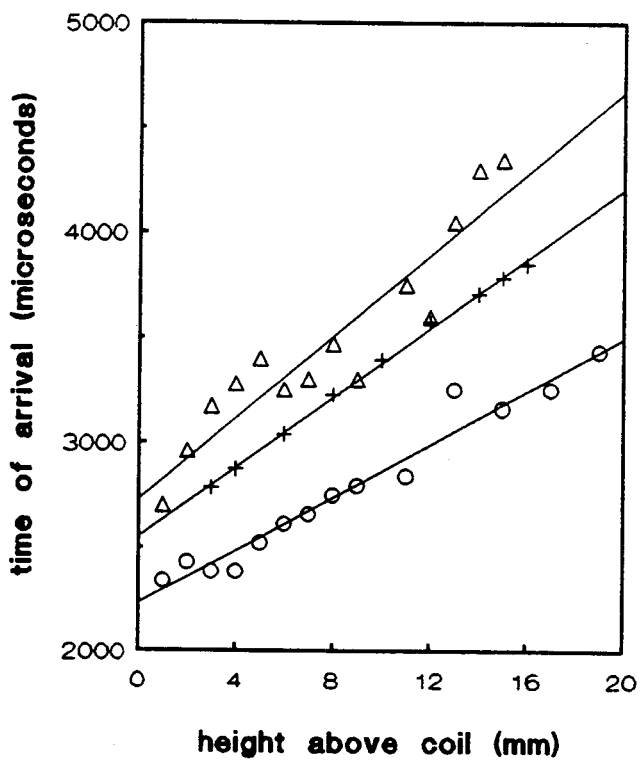

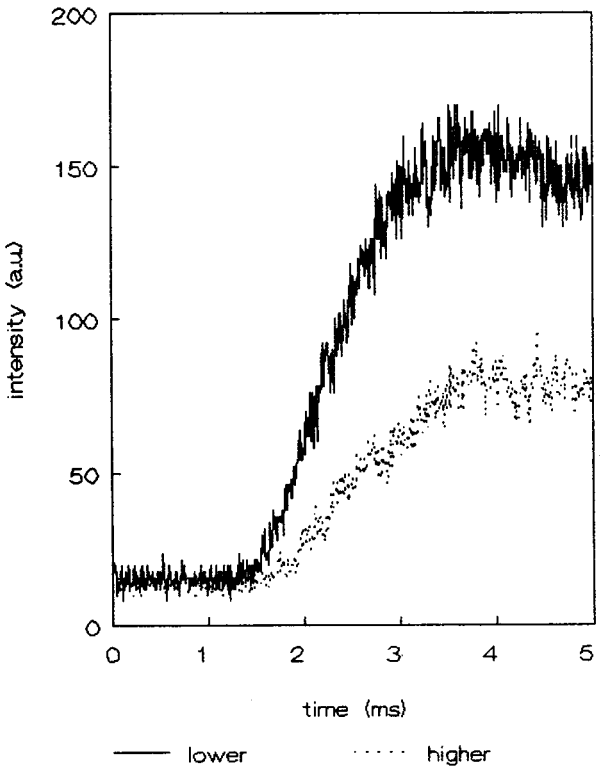


Fig. IV.11. Typical responses of Hα line to hydrogen pulses at two different heights in the plasma. Note that the maximum is reached at the same time.

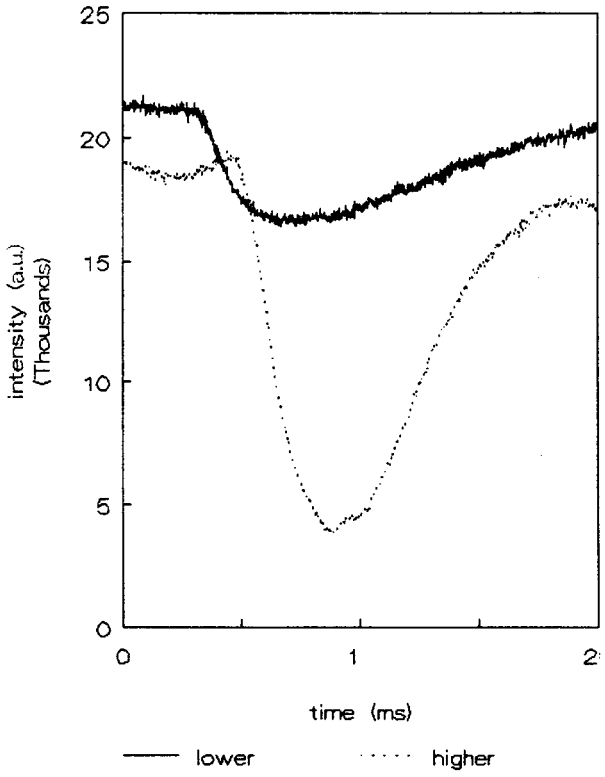


Fig. IV.12. Typical responses of Ar 6d line to neon pulses at two different heights in the plasma. As expected for a travelling phenomenon, the maxima are shifted in time for different heights.

the above considerations follows from Fig. IV.11. When the responses of Hα line emission to a $H_2$ pulse are compared for different observation heights in the plasma, we see that maxima have approximately the same time of arrival. In Fig. IV.12 we present analogous responses of Ar 6d to a Ne pulse. It can be immediately noted that the maxima are shifted in time and the risetime decreases with height in the plasma (as expected from diffusional smearing). This suggests that the risetime (and consequently the time of arrival) for $H_2$ pulses is probably limited by the excitation (ionization) rate of H and not by transport. One should also remember that dissociation of $H_2$ is a very fast process which consumes energy, so it can lower $T_h$ in the plasma. Therefore the results obtained for Ne injection should be more trusted, as the velocity they provide is probably closer to the real one.

The determined value of velocity is indeed in the order of 10 m/s, which is in a good agreement with the theoretical predictions based on a simple convective energy transport. It is recommended that more experiments be performed in order to improve the gas pulse technique.

# V. MICROSCOPIC CHARACTERIZATION OF THE ICP

## V.1 INTRODUCTION

The major part of this chapter contains a study of the dynamic processes following the power interruption. The disturbance of the energy chain, described in § III induces several processes, occurring with different time scales. The changes of plasma parameters in time supply a vast amount of information about the mechanisms of the occurring processes. Generally, two important phenomena are studied: the energy transfer from the EM field to electrons and heavy particles and the changes of electron density.

Further the influence of additives to the plasma (water and hydrogen) is shown. We discuss several possible processes induced by these additives. However, the experimental verification of these possibilities is not yet available.

## V.2 TIME CONSTANTS

In the power interruption experiment it is possible to distinguish between two major processes: the relaxation of temperature, caused by energy transfer and the relaxation of particles densities, caused by various production/destruction processes. Due to different time scales of these processes a clear distinction between them is given. Therefore it is possible to study them separately and to obtain information about their mechanisms, time constants, etc. A detailed analysis of the experimental data together with interpretation of these phenomena is given below.

When the plasma generator is switched off, the EM field disappears with a characteristic time constant $\tau_b = 3\times10^{-6}$ s. This has been found by monitoring the decay of the magnetic field induced in a pick up coil. However, the relaxation time of the emission intensities is larger. Taking as an example a typical Saha like response of an argon line we see that the maximum of intensity (when $T_e$ drops to $T_h$) is observed 8 - 10 $\mu$s after the switching off. In Fig. V.1 the time behavior at the cooling jump of several argon lines is shown. It can be seen immediately that the maximum of intensity is reached always at the same time, regardless of the ionization energy of the level. If the relaxation time of the emission was limited by the rate of transport within the atomic system, we would expect that for the levels lower in the system (like 4p) the maximum will appear later. Since there is no difference in the rise time between the highest and the lowest level, it can be concluded that the relaxation of the atomic system is much faster than the temperature changes. In fact the Saha equilibrium in the system is following the temperature changes, restoring itself in every moment. The estimated time scale for reestablishing of elementary balances is $\tau_s \simeq 10^{-9} - 10^{-8}$ s and the experiment does not contradict it. The rise time of the emission intensities is determined by

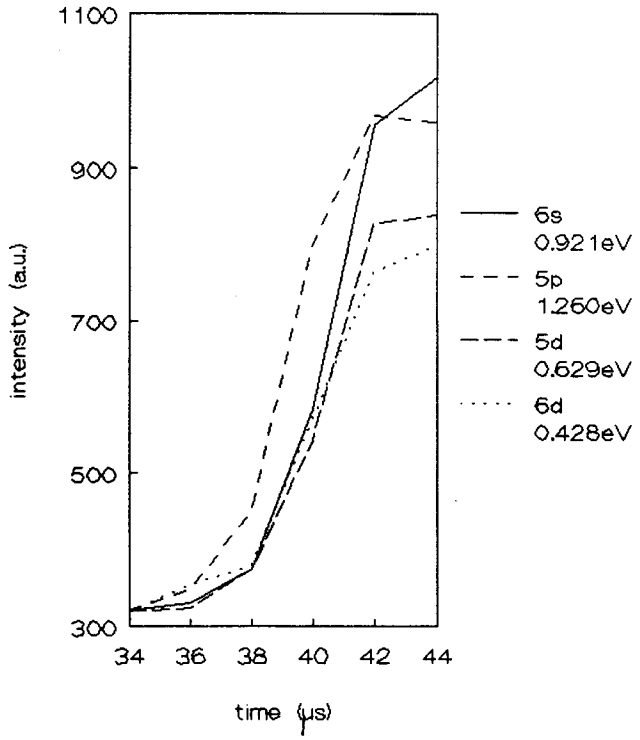


Fig. V.1. Time behavior of several argon lines at the cooling. The ionization energies of these **levels** are given. These jumps originate from Abel inverted scans, in normal conditions: dry plasma, flows: 12/0/0.7 l/min, power input: V = 3 kV, I = 0.4 A, 5 mm ALC. Here r = 6 mm.

the relaxation of temperature, with a characteristic time scale $\tau_e$, experimentally determined to be about $10^{-5}$ s.

The decay of emission intensity during the off-period occurs with another time scale (see § III). This time scale ($\tau_n$) is related to the destruction of radiating particles, which is the slowest of the mentioned processes. There is, however, another process, which can be even slower. This is the cooling of the heavy particles due to convection and heat conduction, with a time constant $\tau_h$. This process has been shown not to influence the instantaneous responses [FEY.91/1], provided the $T_h$ gradients are not too large. Therefore during the off-period $T_h$ decays significantly only in the places where large $T_h$ gradients are present (i.e. outside the plasma). Generally we may state that: $\tau_s < \tau_b < \tau_e < \tau_n < \tau_h$.

In the further considerations we shall concentrate on $\tau_e$ and $\tau_n$. We assume that the first two time constants are small enough, so they do not influence the other ones. We are aware that this assumption is not completely valid in case of $\tau_b$. However, the error introduced by this simplification anyway cannot be recognized within the low time resolution of the multichannel scaler. Moreover, $\tau_b$ is a purely electronic property of this very setup, so it is not important from the point of view of fundamental plasma processes.

## V.3. THE ENERGY TRANSFER

In this section we shall describe the energy balance for electrons. The properties of this balance will appear to have very important consequences. By introducing several simplifications we will be able to study the phenomena following switching the plasma generator off and on. Thus the time constant for energy transfer ($\tau_e$) will be determined and the relation between the electron temperature and density will be found.

The energy equation for electrons in the plasma heated by EM field is:

$$3/2\ \partial(n_e k T_e)/\partial t \ + \ 3/2\ \mathbf{w}\cdot\nabla\ (n_e k T_e) \ + \ 5/2\ n_e k T_e\ \nabla\cdot\mathbf{w} \ + \ \nabla\cdot\mathbf{q} \ =$$

(temporal change + convection + expansion + heat conduction)

$$\sigma_e\ E^2 - 3\ m_e/m_h\ (\nu_{ei} + \nu_{ea})\ n_e\ k\ (T_e - T_h) \quad \text{(local energy balance)}$$

$$- E_{ion}\ \dot{n}_e \quad \text{(energy changes due to ionization/recombination)}$$

$$- \Sigma_{ik}\ h\nu_{ik}\ A(i,k)\ \Theta(i,k)\ n_i \quad \text{(radiative losses)} \qquad \text{V.1}$$

where:

**w** drift velocity of the plasma,

$\sigma_e$ electric conductivity,

E electric field

$\dot{n}_e$ net $n_e$ change (due to ionization - recombination)

$\nu_{ei}$, $\nu_{ea}$ electron - ion and electron - atom collision frequency for momentum transfer

A(i,k), $\Theta$(i,k) -radiative transition probability and escape factor, respectively.radiative losses in the steady state ICP are only of little importance [FEY.91/2] and therefore they will be neglected.

In the above equation we can distinguish between the "fast" and "slow" terms. The "fast" one is the local energy balance and the "slow" one is ionization. If $n_e$ and $T_e$ gradients are small enough the transport phenomena are also slow. As the "fast" and "slow" processes equilibrate on different time scales, it is possible to separate them. Thus on a long time scale we shall demand that the energy balance be in equilibrium, while on a short time scale the "slow" processes have no influence. The separation between "slow" and "fast" processes allows to simplify (V.1), so its interpretation will be easier. This formalism is only useful in the active zone, where this separation can be made. When there is no energy input (e.g. high above the load coils) the "fast" terms vanish and $T_e = T_h$.

In the further considerations we shall limit ourselves to a simple case of nearly homogeneous plasma. It means that we assume the $T_e$, $n_e$, **w** gradients to be small enough, so the

flows caused by them are much slower than the processes contributing to the local energy balance. Generally one has to be very careful with the above assumption. As the gradients in the plasma are large, the application of this approximation is limited practically only to the region in the middle of the skin in the dry plasma (see § II, profiles). When water is added in the plasma the transport processes become extremely fast (see [STO.91/1,3]), so the above approximation is probably not valid anymore.

Thus we limit ourselves to the region in the middle of the skin (r = 4 - 6 mm from the center). There we can neglect the transport terms in (V.1), as being not important on a time scale of few microseconds. Therefore the temperature changes will be controlled only by the local energy balance:

$$\partial(n_e k T_e)/\partial t = 2/3\ \sigma_e\ E^2 - 2\ m_e/m_h\ (\nu_{ei} + \nu_{ea})\ n_e\ k\ (T_e - T_h) \qquad \text{V.2}$$

where the energy gained by electrons from the EM field is transferred to heavy particles in elastic collisions. The inelastic losses are in the order of the net ionization flow, so they are of no importance.

Before using (V.2) we have to comment it. The two terms on the right hand side of (V.2) will be discussed below.

The second term on the right hand side of (V.2) describes the energy loss of electrons in collisions with heavy particles (ions and atoms). The number of collisions per unit time (collision frequency) is a function of electron temperature and density.

A well known formula for collision frequency gives:

$$\nu_{ei,a} = n_{i,a} \langle \sigma_{ei,a}\ v_e \rangle \qquad \text{V.3}$$

where n is the density of particles with which the electrons collide (ions or atoms, respectively), $\sigma$ is the cross section (velocity dependent) and $v_e$ the velocity of an electron. The factor $\langle \sigma v \rangle$ (called also rate coefficient) in the above formula is obtained by integrating $\sigma$ over the velocity distribution of the free electrons. This might bring an error into our considerations. In the formulas used below the rate coefficient is calculated assuming the Maxwellian electron velocity (energy) distribution:

$$f(\epsilon) = 2\pi^{-1/2}\ (kT_e)^{-3/2}\ \epsilon^{1/2}\ \exp(-\epsilon/kT_e) \qquad \text{V.4}$$

It can be shown, that the Electron Energy Distribution Function (EEDF) in the ICP is not Maxwellian (see [STO.91/3]). The high energy tail of the distribution is influenced by net ionization of argon. The most energy consuming step of this process is excitation from 3p (ground state) to 4s. This takes about 10 eV. As the Maxwellization of the EEDF is not as fast as the excitation [MUL.86] to 4s, the high energy tail will be deformed. Namely, the fraction of high energy electrons will be smaller than

predicted by Maxwellian distribution. Therefore we have to evaluate the error introduced by using the Maxwellian distribution. In the formula (V.3) it is important, how fast the cross sections grow with electron energy. If they increase significantly, the contribution from the high energy tail in (V.3) might be large, despite the fast decay of this tail. The cross section for electron - ion collisions decreases with energy according to:

$$\sigma_{ei} = \frac{q^4 \ln \Lambda_c}{16 \pi \epsilon_0{}^2 \epsilon^2}$$

where $\ln \Lambda_c$ is the Coulomb logarithm (it is weakly $n_e$ and $T_e$ dependent. In the ICP $\ln \Lambda_c \approx 6$). Thus for $\epsilon \simeq 10$ eV $\sigma_{ei}$ is about 100 times smaller than for $\epsilon \simeq 3/2\ kT_e$. The cross section for electron - atom collisions does not have such a simple analytical form. It can be found in [MIT.73]. It follows from there, that for $\epsilon \simeq 10$ eV this cross section is about 100 times higher than for $\epsilon \simeq 3/2\ kT_e$. Since for low energies the electron - ion collisions are anyway dominant, we can conclude that the total collision frequency will not increase significantly. Finally, we may state that the relative error we commit in (V.3) using (V.4) will be in the order of the fraction of electrons in the high energy tail. This error is negligible.

Hereafter we shall use the integrated form of (V.3). The electron - ion collision frequency for momentum exchange is given by the formula:

$$\nu_{ei} = 8/3 \quad (\pi/2)^{1/2} \quad (e^2/4\pi\epsilon_0 m_e)^2 \quad (m_e/kT_e)^{3/2} \quad n_+ \quad \ln \quad \Lambda_c, \quad [s^{-1}] \qquad \text{V.5}$$

where $kT_e$ is in J, $n_+ = n_e$ in $m^{-3}$. These collisions, due to their Coulomb nature have the largest cross section. Therefore if the electron density is high enough they will be dominant. For the typical electron densities in the ICP they are still dominant, nevertheless the electron - atom collisions must be also taken into account, especially at higher temperatures. The electron - atom collision frequency given here is based on the calculation of [BEN.90] and in the range 0.5 - 1.5 eV can be approximated by:

$$\nu_{ea} = (1.2359 \ln T_e - 9.1473) \times 10^{10} \ [s^{-1}] \qquad \text{V.6}$$

These frequencies are related to the time constants of momentum transfer from electrons to heavy particles. The change of temperature is caused by the energy transfer. This is much less effective due to small mass of the electron. Therefore the frequencies will be multiplied by a small factor $2m_e/m_h$. For argon $m_h = 40\ m_p$ (mass of proton).

Other unknown quantities in (V.2) are the conductivity $\sigma_e$ and the electric field E. Their dependencies on $n_e$ and $T_e$ should be found. The conductivity $\sigma_e$ is the following function of $n_e$ and $T_e$:

$$\sigma_e = \frac{n_e e^2}{m_e(\nu_{ei} + \nu_{ea})} \qquad V.7$$

It is very weakly $n_e$ independent, since the dominant term in the denominator, $\nu_{ei}$ is proportional to $n_e$. The E field decays with the distance from the edge of the plasma (x) according to:

$$\partial E/\partial x = -\delta(x)^{-1} E \qquad V.8$$

where $\delta$ is the skin depth. The dependence of $\delta$ on plasma parameters is given by:

$$\delta = (1/2\,\mu_0\,\omega\,\sigma_e)^{-1/2} \qquad V.9$$

A typical value of the skin depth is 2 - 3 mm. It decreases with temperature (via $\sigma_e$ dependence) and it hardly depends on electron density.

The proper solution of (V.8) is an integral: $E = E_0 \exp(-\int \delta^{-1}(x)\,dx)$. However, since $\delta$ is $T_e$ dependent, one would have to introduce the electron temperature profile in (V.8). As this is hardly known, it is better to use the following approximation: $T_e(x) = T_{e0}\,\Theta(x)$, where $\Theta$ is the step function (Heaviside function), $x = 0$ is the edge of the plasma. We assume the plasma boundary to be 7 mm away from the center. $T_{e0}$ is the temperature in the middle of the skin (we use all this formalism only for the region in the middle of the skin). We are aware, that this simplification is very drastic, but if we introduce some arbitrary $T_e$ profile the result will be much more complicated, while we will not gain significantly more accuracy. Therefore we can write:

$$E = E_0 \exp(-x/\delta) \qquad V.10$$

i.e. the field decays exponentially with the distance from the edge of the plasma.

Having information about all the terms in (V.2) we can concentrate on special cases, when (V.2) can be used.

### V.3.1 The kinetics of the cooling jump

The determination of $\tau_e$, the time scale of changes of the electron temperature has created some confusion in the past. The estimated value was always smaller than the experimental one. Here we shall first discuss a well known method of estimating $\tau_e$, which is based on the reasoning described below.

In the steady state the electrons {e} transfer their energy to the heavy particles {h} with the same rate P with which they receive energy from the EM field. At the moment the field is switched off they will keep transferring their energy with the rate P until their energy surplus ($\Delta E$) is gone.

The time constant of this process can be evaluated by :

$$\tau_e = \Delta E / P \qquad \text{V.11}$$

Taking the following expression for the energy surplus: $\Delta E = 3/2\ n_e\ k\ (T_e - T_h)\ V$, where V is the volume in which the energy is incoupled, we can rewrite (V.11) as:

$$\tau_e = 3/2\ n_e\ k\ (T_e - T_h)\ V / P \qquad \text{V.12}$$

The upper estimation of (V.12) is $\tau_e \lesssim 1\ \mu s$, which is in any case too small. However, this method is supposed to give only an estimation of the order of magnitude, so we should be aware of its inaccuracy. There are many uncertainties in (V.12). The systematically too low value of $\tau_e$ might imply that the volume V is much larger than we think. The power input is also dependent on the amount of electrons in the plasma. Moreover, it is also possible that a significant part of the power P is scattered instead of being coupled to the electrons.

Therefore the determination of local values of $\tau_e$ needs another approach, in which only the local elementary plasma processes are involved. When the field disappears, the main (fastest) process cooling the electrons are collisions. Therefore we may use the equation (V.2), where the "fast" processes are separated from the "slow" ones. In the absence of the field the problem reduces to solving a simple differential equation:

$$\partial T_e/\partial t = -\ 2\ m_e/m_h\ (\nu_{ei} + \nu_{ea})\ (T_e - T_h) \qquad \text{V.13}$$

Having this equation we can immediately estimate a characteristic frequency of $T_e$ decay to be $2m_e/m_h(\nu_{ei} + \nu_{ea}) \simeq 10^5 - 10^6\ s^{-1}$. The actual time decay of $T_e$ has to be obtained by integrating (13). The solutions for several possible electron densities are plotted in Fig. V.2. It can be seen that typically the temperature drops in 3 - 5 $\mu$s, which together with the decay time of the field (3 $\mu$s) is close to the experimental result (though still too fast). Moreover it can be seen that if the electron density is larger, the decay is faster (time constant is smaller). This is quite logical, because when the electron density is high, the ion density is also high. Therefore the collisional energy losses with ions are faster. The formula (V.12) gives a contradictory dependence on $n_e$: the process seems to be slower for large $n_e$. Therefore it cannot represent a correct time constant.

The Fig. V.3 shows a simulated time behavior of an argon 6s - 4p line ($\lambda$ = 703 nm) for several electron densities. The Saha value for the density of 6s is assumed. The equation (V.13) provides some additional information about the rise time of the temperature (emission intensity). As shown before, the temperature changes are faster for high electron density. This in principle can be verified experimentally (though the time resolution of the MCS is not high enough for this purpose).

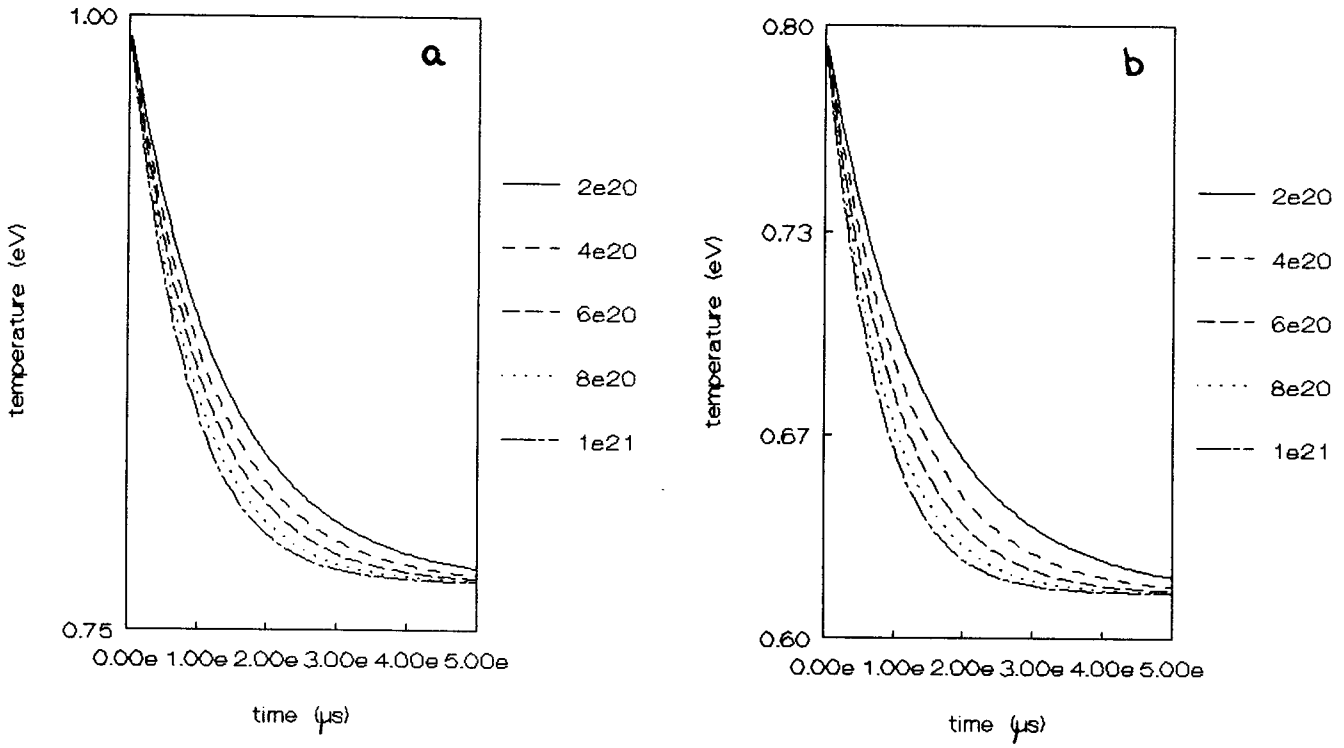


Fig. V.2. The simulation of time behavior of temperature at the cooling for several electron densities. The steady state conditions are assumed to be:
a) $\gamma$ = 1.3, $T_e$ = 1 eV, $T_h$ = 0.77 eV
b) $\gamma$ = 1.3, $T_e$ = 0.8 eV, $T_h$ = 0.615 eV.

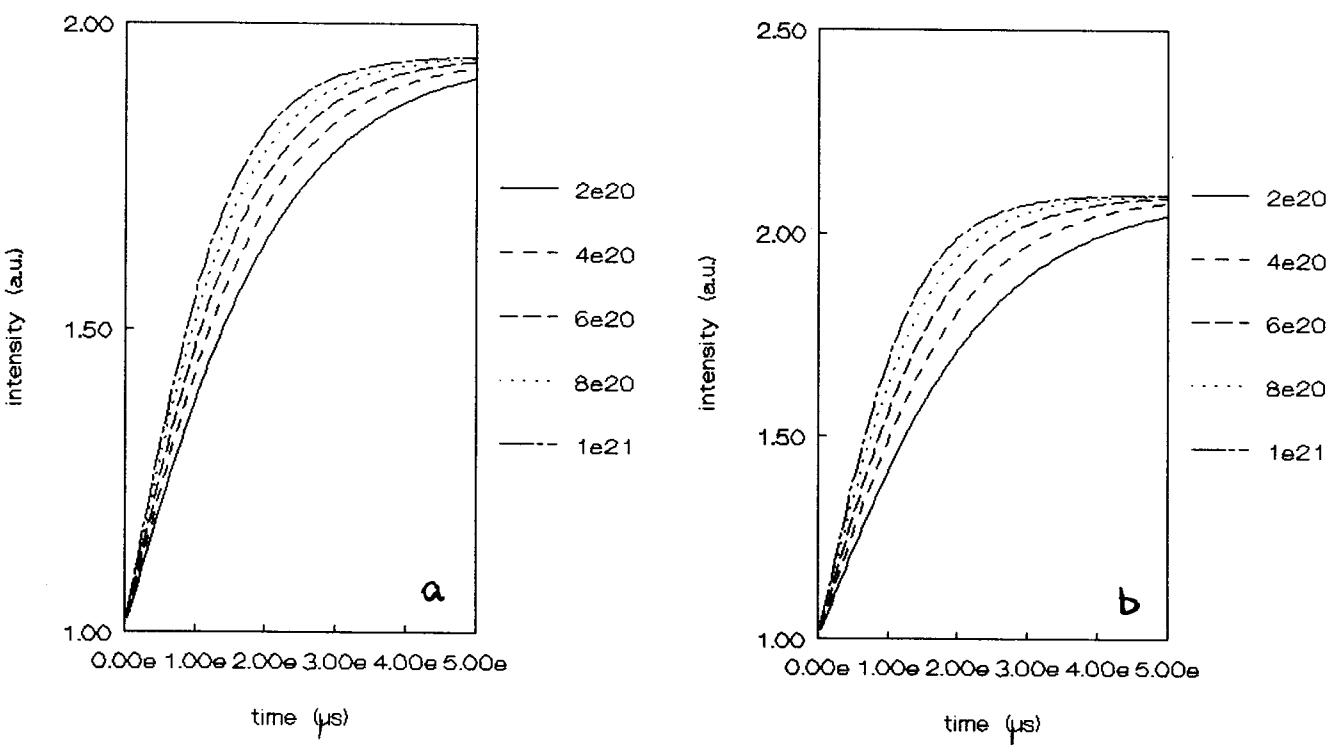


Fig. V.3. The simulation of time behavior of emission intensities (according to Saha) at the cooling for several electron densities. The steady state conditions are assumed to be:
a) $\gamma$ = 1.3, $T_e$ = 1 eV, $T_h$ = 0.77 eV
b) $\gamma$ = 1.3, $T_e$ = 0.8 eV, $T_h$ = 0.615 eV.

Fig. V.4. Experimental time behavior of Ar 6s line at different places in the plasma. The maximum is achieved at the same time, but the temperature changes are smaller at r = 3 mm than at r = 6 mm.

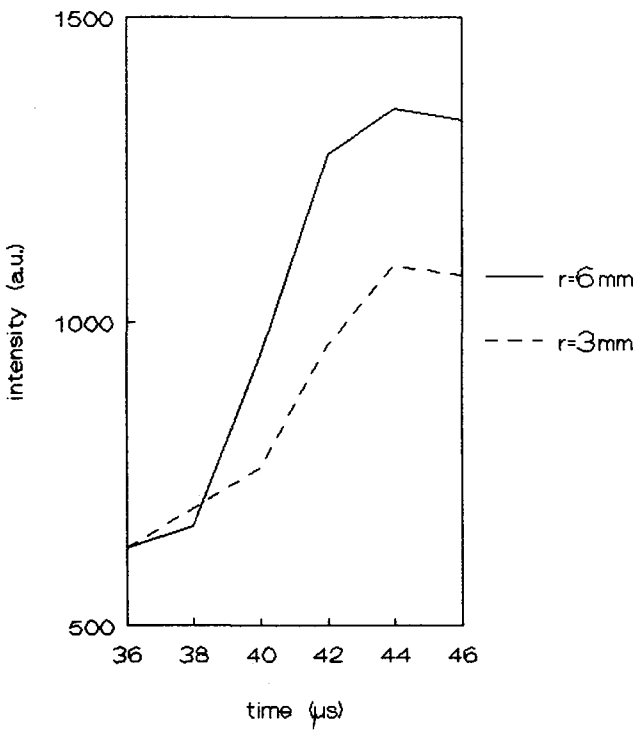


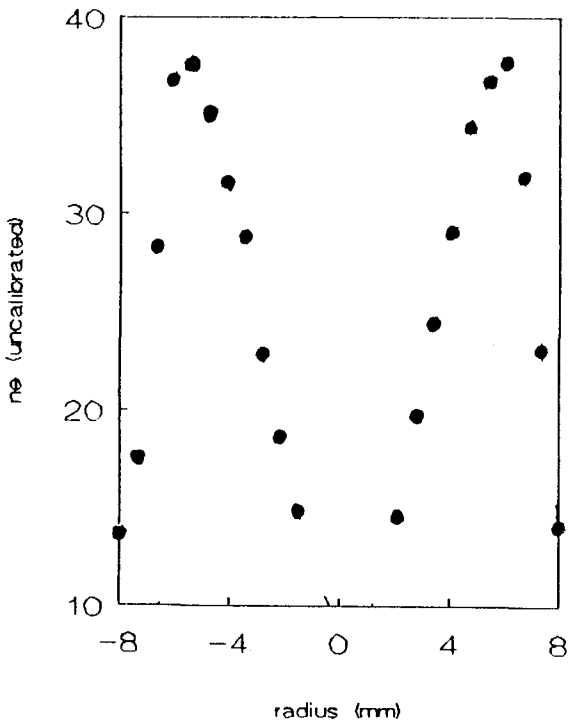


Fig. V.5. A relative electron density profile. From this it follows that $n_e$ at r = 6 mm is higher than at r = 3 mm.

It is very well known that in the middle of the plasma and far outside the electron density is lower than in the skin. We can compare the rise times for Abel inverted cooling jumps of 6s - 4p line. We cannot move very far to the middle, as the emission intensities and cooling jumps become too small. We also cannot consider the data from outside the skin. The approximation of the homogeneous plasma (V.2) is not valid there, as the transport terms in (V.1) cannot be neglected anymore. Therefore we can only compare rise times at r = 3 and r = 6 mm from the center (Fig. V.4). A radial profile of electron density is shown in Fig. V.5 (the absolute value of $n_e$ is not shown). From this it follows that $n_e$ is higher at r = 6 mm than at r = 3 mm. The steady state temperatures in these places are different, but the final temperature ($T_h$) can be assumed to be the same ($T_h$ profile in the region r = 3 - 6 mm can be assumed to be flat). We see that the maximum is reached approximately at the same time. On the other hand the initial temperatures were not the same: $T_e$ was higher at r = 6 mm. Therefore it can be concluded that the cooling process is faster at r = 6 mm. This effect, however, should be studied more carefully when a better time resolution is available.

### V.3.2 The relation between electron temperature and density

Another interesting consequence of the separation between "fast" and "slow" terms in (V.1) is the relation between electron density and temperature. This will help to understand the processes occurring immediately after the off-period, when the plasma generator is switched on again. It has been already said in § III (Power Interruption) that $T_e$ at the heating jump is higher than in the steady state. Here we shall give an explanation based on the fact that the local energy balance equilibrates on a short time scale.

The electron density has decreased during the off-time, so the conditions are different from those in the steady state. It is expected that the fastest process (energy incoupling) will push the plasma towards a new quasi steady state. In Fig. V.6 a typical response of a "Boltzmann like" line for several off-periods is shown. It is known that intensity of such a line is only electron temperature dependent (see [STO.91/3]) and increases with increasing $T_e$. It can be seen that the temperature the plasma reaches at the heating jump increases with increasing off-period. The time constant is characteristic for the energy incoupling processes described above. Once $T_e$ has reached the maximum it decreases slowly with a time constant characteristic for $n_e$ changes. This maximum is the new quasi steady state, for which the following is demanded:

$$\partial T_e/\partial t \simeq 0 \qquad \text{V.14}$$

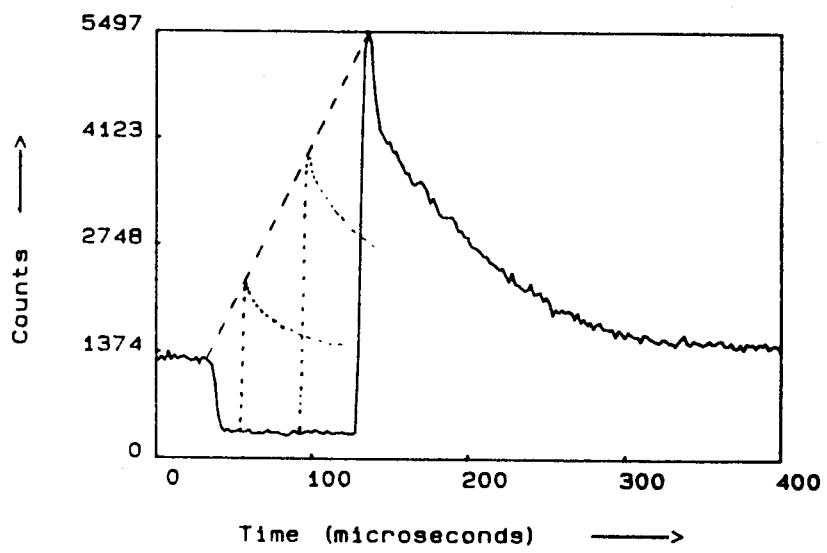


Fig. V.6. The responses of a Mg II line for several off-times. As the emission intensity of Mg increases with increasing $T_e$, it can be concluded that $T_e$ after the heating increases with increasing off-time.

which means that $T_e^{-1}\partial T_e/\partial t$ can be in the order of $\tau_n^{-1}$. This of course does not mean that $\partial n_e/\partial t$ is zero, but the changes in electron density are relatively slow. Therefore the temperature will always have the value imposed by the current $n_e$. The condition for the "steady state" follows from (V.2):

$$\partial(n_e k T_e)/\partial t \simeq n_e\, \partial k T_e/\partial t \simeq$$

$$2/3\ \sigma_e E^2 - 2\ m_e/m_h\ (\nu_{ei} + \nu_{ea})\ n_e k(T_e - T_h) =$$
$$2/3\ \sigma_e E^2 - 2\ m_e/m_h\ (\nu_{ei} + \nu_{ea})\ n_e k T_e(1 - 1/\gamma) \simeq 0 \qquad \text{V.15}$$

Incorporating the expressions for $\sigma_e$, E and $\nu$ in (V.15) allows in principle to determine the electron temperature for a given electron density and $\gamma$. However, some constants in (V.15), like the electric field produced by the generator ($E_0$), are not very well known. Therefore it is safer to calculate only the relative solutions of (V.15), i.e. normalized over the steady state conditions. Indeed, in the undisturbed plasma:

$$2/3\ \sigma_e^s E^{s2} - 2\ m_e/m_h\ (\nu_{ei}^s + \nu_{ea}^s)\ n_e^s\ k\ (T_e^s - T_h) \simeq 0, \qquad \text{V.16}$$

where index s refers to the parameters in the steady state. Dividing (V.15) by (V.16) we obtain:

$$\sigma_e/\sigma_e^s\ (E/E^s)^2 \simeq (\nu_{ei} + \nu_{ea})/(\nu_{ei}^s + \nu_{ea}^s)\ n_e/n_e^s\ (T_e - T_h)/(T_e^s - T_h) \qquad \text{V.17}$$

in which most of the constants drop out.

In order to solve (V.17) a steady state solution has to be assumed. The power interruption technique does not allow to determine $T_e$ and $T_h$ accurately enough. Their ratio ($\gamma$), however, is quite well known (see § IV). Therefore we shall assume several possible steady state $T_e$ and $\gamma \approx 1.3$. The electron density is also not well known, so several possible values have to be assumed. E field depends on the radial position in the plasma (V.10). We will fix this position to be 2 mm away from the edge of the plasma (x = 2 mm). It corresponds to r = 5 mm from the center. In this place there are some experimental data available. In the simulations the radius of the plasma is taken to be 7 mm.

Let us define the function:

$$F(T_e) = \sigma_e/\sigma_e^s\ (E/E^s)^2 - (\nu_{ei} + \nu_{ea})/(\nu_{ei}^s + \nu_{ea}^s)\ n_e/n_e^s\ (T_e - T_h)/(T_e^s - T_h) \qquad \text{V.18}$$

The first thing one should check are the properties of the assumed steady state solution. The values $T_e = T_e^s$, $n_e = n_e^s$ satisfy the equation (V.17) trivially. However, it is also interesting to know the

behavior of $F(T_e)$ around the fixed point. In Fig. V.7 $F(T_e)$ is plotted for the following steady state conditions:

$$T_e^s = 0.7 \text{ eV}, \quad T_h^s = 0.54 \text{ eV}, \quad n_e^s = 1\times 10^{21} \text{ m}^{-3}$$

The crossing point of $F(T_e)$ with the zero axis corresponds with $T_e^s = 0.7$ eV. However, we see that there is one more solution for $T_e = 0.735$ eV. In order to eliminate it we have to note that $F(T_e) \sim \partial T_e/\partial t$. What is very important for a physically reasonable solution is its stability. The solution of (V.16) must be stable, else it cannot describe the steady state. In order to investigate the stability we have to perturb a solution $F(T_e^s) = 0$ by putting: $T_e = T_e^s + \Delta T_e$. This gives:

$$\partial \Delta T_e/\partial t \sim \partial F/\partial T_e \, \Delta T_e, \qquad \text{V.19}$$

so the condition for stability is:

$$\partial F/\partial T_e < 0 \qquad \text{V.20}$$

In Fig. V.7 the "assumed" steady state solution ($T_e^s = 0.7$ eV) for $n_e = 10^{21}$ m$^{-3}$ is stable, while the other one ($T_e = 0.735$ eV) is unstable and therefore it need not be taken into account. However,

Fig. V.7. The simulation of the rate of $T_e$ changes (relative) as a function of $T_e$. The assumed steady state conditions are: $n_e^s = 10^{21}$ m$^{-3}$, $\gamma^s = 1.3$, $T_e^s = 0.7$ eV. The fixed point corresponding to $T_e = 0.7$ eV is still stable ($dT_e/dt < 0$), but it is very close to an unstable region.

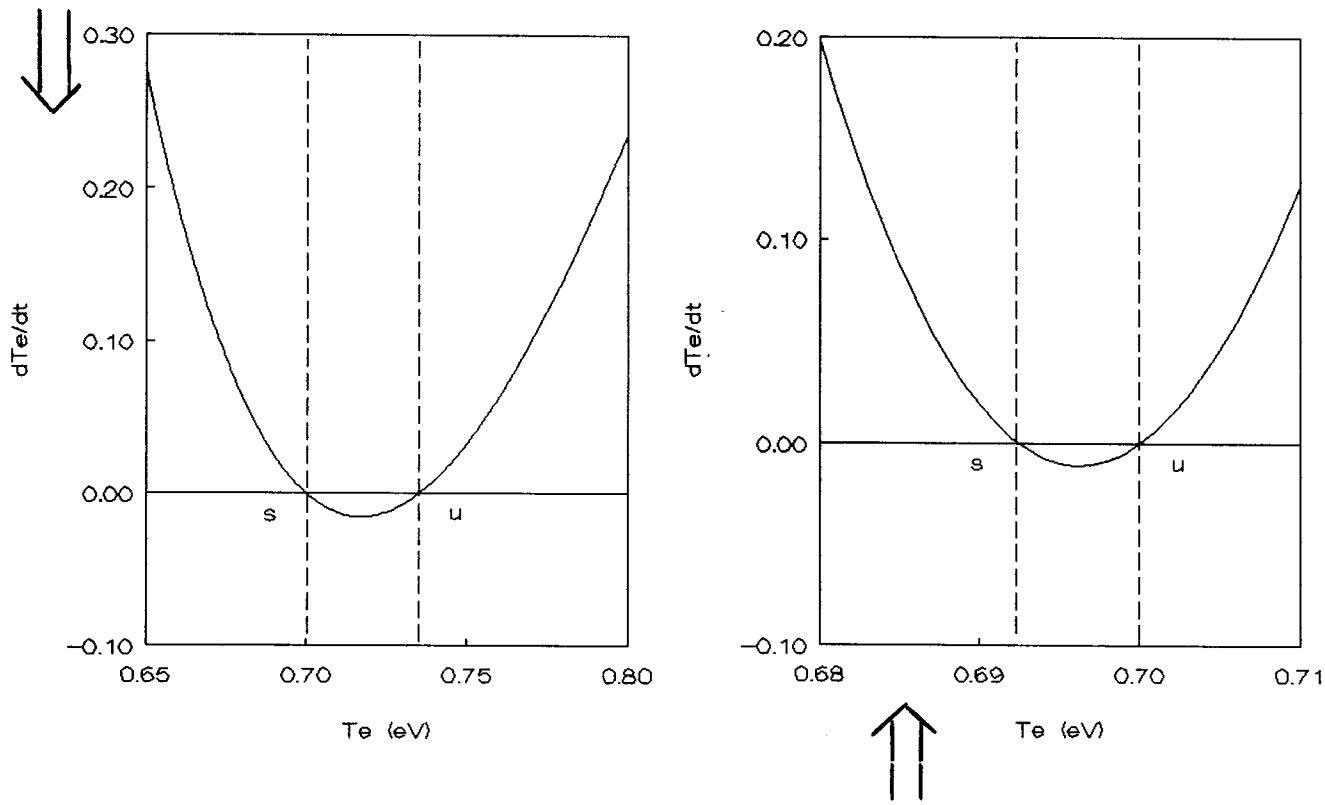


Fig. V.8. The simulation of the rate of $T_e$ changes (relative) as a function of $T_e$. The assumed steady state conditions are: $n_e^s = 1.5\times 10^{21}$ m$^{-3}$, $\gamma^s = 1.3$, $T_e^s = 0.7$ eV. The fixed point corresponding to $T_e = 0.7$ eV is unstable ($dT_e/dt > 0$). The other fixed point corresponds to a lower $\gamma$.

when we consider only slightly different steady state conditions like $T_e^s$ = 0.7 eV, $T_h^s$ = 0.54 eV, $n_e^s$ = $1.5\times10^{21}$ $m^{-3}$ (Fig. V.8) the "assumed" solution becomes unstable while the other one is stable. The same effect can be obtained by lowering the "assumed" temperature. We can see it very well in Fig. V.9, where $F(T_e)$ is plotted for:

$$T_e^s = 0.52 \text{ eV}, \quad T_h^s = 0.4 \text{ eV}, \quad n_e^s = 10^{21} \text{ m}^{-3}$$

The stable steady state solution in Fig. V.9 corresponds to $T_e$ lower than 0.52 eV. This would mean that $\gamma$ is substantially lower. However, we do not take it into account, as it cannot be in agreement with the results of the power interruption experiment.

The physical interpretation of the mathematical analysis presented above is the following: in the steady state we want the energy input (first term in (V.16)) to be large enough in comparison with losses (second term in (V.16)). The losses are $n_e$ dependent, while the gain term is practically $n_e$ independent. This gives us some limitation for the electron temperature and density. At low $T_e$ the energy incoupling is inefficient, due to low $\sigma_e$. The dependence of $\sigma_e$ on $T_e$ is stronger than this of the collisional term. Therefore if $T_e^s$ is low, for small deviations from $T_e^s$ the energy incoupling will not be able to catch up with the collisional losses, especially for high electron densities. This is why the assumed solution will be unstable. In this case the system will choose a lower $\gamma$, which will make the collisional term less dominant. This is what we see in Fig. V.8 and Fig. V.9.

Fig. V.9. The simulation of the rate of $T_e$ changes (relative) as a function of $T_e$. The assumed steady state conditions are like in Fig. V.7-8, only $T_e^s$ is lower (0.52 eV). The fixed point corresponding to $T_e$ = 0.52 eV is unstable ($dT_e/dt > 0$). The other fixed point corresponds to a lower $\gamma$.

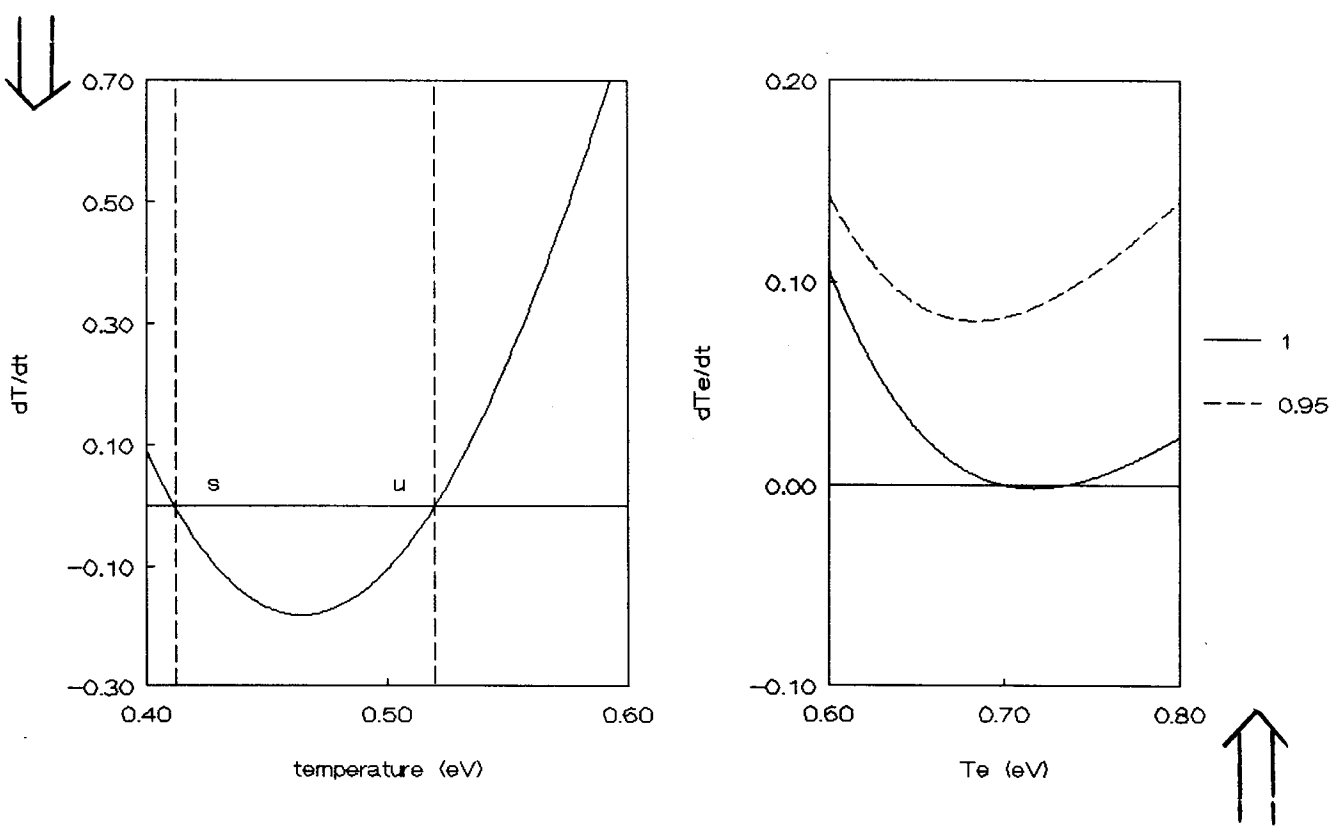


Fig. V.10. The simulation of the rate of $T_e$ changes. Steady state conditions as in Fig. V.7. Dashed line corresponds to $n_e/n_e^s$ = 0.95. We see that there is no fixed point for $n_e < n_e^s$.

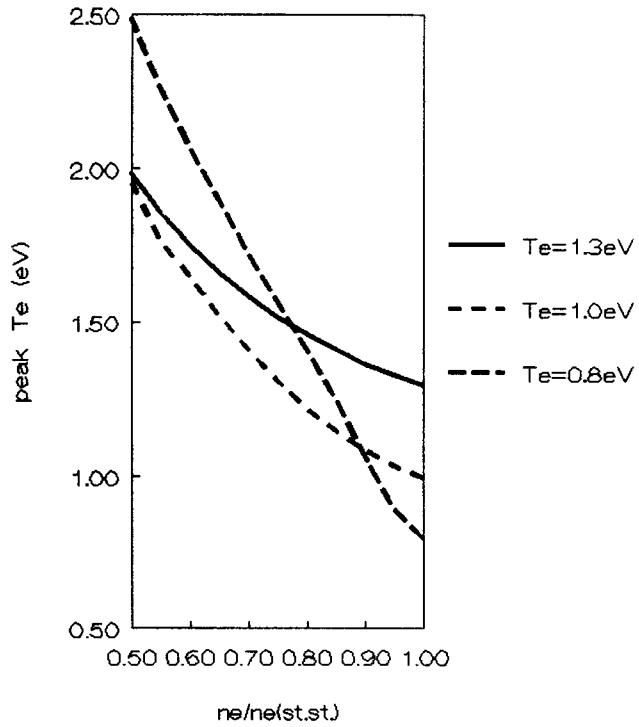


Fig. V.11. The stable peak electron temperature (after the heating) as a function of electron density at the end of the off-period (divided by the steady state $n_e$). Simulated for several assumed steady state conditions. Electron density $n_e^s$ is always $10^{21}$ $m^{-3}$, $\gamma^s$ = 1.3.

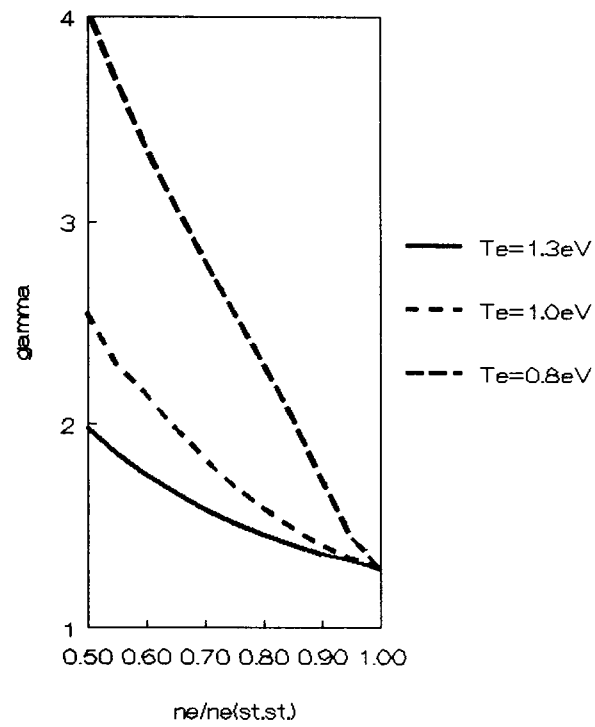


Fig. V.12. The $T_e^p/T_h$ ratio ($\gamma^p$) at the heating. Simulated for the same conditions as in Fig. V.11.

All this reasoning leads to the conclusion, that for our $\gamma$ (determined experimentally as described in § IV) and $n_e$ (which should not be lower than this determined from H$\beta$ broadening [NOW.88]) $T_e^s$ cannot be too low. The stability of the steady state solution imposes a lower limit on them. This limit will depend on the actual value of electron density, place in the plasma, etc. However, the existence of such a limit is not dependent on the assumption of a "nearly homogeneous" plasma. We have to remember that the equation (V.2), which is the basis of the above considerations, contains only one loss term (collisional). In fact, there are more loss terms, which have been neglected (see (V.1)), while there is only one gain term. Above we have shown, that at low $T_e^s$ the collisional losses are already so large, that they dominate the gain term. In a real case it will not be better.

Finally, having well chosen steady state conditions we can determine the peak electron temperature ($T_e^p$), which is reached after the plasma generator is switched on. In order to obtain $T_e^p$ we have to solve (V.17), introducing $n_e/n_e^s < 1$.

If we plot $F(T_e)$ for the same conditions as in Fig. V.7 and decrease the electron density by 5% ($n_e/n_e^s = 0.95$) there is no solution at all (Fig. V.10). This is due to the fact that $T_e^s$ is close to the value below which it becomes unstable. It implies that a solution for the peak $T_e^p > T_e^s$ does not exist. This does not describe the physical situation, as we do observe a stable $T_e^p > T_e^s$. Therefore there is another limitation in choosing the steady state parameters. We shall define the stability limit the following way: the steady state $T_e^s$ is stable if the point $T_e^s$ is stable according to (V.20) and if the solution for $T_e^p$ exists for $n_e/n_e^s = 0.5$. This stability limit is of course electron density dependent. From Fig. V.7, 8 we have seen that if $n_e^s$ is low, the value of $T_e^s$ required for stability need not be so high. In the further considerations we shall fix $n_e^s = 10^{21}$ m$^{-3}$. This should give a lower estimation for $T_e^s$. The real $n_e^s$ in the skin is probably higher than $10^{21}$ m$^{-3}$, so the stable steady state temperature must be even higher.

In Fig. V.11 the dependencies of stable $T_e^p$ on electron density are plotted for various steady state conditions (with constant $\gamma = 1.3$). We see that $T_e^p$ increases strongly with decreasing "assumed" $T_e^s$. When the stability limit (at $T_e^s = 0.8$ eV) is approached $T_e^p \to \infty$ for $n_e/n_e^s \to 0$. Fig. V.12 shows a dependence of the peak $\gamma^p$ ($= T_e^p/T_h$) on electron density. This plot is more useful from the point of view of comparison with experimental data. The experimental data are shown in Fig. V.13. The ratio of the peak electron temperature to the heavy particle temperature when the plasma generator is switched on can be determined the same way as the steady state $\gamma$ (see § IV). In Fig. V.13 the heating jump is plotted as a function of the ionization energy for several levels. The data for heating jump contain much more scatter than those for cooling jump. Nevertheless, the value of $\gamma^p$ can be determined to be about 1.7. The experimental $T_e^p = 1.3$ eV. The ratio of electron density after the off-period to the steady state $n_e^s$ can be found from the emission intensities, as shown in Fig. V.14. The ratio $n_e/n_e^s = 0.8$. If we compare this point with the calculated $n_e$ - $\gamma$ relation (Fig. V.12) we see that the best agreement is obtained for steady state conditions: $T_e^s = 1.0$ eV, $T_h = 0.77$ eV, $n_e^s = 10^{21}$ m$^{-3}$.

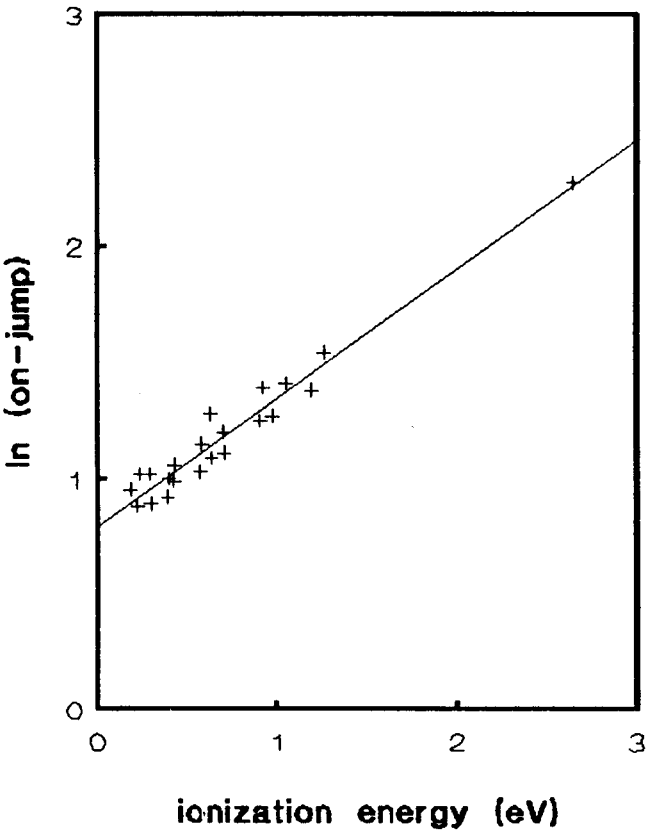


Fig. V.13. The experimental data on the heating jump. The logarithm of the heating jump is plotted as a function of ionization energy for several Ar lines. The conditions are: flows: 12/0/0.7 l/min with water injection, power input: V = 3 kV, I = 0.4 A, 5 mm ALC, r = 4 mm. The $\gamma$ at the heating jump is 1.69, $T_e$ = 1.26 eV

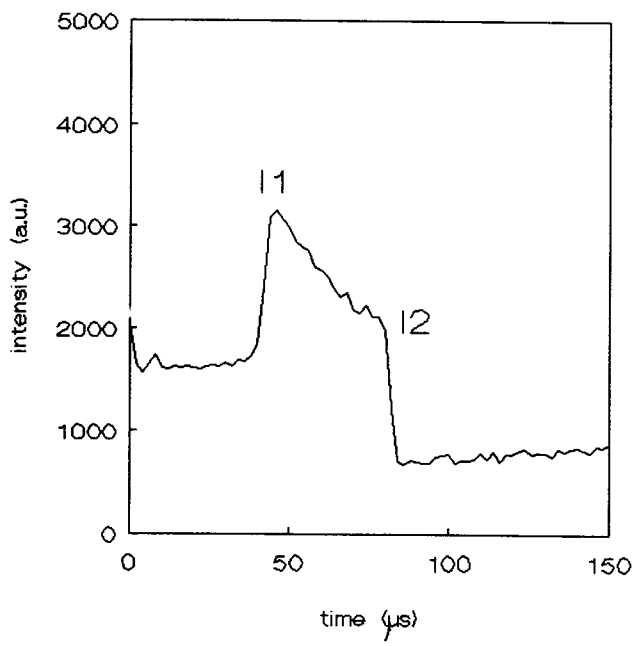


Fig. V.14. The electron density at the end of the off-period can be determined from line intensities, as $I_1/I_2 = (n_{e1}/n_{e2})^2$. $I_1$ corresponds to steady state electron density. Temperature during the off-period is constant.

The calculated relation provides $\gamma^p$ = 1.6, $T_e^p$ = 1.2 eV for $n_e^p/n_e^s$ = 0.8. Therefore the steady state conditions chosen this way seem to be quite reasonable.

This simple model allows not only to explain why the electron temperature at the heating jump is higher than the steady state temperature, but also allows to predict its value with quite good accuracy. Moreover, is suggests that the electron temperature in the steady state cannot be lower than the stability limit, which is estimated to be 0.8 eV. This limit concerns of course the active zone (skin) of the plasma, where the energy is incoupled. We are aware, that several simplifications make the actual result pretty place dependent. However, we have shown, that this limit should not be much lower, even if the full energy equation with all the transport terms is considered. This would support most of the results from § IV. In most of the experiments the value of $T_e$, determined using the power interruption method is larger than reported before [NOW.89]. However, the power input in our experiment is also larger than this of [NOW.89]. It is possible that the temperatures in the present ICP are that high.

It is recommended that the theoretical $n_e$ - $\gamma$ relation be tested for several electron densities (several off-periods) and several places in the plasma.

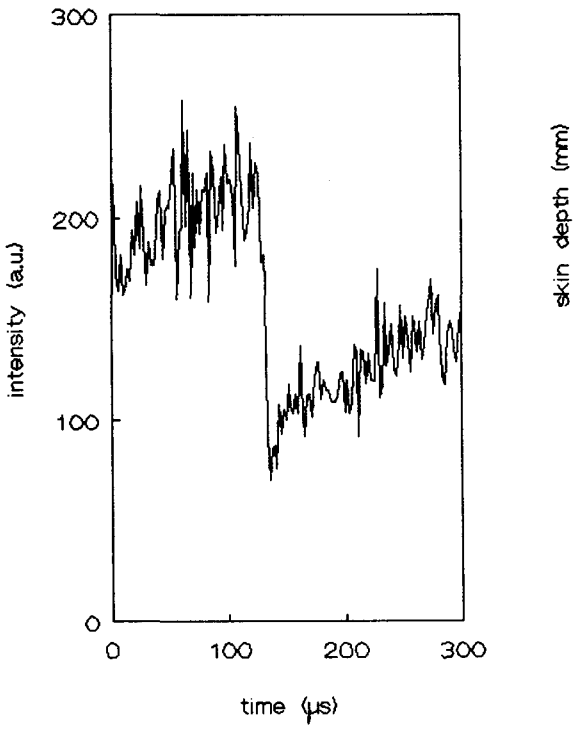


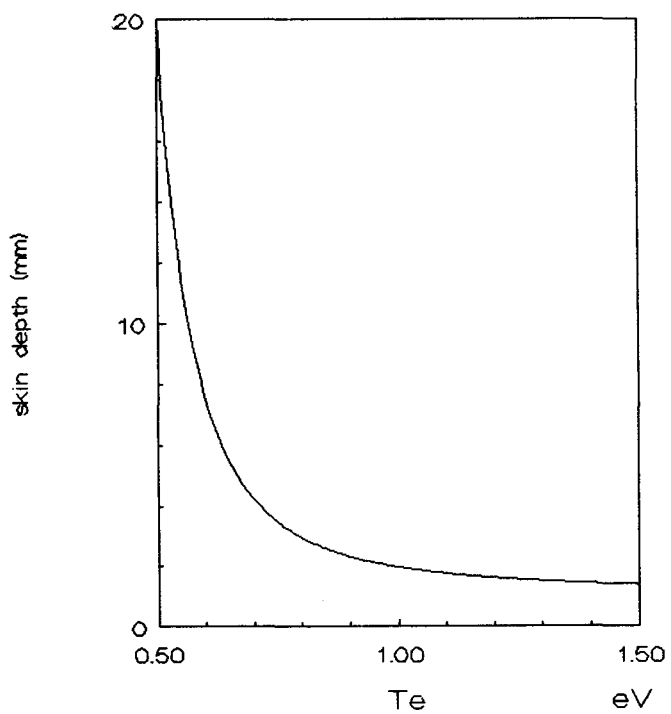


Fig. V.16. The electron temperature dependence of the skin depth (calculated).

Fig. V.15. The instantaneous response at r = 2 mm from the center (obtained from Abel inverted data for dry plasma, low power, 6s Ar line). The cooling jump is not observed, which means that $T_e \approx T_h$. The heating jump is well visible, which indicates a substantial energy input at this place just after the off-period.

### V.3.3 Radial depence of the heating jump

The local description presented above is not sufficient to obtain any quantitative information about the behavior of the center of the plasma during the heating jump. However, as the experiment allows to some extent to study this region we shall give some qualitative remarks.

The plasma skin is the property sustained by the nonuniformity of the energy input. In the absence of the field the $n_e$ and $T_e$ profiles will tend to be flat. Therefore during the off-period the skin is destructed. As the temperature profile becomes flat, the spatial distribution of the field energy is different, when the field reappears in the plasma. This effect has been already indicated in § IV, where the radially resolved responses of an argon line have been shown. Here we shall concentrate on one particular response for r = 2 mm from the center (Fig. V.15). What is remarkable is that the cooling jump is not visible anymore, while the heating jump is quite large. The absence of the cooling jump indicates that in the steady state $T_e \approx T_h$. As the loss terms in the center of the plasma are not larger than in the skin, it requires that the EM heating in the center is negligibly small. This effect is due to the shielding of the E field by the plasma. In Fig. V.16 the skin depth is plotted as a function of electron temperature, according to (V.9). It can be seen that if $T_e$ in the skin drops from 1.0 to 0.77 eV (the optimal conditions found in § V, 2.2), the skin depth increases by a factor of 2. It means that when the generator is switched on again the electric field at x = 2 mm is the same as it was at x = 4 mm in the steady state. This allows a substantial energy input close to the center of the plasma, which results in a large heating jump. The plasma skin is reestablished within a few microseconds. This causes shielding of the field, so the temperature in the center of the plasma cannot increase anymore.

It would be interesting to study the kinetics of the heating jump, just like it has been done with the cooling jump in 2.1. However, too many constants are uncertain, especially when the heating term is introduced. Moreover, this problem cannot be studied locally. The temperature in the skin will always have an influence on the inner parts.

## V.4 ELECTRON DENSITY DECAY

During the off period most of the "Saha like" responses show a decay. The rate of this decay depends on how fast a given excited state is depopulated in the recombining plasma. The experimental time constant of this decay varies between 50 and 1000 $\mu$s. In case of pure argon plasma it is easy to relate this rate to the total electron density decay. The emission intensity of an argon line is proportional to $n_e^2$ (for an optically thin transition, in Saha). Thus by monitoring emission intensities during the off time we can obtain information about the kinetics of the $n_e$ decay. This can give an indication of the dominant destruction mechanism. There are two major candidates for the actual $n_e$ destruction mechanism.

### V.4.1 Three body recombination

$$Ar^+ + e + e \longrightarrow Ar(p) + e$$

The total $n_e$ destruction rate is given by:

$$n_e/\partial t = -\Sigma_p \kappa_{rec}(p)\, n_e^2\, n_+ + \Sigma_p \kappa_{ion}(p)\, n_e\, n_{Ar(p)}$$

of course for argon $n_e = n_+$. In the above formula the contributions of all excited states are included. The collisional ionization/recombination rates differ greatly for various excited states. They are very fast in the top of the atomic system (frequency $\nu \simeq 10^5\ s^{-1}$, see [STO.91/1,3]), while for the ground state they are negligibly small (frequency $\nu \simeq 1\ s^{-1}$, [NOW.89]).

Argon has two main particle reservoirs: atom and ion ground states. In order to decrease the electron density significantly, the ion ground state must be significantly depopulated. The conservation of the total amount of particles implies that the density of particles in the other large reservoir (atom ground state) must increase. It is easy to see, that the direct recombination to the ground state is not sufficient to induce large $n_e$ changes on the considered time scale. Therefore we conclude that the real recombination is not direct but stepwise. It consists of a fast process, which is the recombination to the high excited states and deexcitation to 4s and a slow process, which is deexcitation of the 4s. This slow step limits the rate of the total recombination process. Therefore:

$$\partial n_e/\partial t = \partial n(4s)/\partial t \qquad \text{V.21}$$

There can be two main mechanisms of depopulating 4s. One of them is the collisional deexcitation and the other one is the radiative decay. The kinetic equations for both of them are solved and discussed below.

a) The kinetic equation for the collisional production/destruction of 4s is given by:

$$\partial n(4s)/\partial t = -K(4s,3p)\, n_e\, n(4s) + K(3p,4s)\, n_e\, n(3p) \qquad \text{V.22}$$

The principle of microscopic reversibility supplies the relation between K(4s,3p) and K(3p,4s):

$$K(4s,3p)\, n^S(4s) = K(3p,4s)\, n^S(3p) \qquad \text{V.23}$$

ubstituting (V.23) in (V.22) and remembering that $n(p) = b(p)\, n^S(p)$ we obtain:

$$\partial n_e/\partial t = -K(4s,3p)\, n_e\, n^S(4s)\, (b(4s) - b(3p))$$

The transport within the excited argon system is assumed to be very fast, so $b(4s) \simeq 1$ (which might be true in the recombining plasma). The recombination will continue until the ground state is in Saha equilibrium. At the beginning of the recombination period 3p is far from Saha, so b(3p) is small. Therefore for short off-periods we can assume that:

$$\partial n_e/\partial t \simeq - K(4s,3p)\, n_e\, n^S(4s)$$

Substituting the Saha expression for $n^S(4s)$ leads to:

$$\partial n_e/\partial t = - \kappa_{col}\, n_e^{\,3}, \qquad \text{V.24}$$

where

$$\kappa_{col} = 1/12\, K(4s,3p)\, g(4s)\, (h^2/2\pi m_e kT_e)^{3/2} \exp(E_{ion}(4s)/kT_e)$$

The solution of (V.24) gives the time behavior of $n_e$ according to the collisional mechanism:

$$n_e^{-2} - n_{e0}^{-2} = 2\kappa_{col}(t - t_0)$$

or

$$n_e = (n_{e0}^{-2} + 2\kappa_{col}(t - t_0))^{-1/2} \qquad \text{V.25}$$

The estimated frequency of this kind of process for standard ICP conditions is $10^2\ s^{-1}$ [NOW.89], which is lower than the observed one. However, this does not prove that this mechanism is not important. The estimation is based on a known value of K(3s,4p), which might be wrong even by a factor of 10.

b) The kinetic equation for the radiative decay of 4s can be written as:

$$\partial n_e/\partial t = \partial n(4s)/\partial t = - A(4s,3p)\, \Theta(4s,4p)\, n(4s) \qquad \text{V.26}$$

where $\Theta(4s,3p)$ is the escape factor for this transition. In the steady state ionizing plasma the ground state (3p) density is so large that $\Theta \simeq 0$. However, in a recombining plasma the radiation escape might be important, especially in the outer parts of the skin. A possible explanation for this escape can be the change in line width (see § VI) with temperature and electron density (smaller Doppler broadening for low temperature, no Stark broadening for very low $n_e$). Therefore at the boundary layer of the plasma the radiation emitted from the "hot" region (broad line profile) cannot be completely reabsorbed in the "cold" region (narrow line profile). Substituting the Saha value for n(4s) we obtain:

$$\partial n_e/\partial t = - \kappa_{rad}\, n_e^2 \qquad \text{V.27}$$

with

$$\kappa_{rad} = 1/12\ A(4s,3p)\ \Theta(4s,4p)\ g(4s)\ (h^2/2\pi m_e kT_e)^{3/2}\ \exp(E_{ion}(4s)/kT_e)$$

In this case the time behavior of $n_e$ will be different than for the collisional mechanism. The solution of (V.27) has the form:

$$n_e^{-1} - n_{e0}^{-1} = \kappa_{rad}(t - t_0)$$

or,

$$n_e = (n_{e0}^{-1} + \kappa_{rad}(t - t_0))^{-1} \qquad \text{V.28}$$

The frequency of this process strongly depends on the escape factor $\Theta$, which is place dependent and not very well known. The transition probability is in the order of $10^8$ $s^{-1}$. In order to provide an acceptable frequency ($10^4$ $s^{-1}$) of the radiation escape the escape factor should not be smaller than $10^{-4}$.

### V.4.2 Outward diffusion of electrons

In the outer regions of the plasma the gradients of electron density and temperature are very large. This makes the diffusion very fast. It is possible that during the off-period the diffusion of charged particles competes with or even dominates the recombination described above. It means that the real destruction of them occurs in some other place, where the temperatures are much lower. In this case the kinetic equation will have the following form:

$$\partial n_e/\partial t = - \nabla \cdot (n_e \mathbf{w_e}) \qquad \text{V.29}$$

where $\mathbf{w_e}$ is the diffusion velocity of electrons. An analogous equation holds for ions. The axial gradients of $n_e$ are not as large as the radial ones, so we need only to consider the radial diffusion. Substituting an expression for the particles flux $n_e \underline{w}_e = - D \cdot \nabla n_e$, where D is the ambipolar diffusion coefficient, we obtain:

$$\partial n_e/\partial t = D\, \nabla^2 n_e$$

If we use the following approximation, involving the gradient length $\Lambda$, we obtain:

$$\partial n_e/\partial t = D\, \nabla^2 n_e \approx D/\Lambda^2\, n_e \qquad \text{V.30}$$

According to (V.30) $n_e$ should decrease exponentially with time:

$$n_e = n_{e0} \exp(-Dt/\Lambda^2) \qquad \text{V.31}$$

This mechanism of electron density decay is expected to be most important in the outer regions of the plasma (outer part of the skin). In order to evaluate its frequency one should know the radial gradient length $\Lambda$. This quantity is not known, but in the very outer region of the plasma it can be expected to be smaller than 1 mm. The diffusion coefficient is also not very well known. A typical value is $10^{-3}$ $m^2s^{-1}$. If we assume $\Lambda \simeq 1$ mm the frequency is $10^3$ $s^{-1}$. For $\Lambda < 1$ mm it approaches fast the experimental value.

### V.4.3 Other mechanisms

Since the theoretical values do not completely agree with the experimental ones, some attention has been paid to other possibilities of $n_e$ destruction. One hypothesis involves molecular reactions. The following mechanism has been proposed [OTO.91]:
a) the formation of $Ar_2^+$ molecule:

$$Ar^+ + Ar + Ar \longrightarrow Ar_2^+ + Ar$$

with a rate constant in the order of $10^{-42}$ $m^6/s$
b) dissociative recombination of $Ar_2^+$:

$$Ar_2^+ + e \longrightarrow Ar^* + Ar$$

with a rate constant in the order of $10^{-13}$ $m^3/s$. Ar* is most likely in the 4p state (the rate constant of the above reaction is largest for 4p).

The step which limits the rate of this process is the formation of the molecular ion. The dissociation is much faster. Thus the rate of $Ar^+$ decay would be equal to $10^{-42}$ $n(Ar)^2 = 10^6$ $s^{-1}$. This is of course an upper estimate, in which the reverse process in a) is neglected. In principle this process could describe the observed $n_e$ decay rate. The main objection against this mechanism is that it does not provide a recombination to the ground state. Production of Ar 4p cannot change $n_e$ significantly, as 4p can be easily excited and ionized again. The rate $10^6$ $s^{-1}$ is not much larger than this of a simple three body recombination to an excited argon state. The problem of the "slow step", i.e. the depopulation of the excited states to the ground state still remains.

A promising mechanism has been presented in [NOW.89]. It involves the Charge Transfer between argon ions and molecular nitrogen, according to:

$$Ar^+ + N_2 \longrightarrow Ar + N_2^+$$

It produces an argon atom in its ground state. The $N_2^+$ ion can recombine easily to some excited state of $N_2$ (three body recombination), which in turn can be easily depopulated collisionally or radiatively (there is no large energy gap in $N_2$ system). Indeed, the molecular nitrogen has been found in the outer parts of the plasma, above the load coils (§ IV). However, between the load coils there is no $N_2$, while the time scale of recombination is found to be the same as ALC. Therefore this recombination channel probably cannot have an influence on the bulk of the plasma.

### V.4.4 Experimental data

Based on the experimental data it should be possible to indicate which of the mechanisms presented above is responsible for the $n_e$ destruction. However, the differences in time behavior of $n_e$ for them are not very large (especially for short off periods). Therefore the experimental data should not be treated as the utmost verification.

Fig. V.17 displays radially resolved responses of the 6s Ar line ($\lambda$ = 703 nm) for r = 2 mm, r = 5 mm and r = 7 mm. As in § IV, the radially resolved responses have been obtained by Abel inversion [BRA.90] of lateral data. It is clear that the $n_e$ decay rate increases with the increasing distance from the middle of the plasma. Fig. V.18 shows the dependence of the decay time $\tau_e$ on the radius (the decay time is defined as though the decay was exponential). We can see that in the middle of the plasma it has a time constant $\tau_e \simeq 10^3$ s$^{-1}$ which is quite close to the theoretically predicted one. However, it can be easily noted that the actual decay is not always exponential. We will test the three possible formulae (equation V.25, V.28 and V.31). Remembering that emission intensity (I) is proportional to $n_e^2$ we can plot $I^{-1}$ and $I^{-1/2}$ as a function of time. The three formulae describing $n_e$ decay should give the following dependencies:

collisional $n_e$ decay: $$I^{-1} = \alpha_{col} + \beta_{col}\, t \qquad \text{V.32}$$

radiative $n_e$ decay: $$I^{-1/2} = \alpha_{rad} + \beta_{rad}\, t \qquad \text{V.33}$$

diffusional $n_e$ decay: $$\ln(I) = \alpha_{dif} + \beta_{dif}\, t \qquad \text{V.34}$$

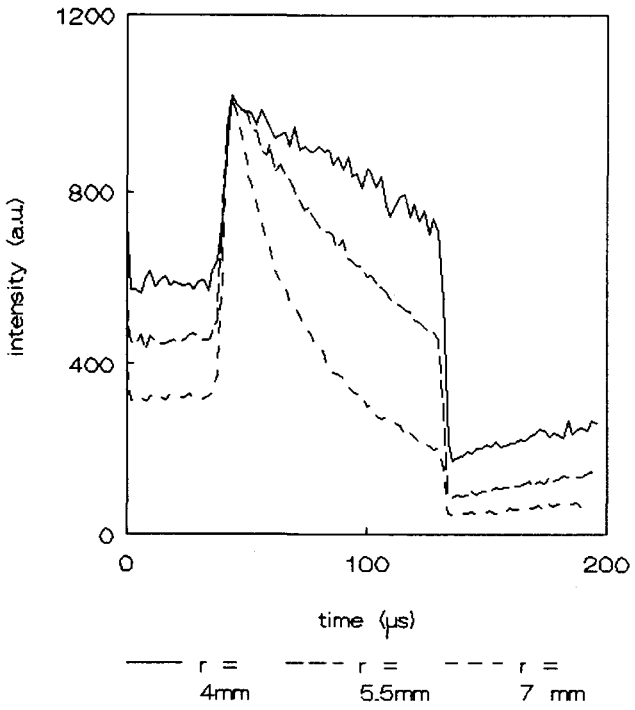


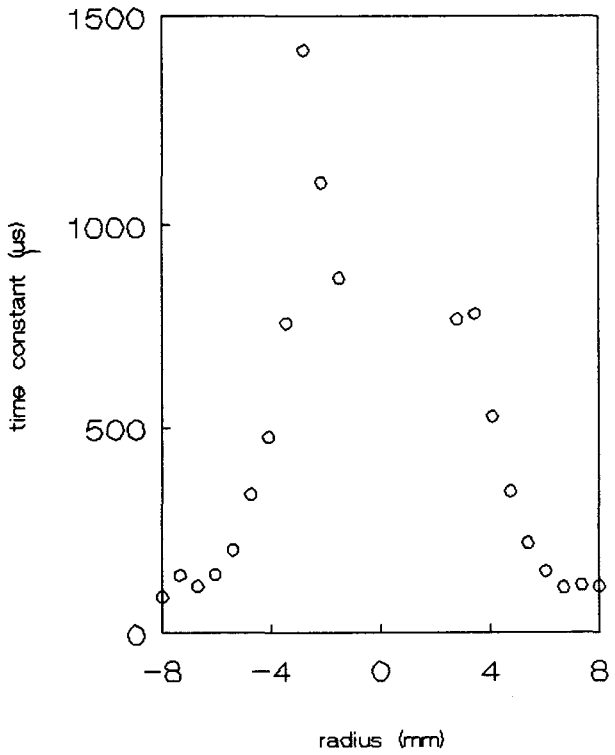


Fig. V.17. The comparison of intensity decays for several distances from the center of the plasma, as obtained from Abel inverted data for Ar 6s line.

Fig. V.18. The radially resolved time constants of $n_e$ decay, obtained from Abel inverted data. Conditions: dry plasma, flows: 12/0/0.7 l/min, power input: V = 3 kV, I = 0.4 A, 5 mm ALC.

Fig. V.19 shows plots of $I^{-1}$, $I^{-1/2}$ and ln(I) versus time for argon 5p - 4s transition ($\lambda$ = 420.1 nm) at r = 6 during the off period. The three curves are fitted with a linear fit. In this case it is easy to decide that the best fit is at Fig. V.19a, which corresponds to the "radiative" $n_e$ decay. Generally the differences cannot be easily seen, so one must compare the correlation factors (R) for these three fits. The R values do not differ that much. On the basis of these results it is difficult to decide what is the real mechanism of $n_e$ decay. However, there is a clear trend. Typically the "diffusional" (exponential) fit (V.34) seems to be the best all over the plasma except for the very edge. In the edge of the plasma the "radiative" fit is clearly better. The "collisional" one is always the worst. These results cannot be a base of a statement, but they might give an indication. It is possible that at the edge of the plasma the radiation can leave the plasma easier, so it will be responsible for depopulation of excited argon states.

Further we shall assume that $n_e$ decay is exponential. This assumption is good enough, as our aim is only to determine and compare the decay constants for other elements in the plasma.

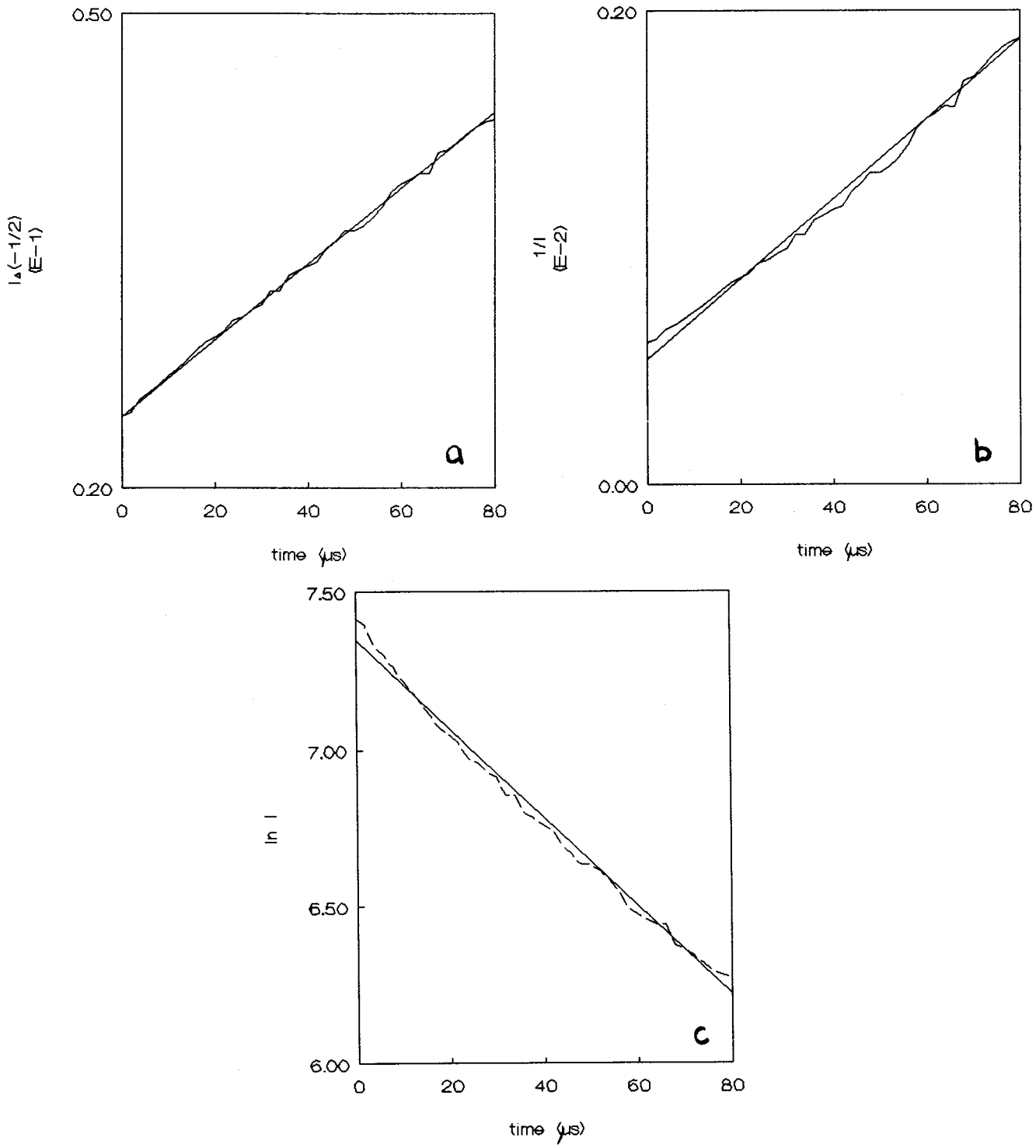


Fig. V.19. The comparison of three fits for the decay of $n_e$. The emission intensity of Ar 6s line in a dry plasma is proportional to $n_e^2$. The conditions are as in Fig. V.18, r = 6.5 mm.

a) $I^{-1/2}$ as a function of time (radiative),

b) $I^{-1}$ as a function of time (collisional),

c) ln(I) as a function of time (diffusional).

If these dependencies are linear they give an indication of the $n_e$ decay mechanism. In this case $I^{1/2}(t)$ can be most accurately approximated by a linear function. The "collisional" fit b) is always the worst.

## V.5 THE INFLUENCE OF HYDROGEN AND WATER

Two ways of introducing $H_2$ into the plasma have been used: in the cooling flow (up to 10% of the cooling flow) or in the central flow. The addition of hydrogen in the cooling flow causes drastic changes in the plasma. The plasma shrinks (even up to 1 cm of diameter) and the skin becomes less pronounced. The comparison of such plasma with the standard ICP under normal conditions is very troublesome. When $H_2$ is added in the central flow the same effects can be observed, but they are not so drastic. In both cases the amount of added $H_2$ is about 300 $cm^3$/min. Comparing this with the amount of Ar (13 l/min) we can estimate the fraction of $H_2$ to be about 1%.

There are several possibilities of ionization of hydrogen, as presented in the following scheme:

$$H_2 \xrightarrow{+\ 4.5\ eV} 2\,H \xrightarrow{+\ 13.6\ eV} H^+ + H$$

$$H_2 \xrightarrow{+\ 15.45\ eV} H_2^+ \xrightarrow{+\ 2.65\ eV} H^+ + H$$

There are also some possibilities of $H_2$ - argon interaction according to:

$$H_2 + Ar^+ \Longleftrightarrow H_2^+ + Ar$$

or

$$H_2 + Ar^+ \Longleftrightarrow ArH^+ + H$$

The first reaction describes a charge transfer between hydrogen molecule and argon, which can occur as the ionization energies of these species are very close. The second reaction might have some implications in the recombination mechanism in the presence of hydrogen, as the dissociative recombination of $ArH^+$:

$$ArH^+ + e \Longleftrightarrow Ar + H^*$$

is a fast reaction leading to a formation of Ar in the ground state. The excited state of hydrogen can be easily depopulated radiatively when the plasma is optically thin for the resonant H transition. This is the case, however, only at very low concentrations of hydrogen (less than $10^{21}$ $m^{-3}$).

Another possible interaction between Ar and H is the excitation transfer between some states of argon and atomic hydrogen. As the states belonging to Ar 4p level are close in excitation energy to $H\delta$, a following reaction can occur:

$$Ar(4p) + H(1) \Longleftrightarrow Ar(3p) + H(6) \qquad V.35$$

Some experimental evidence of this kind of interaction (with hydrogen originating from dissociated water) is presented in [FEY.91/1].

The reactions involving molecules require a significant density of $H_2$ and $H_2^+$ in the plasma. Below we shall estimate the amount of undissociated hydrogen in the plasma. The relation between the densities of $H_2$ and H can be derived using Detailed Balancing [MUL.86], in analogy to the Saha equation:

$$\eta(H_2) = \eta(H)^2 \, (h^2/\pi m_p kT_h)^{3/2} \exp(E_{dis}/kT_h) \qquad \text{V.36}$$

where $m_p$ is the mass of proton, $E_{dis}$ - dissociation energy of $H_2$. It is assumed that the dissociation is performed by collisions with heavy particles. This assumption is very reasonable, as the electrons do not have sufficiently large momentum to break the molecular bonds. Substituting all the known constants in (V.36) (taking an average $T_h$ = 0.5 eV) we obtain:

$$n(H_2)/g(H_2) = n(H)^2/4 \; 8.3\times 10^{-28}$$

which means that if $n(H) \simeq 10^{22}$ $m^{-3}$ (a reasonable value), $n(H_2)/g(H_2) \simeq 10^{16}$ $m^{-3}$. Since $H_2$ has many vibrationally and rotationally excited states, $g(H_2)$ might be large (in the order of $10^3$ - $10^4$), which would increase the molecule density to $10^{20}$ $m^{-3}$. This is an equilibrium evaluation. In reality this number might be even larger, which would allow the molecular reactions to influence the plasma. There are, however, no experimental facts supporting this hypothesis.

The dissociation of hydrogen is probably responsible for the observed shape of the plasma. When the hydrogen approaches the active zone it dissociates almost completely. This process consumes energy, while it is not followed by emission. As a result no emission is collected from the places in which the hydrogen is being dissociated. Therefore the active zone, which is radiating and in which electrons are produced, is shrunk. Such a shrunk profile (with $H_2$ in the cooling flow) is presented in Fig. V.20, next to a pure argon plasma profile.

The response of line emission of hydrogen has been already shown in § III, as an example of a Saha - like response. Here we shall only note that its decay time is about 30% larger than this of argon (at the same place in the plasma, Fig. V.21). We can check whether the difference in decay time between H and Ar can be a consequence of a simple equilibrium relation between two components in the plasma. Suppose that we have two ionization/recombination equilibria:

$$Ar^+ + e + e \Longleftrightarrow Ar + e$$
$$H^+ + e + e \Longleftrightarrow H + e$$

with the corresponding Saha relations:

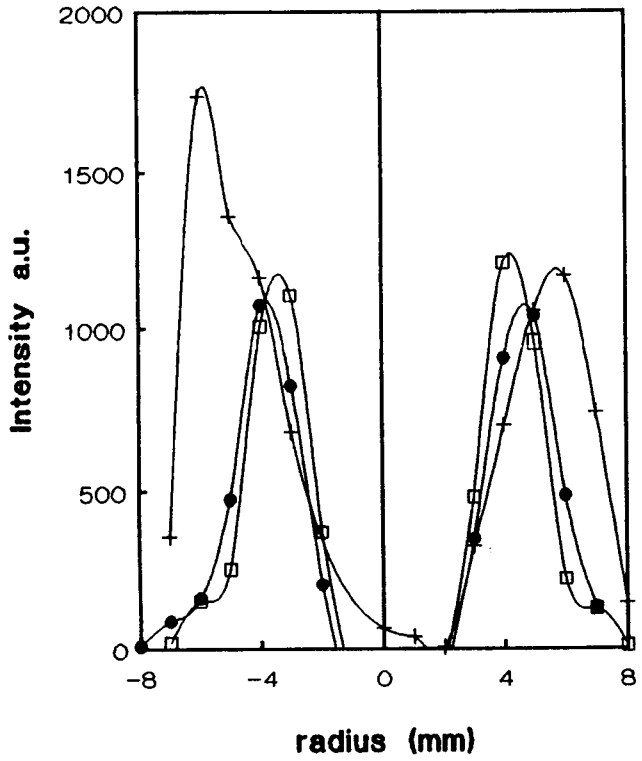


Fig. V.20. The intensity profiles in the ICP for several $H_2$ fractions (hydrogen is introduced in the cooling flow).
+ pure argon plasma
● 0.086 l/min $H_2$ (0.7% $H_2$ in the cooling flow)
□ 0.172 l/min $H_2$ (1.4% $H_2$ in the cooling flow)

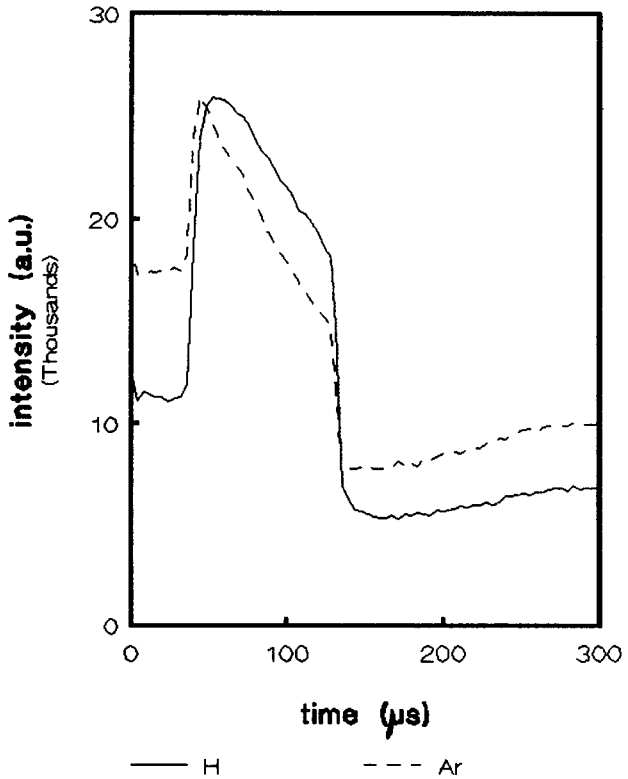


Fig. V.21. A typical response of H line (here H$\beta$) compared with a response of Ar. The decay of H during the off-period is slower.

$$n(H) = n(H^+)\, n_e/2\, g(H)/g(H^+)\, (h^2/2\pi m_e kT_e)^{3/2} \exp(E_{ion}{}^{H}/kT_e) = n(H^+)\, n_e\, S^h$$

$$n(Ar) = n(Ar^+)\, n_e/2\, g(Ar)/g(Ar^+)\, (h^2/2\pi m_e kT_e)^{3/2} \exp(E_{ion}{}^{Ar}/kT_e) = n(Ar^+)\, n_e\, S^{ar} \qquad \text{V.37}$$

Let us define $\beta = S^h/S^{ar} \ll 1$. Then using equations (V.37) we can find the relation between $n(H^+)$ and $n(Ar^+)$:

$$n(H^+) = \frac{n_{tot}(H)\quad n(Ar^+)}{\beta\ n_{tot}(Ar) + (1-\beta)\ n(Ar^+)} \qquad \text{V.38}$$

where $n_{tot}(H)$, $n_{tot}(Ar)$ are the total densities of Ar and H in the plasma. The emission intensities of argon and hydrogen lines can be written as:

$$I(Ar) \sim n(Ar^+)\, n_e$$

$$I(H) \sim n(H^+)\, n_e = \frac{n_{tot}(H)\; n(Ar^+)\; n_e}{\beta\; n_{tot}(Ar) + (1 - \beta)\; n(Ar^+)}$$

The decay of I is limited by the decay of $n_e$ and $n(Ar^+)$. In case of hydrogen we can evaluate the two terms in the nominator, taking $\beta \simeq 10^{-2}$, $n_{tot}(Ar) \simeq 10^{24}$ $m^{-3}$, $n(Ar)^+ \simeq 10^{21}$ $m^{-3}$. Then $\beta\, n_{tot}(Ar)$ is at least an order of magnitude larger than $n(Ar^+)$. It means that $n(Ar^+)$ in the nominator can be neglected and the intensities should decay at the same rate (i.e. like $n(Ar^+)\, n_e$). The large difference shown in Fig. V.21 cannot be explained this way. This suggests that there is some (molecular ?) reaction in the recombining plasma, providing a source of excited hydrogen atoms.

The available experimental data are the Abel inverted responses of an argon line when hydrogen is introduced in the central flow. They provide a possibility of comparing the electron density profiles for a plasma with or without hydrogen. For a dry plasma we can assume that the emission intensity of an excited state $I \sim n_e^2\, S(T_e)$, where $S(T_e)$ is the Saha function. When the generator is switched off $T_e$ drops to $T_h$. The maximum of emission intensity corresponds to Saha values of densities of excited states for $T_e = T_h$ (see § IV). Therefore $I_{max} \sim n_e^2\, S(T_h)$. The radial profile of heavy particle temperature can be assumed to be flat across the plasma, perhaps except for the very outer part of the skin. Therefore the radial profile of the maximal emission intensity at the cooling jump brings some information about the $n_e$ profile. In fact a profile obtained this way has been presented in this chapter in Fig. V.5. If $H_2$ is present in the plasma one has to be more careful, as then $n_e \neq n(Ar^+)$. One can show using (V.38) that in this case the dependence of emission intensity on $n_e$ and $n(H^+)$ will be:

$$I \sim n_e\, n(Ar^+) = \beta\, n_{tot}(Ar) n(H^+) n_e / (n_{tot}(H) - n(H^+)) \qquad \text{V.39}$$

The above expression should give a dependency close to $n_e^2$. In an extreme case, when the plasma is saturated with $H_2$ $n_e \approx n(H^+)$. Then we can see that the dependence of I on $n_e$ should be slightly stronger than $n_e^2$ (due to the nominator, which increases with $n_e$). However, most of H is not ionized (even if Saha equilibrium is assumed). Therefore $I \sim n_e^2$. Let us then assume that $I_{max} \sim n_e^2\, S(T_h)$. In Fig. V.22 such relative $n_e$ profiles (i.e. the profiles of $I_{max}^{1/2}$) are shown. It can be seen that the hydrogen containing plasma is more narrow and the gradients become larger. We expect that this effect will be even more drastic when $H_2$ is introduced in the cooling flow.

The influence of $H_2$ and water on the decay times of Ar lines has been studied. $H_2$ has been introduced in the central flow. The decay times of argon lines in presence of H do not differ from this in pure argon plasma. Using the argument presented above, according to which the intensity of argon lines should be always proportional to $n_e^2$, with or without hydrogen, we can compare the decay times of $n_e$. Fig. V.23 shows a radially resolved decay time of $n_e$ with and without $H_2$. The fact that $n_e$ decay is not influenced by H suggests that even if there is some reaction involved, it does not influence Ar. It might, however, become important at higher H

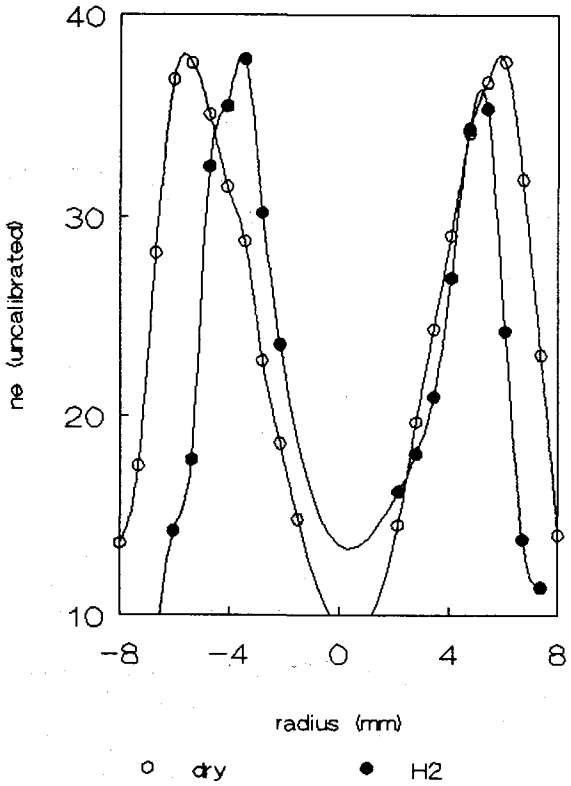


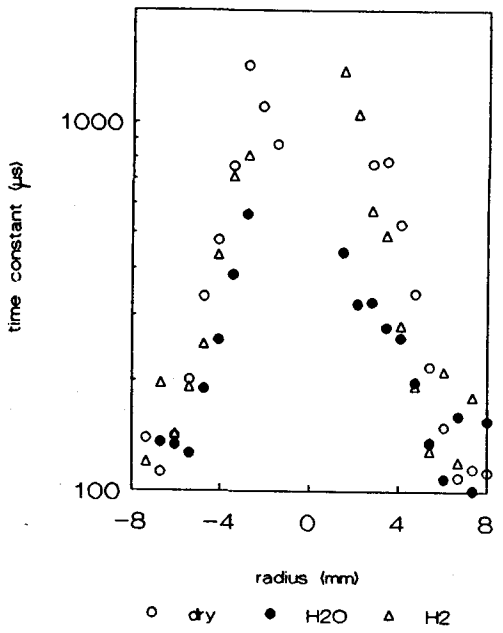


Fig. V.23. The radially resolved $n_e$ decay times from Abel inverted data for Ar 6s. Flows are always 12/0/07 l/min, height 5 mm ALC.
- o pure Ar plasma
- • $H_2O$ injection
- Δ $H_2$ injection (0.05 l/min in the central flow)

Fig. V.22. The relative electron density profiles, obtained from line intensities just after the cooling jump for Abel inverted data for Ar 6s line, assuming flat $T_h$ profile across the plasma. Here the profile for pure Ar plasma is compared with one for plasma containing $H_2$ (0.05 l/min $H_2$ in the central flow). When $H_2$ is introduced in the central flow the plasma also shrinks.

concentrations. In Fig. V.23 we also present radially resolved decay times when water is present in the plasma. It can be immediately seen that the addition of water does influence the argon emission. The decay times become a factor of 2 smaller. The differences are most drastic in the center of the plasma, where water is introduced. This effect is in agreement with the fact that diffusional processes are very important in the wet plasma (see [STO.91/1,3]). Here it is most likely that water droplets create large temperature gradients, which enhance diffusional $n_e$ losses. It has been also checked, that in case of wet plasma the "diffusional" fit for $n_e$ decay (see § V.4.4 ) is the best all over the plasma.

Further we shall concentrate on the experimental data on the plasma containing hydrogen introduced in the cooling flow. The amount of $H_2$ added to the plasma in this case is not larger than the amount of $H_2$ in the central flow, but the changes are very drastic. This indicates, that the diffusion of $H_2$ from the center to the active zone is a slow process.

The main feature of a hydrogen containing plasma is its small size. As a result, the energy incoupling into the plasma is lower. There is no reliable data on electron temperature and density in this plasma. There are, however, several experimental indications that in this plasma electron density is higher than in the pure argon plasma [OHL.87]. We can involve our previous considerations about

Fig. V.24. Logarithm of the cooling jump of Ar 5d line for several $H_2$ flows. $H_2$ is introduced in the cooling flow (12 l/min). The power input is kept constant (3 kV, 0.4 A). The saturation occurs for 0.11 l/min $H_2$ (1% of $H_2$).

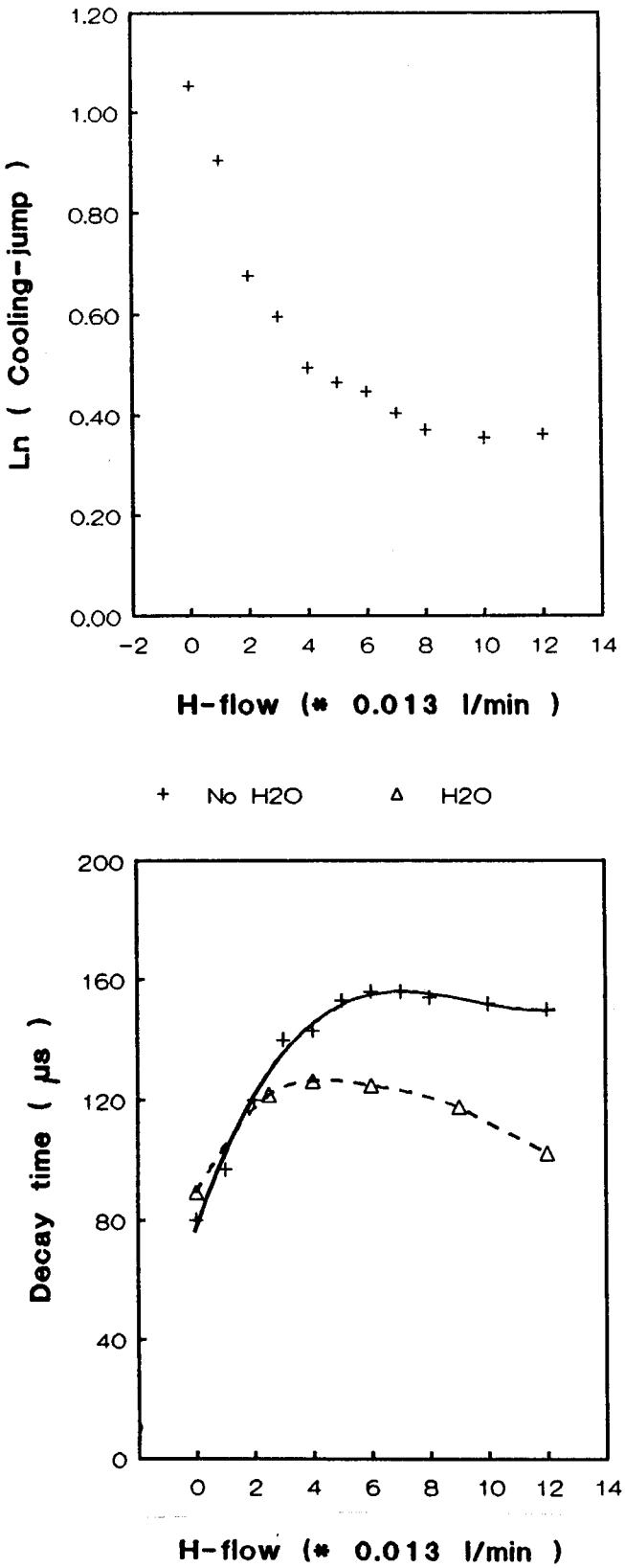


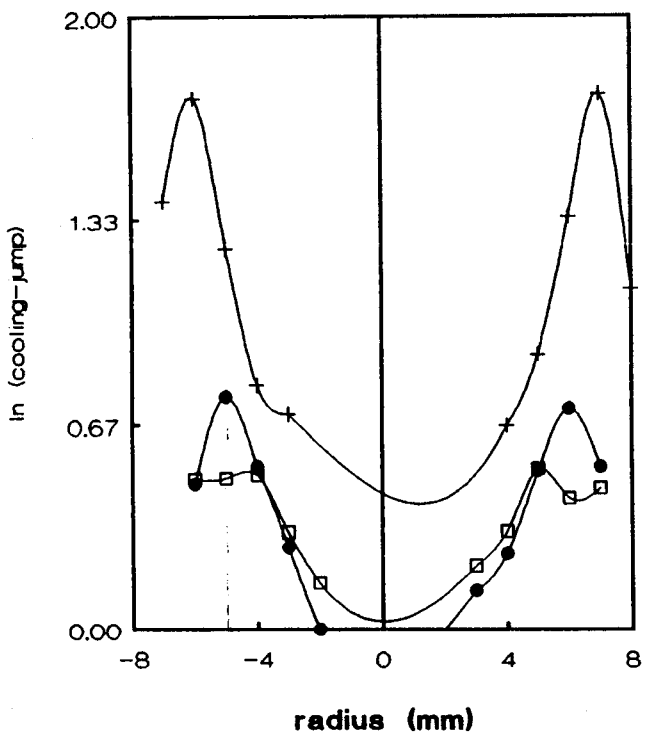


Fig. V.25. The radially resolved logarithm of the cooling jump
+ pure Ar plasma
● 0.7% $H_2$
□ 1.4% $H_2$
The conditions are like in Fig. V.24.

Fig. V.26. Decay time of Ar 5d line for several $H_2$ flows. Conditions are like in Fig. V.24. The decay time increases until a saturation is reached (also at 1% $H_2$). When in addition to $H_2$ water is introduced (central flow) the decay time does not increase that much.

the balance between energy input and losses. As the energy input is not higher (is has been kept constant) and the volume of the plasma is smaller (shrinking), probably $T_e$ is larger. Moreover, as the electron density is higher (V.2), we expect that the difference between $T_e$ and $T_h$ is smaller (i.e. $\gamma$ is smaller). It has been found experimentally that the cooling jumps of Ar lines decrease with increasing fraction of $H_2$ in the plasma, until a saturation is reached (Fig. V.24). The saturation occurs at about 1% of $H_2$ in the plasma. The ratio of H density and Ar density is then about 1/50. On the other hand, the mass ratio of Ar and H is 40. Therefore at 1% of $H_2$ added to the plasma the collision frequency for energy transfer with hydrogen atoms is the same as with argon atoms. The ratio of ion densities is most likely even larger than 1/50, so the collision frequency with $H^+$ is larger than with $Ar^+$. In Fig. V.25 radially resolved jumps for several hydrogen fractions are presented. The decrease of jumps might indicate that $\gamma$ is lower and (or) $T_e$ is higher. However, there is another possibility of explaining the effect shown in Fig. V.24 and 25. Suppose that the excitation transfer between Ar(4p) and H(6) (see (V.35)) is a dominant process (i.e. its rate constant is larger than the rate constant of electronic processes). Then this balance will equilibrate first. The principle of Detailed Balancing requires:

$$\eta(\mathrm{Ar(4p)})\ \eta(\mathrm{H(1)}) = \eta(\mathrm{Ar(3p)})\ \eta(\mathrm{H(6)}) \qquad \text{V.40}$$

The cooling jump of H(6) is smaller that this of Ar(4p), as the ionization energy of H(6) is smaller that this of Ar(4p). However, if the coupling through the excitation transfer is strong enough these jumps will become equal, in order to satisfy (V.40). This can influence jumps in all the argon system. However, since the rate constant for this excitation transfer is not known, the presented mechanism is only a hypothesis.

The influence of $H_2$ can be clearly seen in the decay times of Ar lines. The decay time of the 5d line is shown in Fig. V.26. The saturation occurs for the same amount of added $H_2$ as in Fig. V.24. The increase in the time constant of Ar lines decay in presence of $H_2$ is not fully understood. Equation (V.39) implies that for high $H_2$ fractions argon lines should decay like $n_e^2$ or even faster. Therefore we can state that the increase in time constant for argon lines is really due to increase in $n_e$ decay time. It is possible that the recombination rates of argon and hydrogen are equalized by means of excitation transfer (V.40). This would require that the recombination rate of hydrogen is smaller than this of argon, which is also possible.

When in addition to $H_2$ water is present in the plasma the decay time does not increase that much (Fig. V.26). This is in agreement with the previous observations (see Fig. V.23).

Above we have presented some preliminary results on the influence of hydrogen on the argon ICP. This influence is very complicated, as it involves both changes of the physical properties of the plasma as well as some chemical interaction between the two elements. More experimental work is needed to verify the hypotheses presented in this chapter and to explain some not understood phenomena.

# VI ABSORPTION MEASUREMENTS

## VI.1 INTRODUCTION

So far the ICP has been treated as a plasma, which is optically thin for all the argon transitions except for the resonant Ar transitions in vacuum UV. However, it has been found that some of the 4p - 4s lines are also partially reabsorbed. This feature appears to be useful in studying the behavior of Ar(4s), in the steady state as well as in the power interruption experiment. Since no information about Ar(4s) is accessible from emission measurements, optical thickness of some transitions to 4s is actually the only chance to obtain it. The absorption measurements have been performed either using plasma radiation, reflected back into the plasma, or an external light source (a cascaded arc). The first method has appeared to be simplest and most successful.

## VI.2 THE PRINCIPLE OF THE METHOD

### VI.2.1 Theory

The radiation transfer in a plasma obeys the equation:

$$\frac{d\ I(\nu)}{d\ x} = j(\nu) - \kappa(\nu)\ I(\nu) \qquad \text{VI.1}$$

where $I(\nu)$ is the light intensity at frequency $\nu$, emitted in x direction, $j(\nu)$ is the volume emissivity, related to the decay processes, $\kappa(\nu)$ is the absorption coefficient. The equation (VI.1) describes simply a balance between emission and absorption, valid for any kind of radiation (free - free, free - bound, bound - bound). When the balance is in equilibrium, the right hand side of (VI.1) equals zero and $j(\nu)$ and $\kappa(\nu)$ are related through the Planck black body function. When the equation (VI.1) describes line (bound - bound) emission from a level u (upper) to a level l (lower), the absorption coefficient $\kappa(\nu)$ is given by:

$$\kappa(\nu) = \frac{c^2}{8\ \pi\ \nu^2}\ g(u)\ A(u,l)\ (\eta(l) - \eta(u))\ \phi(\nu) \qquad \text{VI.2}$$

where $\nu$ is the frequency of the transition, g(u) is the statistical weight of the upper level, A(u,l) is the transition probability, $\phi(\nu)$ is the line profile factor, satisfying $\int \phi(\nu)\ d\nu = 1$. If $\nu$ (the energy gap between the states) is large enough then $\eta(l) \gg \eta(u)$ and $\eta(u)$ in the equation (VI.1) can be neglected. Then the absorption coefficient $\kappa$ gives us information about the density of the lower level.

When we only want to study the decay of an external light beam through the plasma, the emissivity term in (VI.1) drops out and the absorption is described by the law of Lambert - Beer. The integrated form of this law is given by:

$$\ln \frac{I_t}{I_0} = - \int \kappa(\nu,x)\, dx \qquad \text{VI.3}$$

where $I_t/I_0$ is the ratio of intensity of transmitted light to the initial intensity (of the external light source, without absorption). The integral of $\kappa$ over the path of the light beam in the absorbing medium is called optical depth ($\tau$). A detectable absorption requires $\tau$ to be not smaller than 0.1. Here we shall give some estimates of $\tau$ for some 4p - 4s transitions.

Let us suppose that $\kappa$ is approximately constant across the plasma (it implies a flat density profile). This assumption has been already used and justified in § V. It allows to simplify (VI.3). Thus we obtain:

$$\tau = \frac{c^2}{8\,\pi\,\nu^2}\, g(u)\, A(u,l)\, (\eta(l) - \eta(u))\, \phi(\nu)\, x \qquad \text{VI.4}$$

The energy gap of these transitions is about 1.5 - 2 eV ($\lambda$ = 600 - 800 nm). First we have to check whether it is allowed to neglect $\eta(u)$. Suppose that the levels 4p and 4s are Boltzmann coupled. It means that $\eta(u) = \eta(l) \exp ( - \Delta E/kT_e)$. For $kT_e \approx 1$ eV $\eta(u)/\eta(l) \simeq 0.1 - 0.2$. This implies an error of 10 - 20% in $\kappa$ if we neglect $\eta(u)$. Perhaps the real error is somewhat smaller. Due to ionizing plasma 4s might be more overpopulated than 4p, which makes the density ratio smaller. Anyway, there are several other sources of error, like uncertainty in the optical path, transition probabilities, etc. For the order of magnitude estimation of $\tau$ we can neglect $\eta(u)$. Eventually we can evaluate the optical depth for the strongest of 4p - 4s transitions, at $\lambda$ = 811.5 nm ($2p_9$ - $1s_5$). We use the following data: $A(2p_9,1s_5) = 3.66\times10^7$ s$^{-1}$ [WIE.69], $g(2p_9) = 7$. The line shape is approximated by a triangle with half width $\Delta\lambda \simeq 0.2$ Å. The absorption coefficient will be estimated at the maximum of the line. Therefore $\phi = (\Delta\nu)^{-1}$, where $\Delta\nu = c/\lambda^2\, \Delta\lambda \simeq 10^{10}$ s$^{-1}$. The optical path x is at most 2 cm. This gives $\tau \simeq 10^{-17}\, \eta(1s_5)$. The state density of $1s_5$ can be evaluated from the Saha equation. Its ionization energy is 2.68 eV. The Saha value of $\eta(1s_5)$ for $n_e \simeq 10^{21}$ m$^{-3}$ and $T_e \simeq 1$ eV is therefore in the order of $10^{15}$ m$^{-3}$ (if $n_e$ is twice as large and $T_e$ is 0.7 eV it might become $10^{17}$ m$^{-3}$). Moreover, in the ionizing plasma 4s is probably substantially overpopulated with respect to Saha. We see that these densities bring $\tau$ into the order of 0.1, which is required for a detectable absorption.

The reabsorption of some 4p - 4s transitions has been found in a power interruption experiment. The instantaneous response of the transition mentioned above ($2p_9$ - $1s_5$) is shown in Fig. VI.1a. In Fig. VI.1b a normal response of an optically thin transition $2p_7$ - $1s_5$ ($\lambda$ = 772.4 nm) is shown for comparison. First we see that the emission intensity decreases when the generator is switched off. Then it increases slightly during the off - period (except for the first few microseconds).

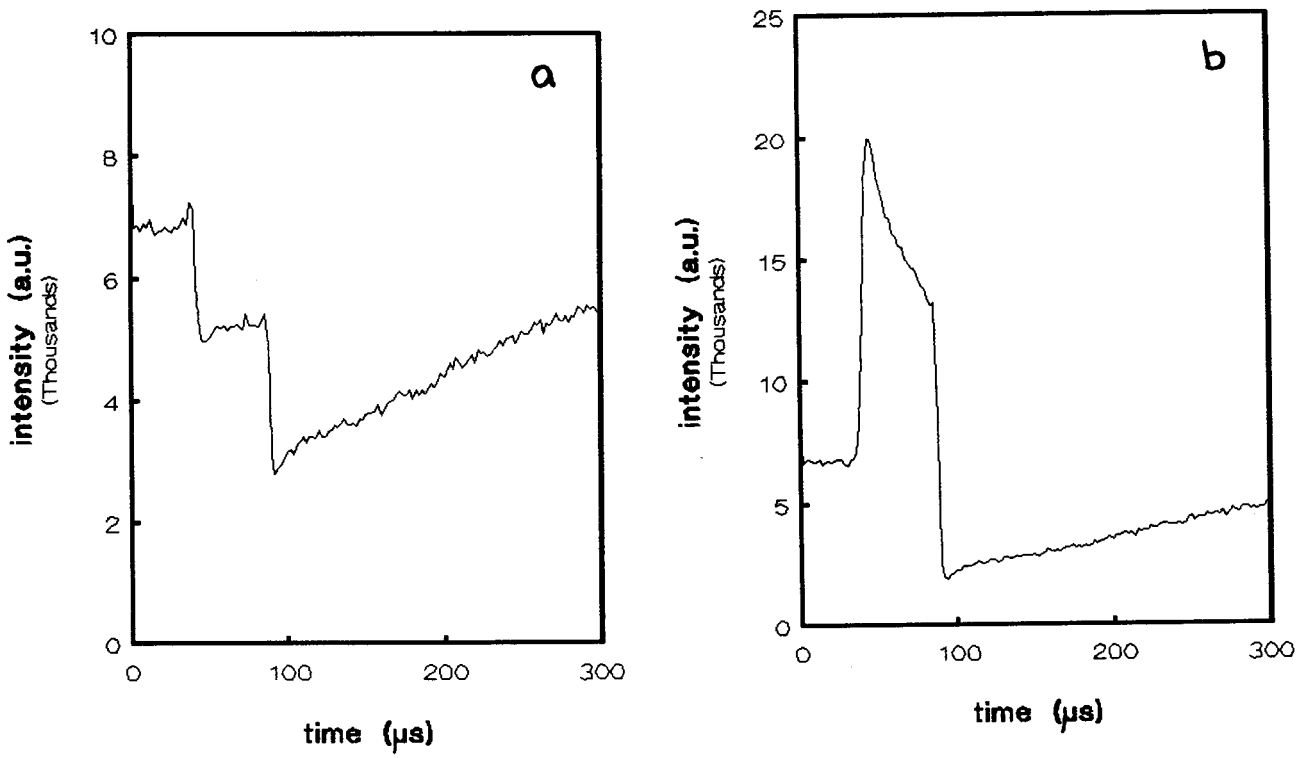


Fig. VI.1. A typical response of the Ar 811.5 nm line (a). A normal response of an optically this 4s - 4p line ($\lambda$ = 772 nm) is shown for comparison.

This can be explained assuming partial reabsorption of this emission. In this case the spontaneous decay rate will equal $A(2p_9,1s_5)\ \Theta(2p_9,1s_5)\ n(2p_9)$, so:

$$I = A(2p_9,1s_5)\ \Theta(2p_9,1s_5)\ n(2p_9)\ h\nu \qquad \text{VI.5}$$

and the escape factor $\Theta$ can be expressed in terms of the optical depth [MUL.86]:

$$\Theta = (1 - \exp(-\tau)) / \tau \qquad \text{VI.6}$$

It can be easily seen that $\Theta$ increases with decreasing $\tau$. The formulae (VI.5) and (VI.6) determine the behavior of I in time. According to Saha, if the density of $2p_9$ during the cooling jump increases by a factor of $\beta$, this of $1s_5$ should increase by a factor $\beta \exp(1.5(\gamma - 1)/kT_e) \approx 1.6\,\beta$. Using (VI.4) and Saha relation we see that $\tau$ increases by the factor:

$$\frac{\tau^*}{\tau} = \beta \frac{\exp(1.5/kT_h) - 1}{\exp(1.5/kT_e) - 1} \approx 1.7\,\beta$$

As usually, * refers to the value of a parameter after cooling. Note that in order to explain these effects it is not allowed to neglect $\eta(u)$ in (VI.4); a more careful treatment is needed. Substituting (VI.6) to (VI.5) we can calculate the ratio of intensities before and after the cooling:

$$\frac{I^*}{I} = \frac{1 - \exp(-\tau^*)}{1 - \exp(-\tau)} \frac{\tau}{\tau^*} \frac{n^*(2p_9)}{n(2p_9)} \approx$$

$$\approx \frac{1 - \exp(-1.7\beta\tau)}{1 - \exp(-\tau)} 0.6 \qquad \text{VI.7}$$

If in the steady state $\tau$ is large enough ( $\simeq$ 1) intensity after the cooling jump can decrease even by 40%. In a real case (ionizing plasma) the jump of 4s is somewhat smaller, so the intensity ratio is not so low.

Similarly, suppose that $1s_5$ and $2p_9$ densities decay during the off-period with the same rate, i.e. $n(2p_9) = n_0(2p_9) \exp(-\alpha t)$, $n(1s_5) = n_0(1s_5) \exp(-\alpha t)$. Then from the expression (VI.4) it follows that $\tau$ decreases with time as $\tau = \tau_0 \exp(-\alpha t)$. Then the time behavior of of emission intensity is given by:

$$I(t) \sim \frac{1 - \exp(-\tau(t))}{\tau_0 \exp(-\alpha t)} n_0(2p_9) \exp(-\alpha t) \sim 1 - \exp(-\tau(t)) \qquad \text{VI.8}$$

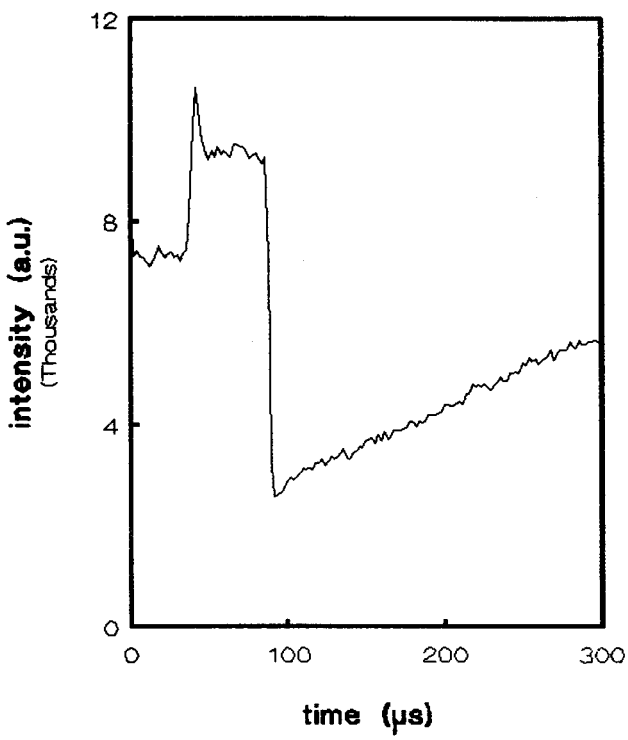


Fig. VI.2. A response of Ar 4s - 4p line ($\lambda$ = 842.5 nm), partially reabsorbed.

If $\tau$ is large enough I(t) should stay approximately constant during the off-period. If I(t) increases it means that $\tau$ should decrease faster than $n(2p_9)$, i.e. $n(1s_5)$ should decrease faster than $n(2p_9)$. However, the increase of intensity shown in Fig. VI.1a is rather minor.

For some other partially reabsorbed transitions, like $2p_8$ - $1s_4$ (resonant), $\lambda$ = 842.5 nm at the cooling jump the emission intensity increases and stays constant during the off-period. (Fig. VI.2). In this case $\tau$ is smaller due to smaller transition probability, so according to (VI.7) the ratio $I^*/I$ can be larger than 1. During the off-period we do not see a decay, as one would expect from (VI.8). It can mean that the decay of $1s_4$ is faster than this of $1s_5$. It can be partially understood, as the resonant $1s_4$ can be depopulated radiatively, while the metastable $1s_5$ cannot. Theoretical calculations [BEN.91] predict a poor collisional coupling between these two levels, so the difference in decay times is in principle possible.

These unexpected responses of several 4p - 4s levels have triggered series of absorption measurements. The results are presented below.

### VI.2.2 Description of the method and results

Most of the absorption experiments presented here have been performed without any external light source. A mirror has been placed behind the plasma, as shown in Fig. VI.3. A part of the plasma radiation is reflected back into the plasma and acts as the "external" beam. The plasma is in focus of the spherical mirror. As the focal length (50 cm) is much larger than the radius of the plasma, the light reflected from the mirror will return to approximately the same place in the plasma it has been emitted from.

The intensity of light reflected back into the plasma ($I_0$) is not known. However, the intensity collected with ($I_m$) and without mirror ($I_{nm}$) can be compared. For an optically thin line we have:

$$I_0 = \frac{I_m - I_{nm}}{I_{nm}} I_{nm} = \xi I_{nm}$$

The coefficient $\xi$ indicates the fraction of light reflected back to the plasma. We shall further assume, that the reflectivity of the mirror is constant in the wavelength range of 4p - 4s transitions, so $\xi$ is always the same. In principle the mirror should be calibrated. The intensity of transmitted light in an optically thick case is analogously:

$$I_t = \frac{I_m - I_{nm}}{I_{nm}} I_{nm}$$

Using (VI.3) we can write for an optically thick line:

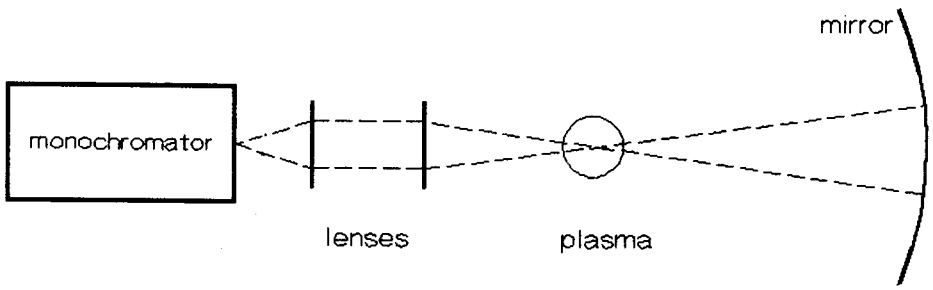


Fig. VI.3. Setup for absorption measurements. The (removable) spherical mirror is used to reflect the plasma radiation back to the plasma. The plasma is placed in the focus (r = 50 cm) of the mirror.

$$\ln I_t/I_0 = \ln \{(I_m - I_{nm})/ \xi I_{nm}\} = -\tau$$

or

$$\ln \{(I_m - I_{nm})/I_{nm}\} = -\tau + \ln \xi \qquad \text{VI.9}$$

The optical depth is proportional both to the transition probability and density of the lower state. Here we have to neglect the contribution of the upper state in the expression for $\tau$, as the upper states were not the same for all transitions. We can plot the ratio on the left hand side of (VI.9) as a function of transition probabilities for the transitions to the lower level $1s_5$ or $1s_4$. The ratio of slopes of these two lines should give the ratio of densities of $1s_5$ and $1s_4$ (averaged over the plasma profile). The measurements were performed 2 mm ALC, at r = 3 mm from the center (laterally). The ratios in the steady state are shown in Fig. VI.4. The result is:

$$\frac{n(1s_5)}{n(1s_4)} = 2.9$$

The ratio of densities of the metastable and resonant levels can be calculated theoretically, using a collisional - radiative model for argon [BEN.91]. The theoretical ratio is about 5. The same ratio calculated assuming a good collisional coupling (the ratio of Boltzmann densities) equals 1.8 (for $T_e$ = 1 eV). The value obtained from the absorption measurement is between these two, therefore we can consider it to be reasonable. Of course we should remember about many sources of error in this measurement. One of the errors is due to a difficulty in finding the maximum of a line. From (VI.2) it follows, that the absorption varies over the line profile. If the wavelength at which we

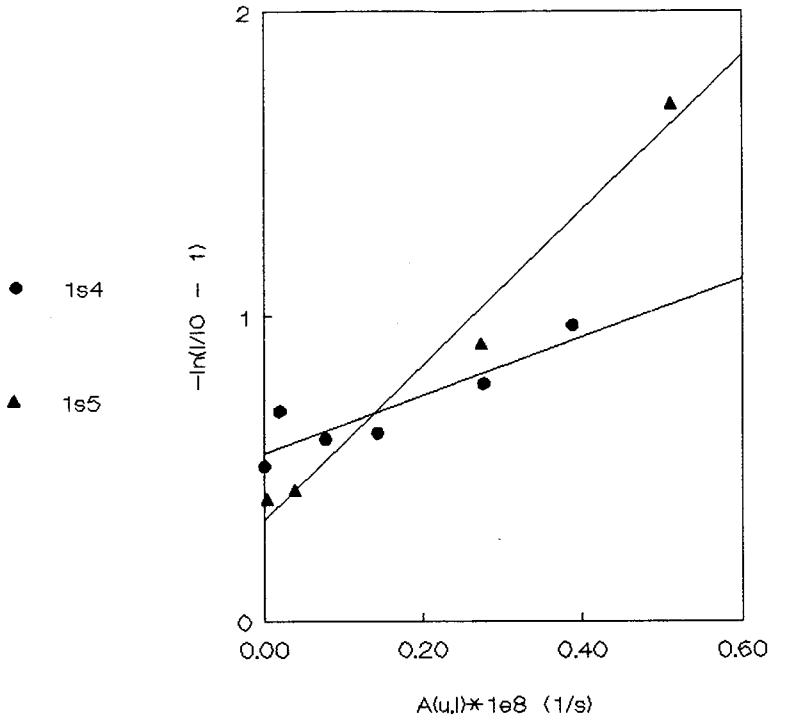


Fig. VI.4. The results of absorption measurements in the steady state. The conditions are standard (dry plasma, flows 12/0/0.7 l/min, power input 3 kV, 0.4 A), heigth 2 mm ALC, r = 0 mm (through the middle of the plasma). The ratio $(I_m - I_{nm})/I_{nm}$ is plotted as a function of transition probability corrected for statistical weigths: g(u)/g(l) A(u,l).

- ▲ the landing level is metastable ($1s_5$)
- ● the landing level is resonant ($1s_4$)

The slopes are proportional to densities of these levels, respectively. Their ratio is 2.9.

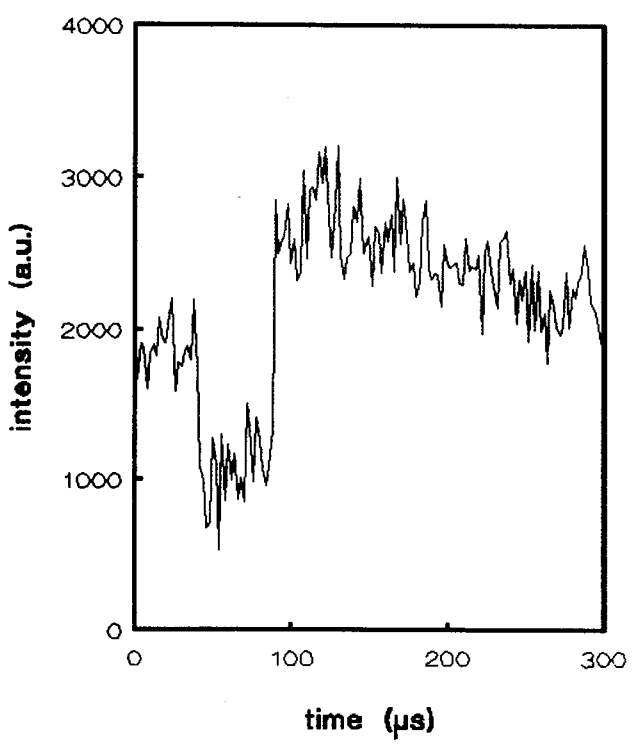


Fig. VI.5. A typical time behavior of ratio $(I_m - I_{nm})/I_{nm}$ for a partially reabsorbed line (here $\lambda$ = 811.5 nm) during the power interruption. This ratio is "inverted" with respect to a normal response. The jump down at cooling corresponds to increase of 4p density, the increase during the off-period corresponds to decay of 4s, etc.

measure is slightly detuned, the absorption is much smaller. The transition probabilities [WIE.69] used in Fig. VI.4 might contain an error up to 50%.

The combination of absorption measurement with the power interruption provides an interesting tool to study the response of 4s level. In Fig. VI.5 a ratio from (VI.9) (scaled by a constant) for 811.5 nm line as a function of time is shown. In Fig. VI.6 the ratios from (VI.9) are plotted against transition probabilities for the steady state, analogously to Fig. VI.4. The obtained density ratio is:

$$\frac{n(1s_5)}{n(1s_4)} = \frac{8.32}{2.26} = 3.7$$

so the result is fairly reproducible. The ratio of densities is always larger than this obtained assuming Boltzmann coupling. This supports the theoretical result. In Fig. VI.7 a ratio from (VI.9) after the cooling is plotted. It brings:

$$\frac{n(1s_5)}{n(1s_4)} = \frac{13.96}{4.73} = 3.0$$

From the ratio of slopes for steady state and off period we can obtain jumps for $1s_5$ and $1s_4$. They are:

$$\frac{n(1s_5)^*}{n(1s_5)} = 1.7$$
$$\frac{n(1s_4)^*}{n(1s_4)} = 2.1$$

The ionization energy of $1s_4$ is higher than this of $1s_5$. Nevertheless, the jump of $1s_4$ is higher than this of $1s_5$. This suggests that the metastable level is more overpopulated in the steady state than the resonant one. Both jumps are rather small, considering large ionization energy of 4s. Typical jumps of 4p (measured for optically thin transitions) are around 2 - 3. The low jumps of 4s are not due to lack of spatial resolution in the absorption measurement. The value of the 4p jump is obtained from a lateral scan at the same place as the absorption measurement. The spatial profiles of 4s and 4p are not likely to be very different. Neglecting the density of 4p in (VI.2) might decrease the jumps of 4s by 20%. However, the jump of 4s should be also a factor of 1.6 larger than this of 4p (see § VI, 2.1). Therefore we conclude that the jump of 4s is lower than it should be according to Saha. This is to be expected in an ionizing plasma (see § IV).

In Fig. VI.8 a full time behavior of the ratio $(I_m - I_{nm})/I_{nm}$ for the 811.5 nm line is shown. An interesting detail is lack of the delayed response. This would imply that the amplitude of this response in the 4s density is not larger than in 4p density (the argument is the same as the one about cooling jumps). If this effect is due to temperature fluctuation that according to Saha the jump for 4s should be larger than for 4p. This fact will be used in § VII to give an indication that the

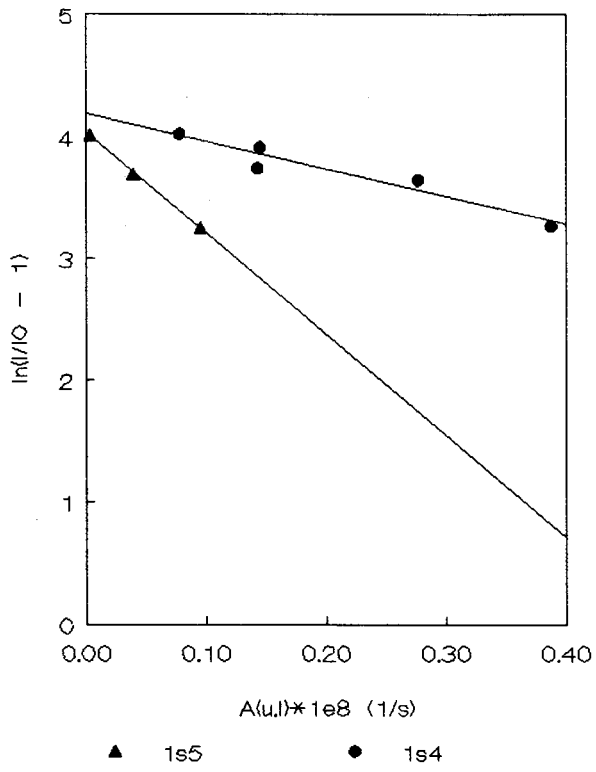


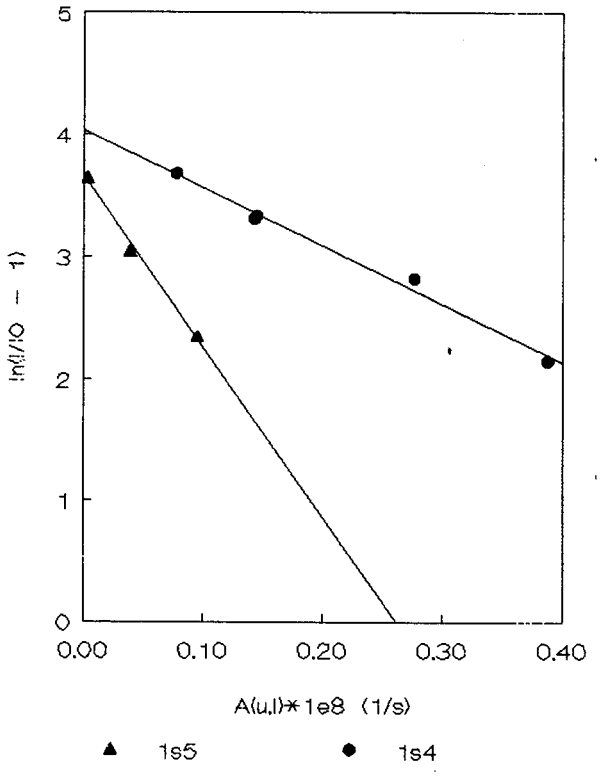


Fig. VI.7. The ratio $(I_m - I_{nm})/I_{nm}$ after the cooling is plotted against transition probabilities (like in Fig. VI.4). The ratio of slopes after the cooling is 3.0.

Fig. VI.6. The ratio $(I_m - I_{nm})/I_{nm}$ obtained in the power interruption experiment is plotted versus transition probability in the steady state, like in Fig. VI. 4. Here the conditions are the same, only r = 3 mm. The ratio of slopes is 3.7.

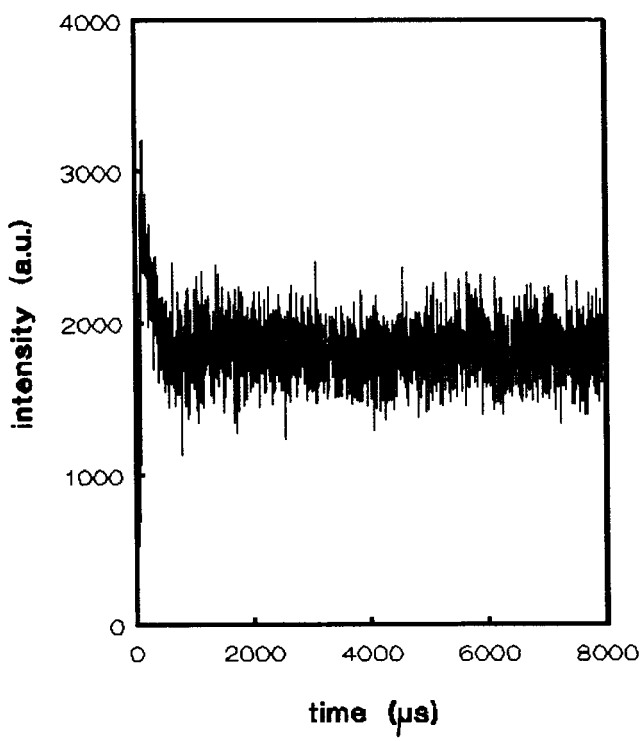


Fig. VI.8. A full time behavior of the ratio from Fig. VI.5. Note the absence of the delayed response.

delayed response is caused only by a fluctuation of electron temperature and density without changes in the ground state density (just like the instantaneous responses).

The experiment described above should be repeated using an external source of light. This would allow to avoid problems like reflectivity of the mirror. Moreover, the determination of $I_t/I_0$ would be straightforward. An attempt has been made to use a cascaded arc [WIL.91] as a light source. However, the emission lines of Ar from the arc are much broader than these from the ICP, so the reabsorption is hardly visible (Fig. VI.9). Despite using filters, the light intensity from the arc is so high, that it disturbs the balances in the ICP.

The measurements we have presented are not accurate enough. They should be repeated preferably using an external light source. It would be recommended to use a tunable laser as a light source (in addition to Laser Induced Fluorescence measurements). The techniques are very powerful for studying the levels inaccessible in emission. It would be very useful to know the behavior of 4s, as it can bring a lot of information about the deviations from equilibrium in the plasma. The preliminary results obtained using our inaccurate technique serve only as a challenge to study the problem more carefully in future.

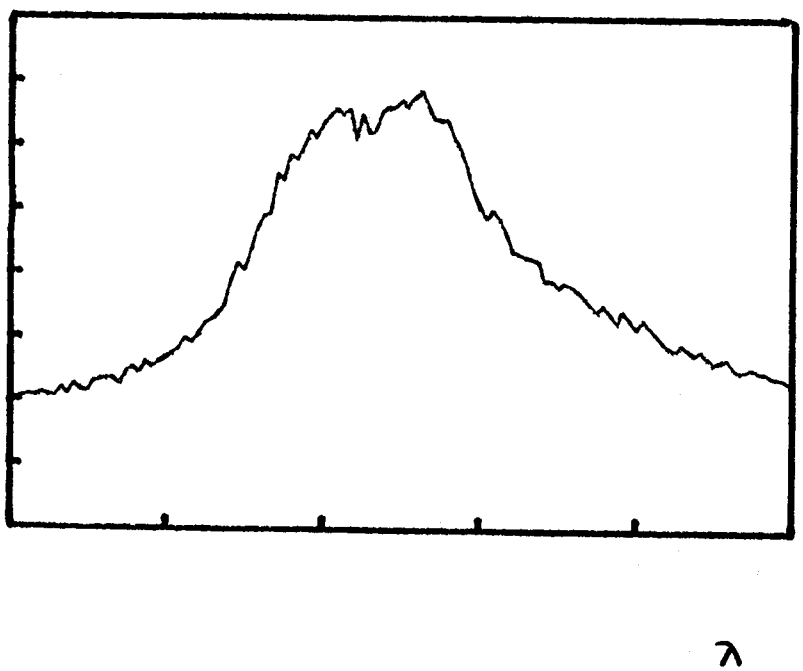


Fig. VI.9. A profile of the emission line from the cascaded arc ($\lambda$ = 811.5 nm). The full scale is 0.3 nm. On the top of the line profile the absorption dip from the ICP is visible.

# VII THE DELAYED RESPONSES

## VII.1 INTRODUCTION

The power interruption experiment gives two kinds of responses. In the previous chapters the instantaneous local responses have been discussed. In this chapter the delayed macroscopic response is treated. First it is shown by linearizing the continuity and the energy equation that a disturbance of electron temperature and density created underneath the load coil can propagate through the plasma with a velocity equal to the drift velocity of the plasma. The chapter continues with experimental data on the delayed response. Finally it is shown that this kind of disturbance is always present in the plasma (also in the steady state). The interruption experiment is only a way to trigger the event so it is observed more easily (there are also other methods of disturbing the local energy balance). The response is not an artifact due to the interruption. It is a fundamental plasma process which can be triggered by the power interruption.

## VII.2 THE PROPAGATION OF FLUCTUATIONS IN THE ICP

The power interruption experiment is an efficient method of creating disturbances in the plasma. There are several kinds of mechanisms of wave propagation for such disturbances. The most common mechanism is just a simple sonic wave propagation. This is also the most prominent effect of the power interruption experiment. The formation of this wave requires only the existence of a pressure gradient in the following (simplified) Navier - Stokes equation:

$$\partial \mathbf{w}/\partial t + (\mathbf{w}\cdot\nabla)w = -(\nabla p)/mn, \qquad \text{VII.1}$$

The above equation serves only to demonstrate a possibility of propagation of a dispersionless sonic wave. Therefore we do not consider the full equation: the viscosity term has been neglected. Also the EM force need not be taken into account, as the collision frequency of charged particles in the ICP is so large, that the plasma does not show any collective behavior in the EM field. A dispersion relation for a sonic wave can be found by linearizing the above equation together with the continuity equation for the gas, given below with respect to small perturbances in pressure ($\delta$p) and density ($\delta$n):

$$\partial n/\partial t + \nabla(n\mathbf{w}) = 0, \qquad \text{VII.2}$$

The source term in (VII.2) can be neglected as being too small to influence the bulk of gas. The

adiabatic relation between the pressure and velocity requires: $\delta p = c_0 \delta n$, where $c_0$ is the speed of sound. This treatment provides a dispersionless sonic wave, propagating with $c_0 = (kT_h/m_h)^{1/2}$ [LAN.87]. In the case of ICP it equals 1500 m/s. Such an unbalanced gradient of the total gas pressure is readily created in the power interruption experiment.

Another effect, which is most likely also present in the ICP is the propagation of so called ion sound waves. They are caused by local spatial separation of the positively and negatively charged particles. The dispersion relation for such a wave is [KAR.75]:

$$\omega = (k(T_e + \gamma T_h)/m_i)^{1/2}\, k / (1 + k^2D^2) \approx (k(T_e + \gamma T_h)/m_i)^{1/2}\, k\, (1 - D^2k^2 + ...)$$

where D is the Debye length. It can be easily seen that for long waves (with respect to the Debye length, $D^2k^2 \ll 1$), which can be expected in the ICP the group velocity of the disturbance is even larger than this of a "normal" sonic wave.

These two effects still do not clarify the origin of a wave like delayed response which travels with the drift velocity of the plasma. The time scale of the observed disturbance is in the order of a millisecond. The "fast" disturbances described above propagate with a speed of sound, so they will be present in the plasma only for a few microseconds. This time is so short that they will not leave any significant trace, as the fundamental processes like energy incoupling and especially ionization/recombination are slower. Therefore another mechanism has to be found.

It has been shown, that the local energy balance provides a relation between the electron temperature and density (see § V). From § V it follows that when the ICP power is switched on the electron temperature will exceed its steady state value. In case of a uniform plasma this disturbance will monotonically decay towards the steady state $T_e$. However, if there are significant longitudinal gradients of $n_e$ and $T_e$ (like in the region below the coils), the disturbances of $n_e$ and $T_e$ will be propagated spatially due to gradient terms in the continuity and energy equation. Further the properties of such propagation will be investigated.

In order to describe fully any disturbance in the ICP, generally the full time dependent behavior of this plasma should be considered. Such a task is extremely time consuming and by no means can be treated analytically. Nevertheless it does not mean that before such a general description is created it is impossible to find the cause of the observed effects. Remembering that our goal is only to obtain the insight into the processes, leading to propagation of such disturbances we will not aim at the high accuracy of the obtained results. In order to provide a possible mechanism we have to introduce several simplifications:

1) The considered disturbance is assumed to be small, so the nonlinear flow equations can be linearized. This simplification is very drastic and not correct when a full description is required. It will appear, that in fact the disturbance should be described by a nonlinear equation. However, the nonlinear effects can bring some information about the shape of the wave packet, the amplitude - frequency relation, etc., while at this state of knowledge we only need to know the origin of the

disturbance and its velocity. This can be obtained from a simple linearized equation. The nonlinear treatment is extremely complicated and it probably involves analysis the full system of flow equation. As it will appear later in this chapter, the physical properties of the ICP, like the rate of energy input, ionization, etc. are not known well enough to serve as a base of an accurate treatment.

2) We assume the disturbance to be a purely longitudinal effect, so all the radial changes can be neglected. This is a basis of a slab model. By assuming this we exclude from our considerations some effects which could be due to radial recirculation of the gas, etc.

3) The disturbance is purely an electron effect. It is not related to the pressure gradients of neutral particles (anyway, due to a small ionization degree, the role of ionized particles in the total flow equations is small). It allows to exclude the flow equations for heavy particles, as they are assumed to be all the time in the steady state. This assumption is valid for small disturbances (e.g. the ones created in the steady state or by a short power interruption). An experimental fact supporting this assumption has been discussed in § VI (Absorption measurements). It has been shown that the amplitude of the disturbance does not increase with ionization energy of a level as it should according to Saha. For the lower levels (4p and 4s) it is too low. This resembles very much the dependence of the cooling jump (which is only due to $T_e$ changes) on the ionization energy. Moreover, the amplitude of the disturbance can be even 100% of the steady state intensity value. If this were caused by a fluctuation in the ground state density, it would require the ground state density also to increase twice. If the total gas pressure has to stay constant (it has to, else a sonic wave propagates) the heavy particles temperature has to decrease twice ($p = nkT_h$). This change is very drastic and as it will appear in the experimental part, not justified. Possibly there might be a combined electron - heavy particles effect, in which $\gamma$ stays constant. The experimental verification of it is still not completely clear.

4) The drift velocity of electrons is the same as the gas velocity ($w_e = w$). This is a consequence of the assumption 2). As the motion of gas is approximated to be one dimensional, the charged particles have to move at the same velocity. If the electron velocity differs from the heavy particles velocity the electric field appears due to charge separation and the quasi neutrality is reestablished on a time scale of one microsecond (a typical time scale for propagation of ion sound waves, mentioned above). Therefore we need not consider the momentum equation for electrons (it is assumed to be satisfied automatically).

5) The effects like heat conduction, diffusion and radiative losses are neglected. They might, however, cause an additional smearing out of the disturbance profile. Heat conduction and radiative losses have been estimated to be smaller than the convective terms. As their actual influence as well as their dependencies on plasma parameters are not known, we shall not include them in our equations. We shall remember, however, that they form an additional loss term, probably not large enough to quench the wave profile.

6) The collisional ionization/recombination mechanism is used, as being the best known one. There are many possible recombination channels (see § V), but most likely there is only one

ionization channel (collisional). The collective ionization constant for the collisional process [BEN.90] has an easy analytical form. However, this constant has been calculated for a low pressure plasma at high temperatures. This is the only available data, but we should be aware that it need not fit perfectly for the ICP conditions.

7) The energy input and collisional losses have been proven to be much faster than the ionization/recombination processes and the observed time scale of the disturbance. However, we cannot assume this balance to be all the time in equilibrium. The energy input terms are larger than convection and ionization. Therefore for a system for which the energy input is almost completely balanced by the losses the difference $\sigma E^2 - (\nu_{ei}+\nu_{ea})n_e(T_e-T_h)$ will be much smaller than any of the terms separately, but it can be in the order of convection and ionization terms.

Therefore the considered set of equations can be finally written in the form (see § V):

**1) energy equation:**

$$3/2\ \partial(n_eT_e)/\partial t + 3/2\ w\ \partial(n_eT_e)/\partial z + 5/2\ n_eT_e\ \partial w/\partial z = \sigma_e E^2 - 3/2\ (2\ m_e/m_h)\ (\nu_{ei} + \nu_{ea})\ n_e\ (T_e - T_h) - (\kappa_{ion}\ n_a n_e - \kappa_{rec}\ n_e^3)\ E_{ion} \qquad \text{VII.3}$$

**2) continuity equation:**

$$\partial n_e/\partial t + \partial(n_e w)/\partial z = \kappa_{ion}\ n_a n_e - \kappa_{rec}\ n_e^3 \qquad \text{VII.4}$$

Further we shall introduce:

$$\sigma_e E^2 - 3\ m_e/m_h\ (\nu_{ei} + \nu_{ea})\ n_e\ (T_e - T_h) \equiv \phi(n_e,T_e)$$
$$\kappa_{ion}\ n_a n_e - \kappa_{rec}\ n_e^3 \equiv J(n_e,T_e)$$

Electron temperature will be here expressed in eV, $n_e$ in $m^{-3}$. The longitudinal steady state profiles of $n_e(z)$, $T_e(z)$, $T_h(z)$ and $v(z)$ satisfy the appropriate steady state equations. Now a disturbance from the steady state can be introduced in the form of a planar wave:

$$n_e = n_{e0} + A \exp i(kz - \omega t), \qquad \text{VII.5}$$
$$T_e = T_{e0} + B \exp i(kz - \omega t). \qquad \text{VII.6}$$

Introducing (VII.5) and (VII.6) into (VII.3) and (VII.4) and linearizing these equations with respect to A and B we obtain:

$$\alpha_{11} A + \alpha_{12} B = 0$$
$$\alpha_{21} A + \alpha_{22} B = 0, \qquad \text{VII.7}$$

where:

$$\alpha_{11} = T_{e0}\, i(kw - \omega) + 5/3\, T_{e0}\, \partial w/\partial z - 2/3\, \partial\phi/\partial n_e + 2/3\, E_{ion}\, \partial J/\partial n_e$$
$$\alpha_{12} = n_{e0}\, i(kw - \omega) + 5/3\, n_{e0}\, \partial w/\partial z - 2/3\, \partial\phi/\partial T_e + 2/3\, E_{ion}\, \partial J/\partial T_e$$
$$\alpha_{21} = i(kw - \omega) + \partial w/\partial z - \partial J/\partial n_e$$
$$\alpha_{22} = - \partial J/\partial T_e$$

Further we introduce the following notation:

$$P \equiv kw - \omega,$$
$$\partial J/\partial n_e \equiv J_n$$
$$\partial J/\partial T_e \equiv J_t$$
$$\partial\phi/\partial n_e \equiv \phi_n$$
$$\partial\phi/\partial T_e \equiv \phi_t$$
$$\partial w/\partial z \equiv \delta$$

The spatial profile of the gas velocity is not completely known (like many other things in the above equations). This might create a problem in evaluating $\delta$. In order to simplify our considerations we will assume that w grows linearly in the region below the coils ($\delta$ = const > 0) and further it stays constant ($\delta$ = 0).

The existence of nontrivial solutions of (VII.7) requires $\alpha_{11}\,\alpha_{22} - \alpha_{12}\,\alpha_{21} = 0$, which leads to the dispersion relation:

$$n_{e0}\,(iP)^2 + \{J_t T_{e0} - J_n n_{e0} + 8/3\, n_{e0}\delta - 2/3\, \phi_t + 2/3\, E_{ion}\, J_t\}\, iP +$$
$$+ 5/3\, \delta\,(J_t T_{e0} - J_n n_{e0}) + 2/3\,(J_n\phi_t - J_t\phi_n) + 5/3\, n_{e0}\delta^2 - 2/3\, \phi_t\delta$$
$$+ 2/3\, E_{ion} J_t\delta = 0 \qquad \text{VII.8}$$

The solutions of this equation are:

$$iP = - \{J_t T_{e0} - J_n n_{e0} + 8/3\, n_{e0}\delta - 2/3\, \phi_t + 2/3\, E_{ion}\, J_t\}/2n_{e0} \pm \sqrt{\Delta}/2n_{e0} \qquad \text{VII.9}$$

where $\Delta$ is the discriminator of the equation (VII.8).

The planar wave has the form (VII.5) or (VII.6). Substituting $\omega = \omega_r + i\omega_i$ in (VII.5) or (VII.6) we obtain:

$$\exp i(kz - \omega t) = \exp i(kz - \omega_r t)\, \exp(\omega_i t)$$

The real part of $\omega$ determines the group velocity of the wave, while the imaginary part of $\omega$ describes the amplification (damping) of the amplitude. Having an expression for P we can calculate $\omega_r$ and $\omega_i$. Remembering that $P = kw - \omega$ we find:

$$\omega_r = kw - Re(P) \qquad \text{VII.10a}$$

$$\omega_i = - Im(P) \qquad \text{VII.10b}$$

Form (VII.9) we see that if $\Delta \geq 0$ then $Re(P) = 0$ and the group velocity of this wave ($\partial\omega_r/\partial k$) equals the drift velocity of the gas. The imaginary part of $\omega$ determines the time behavior of the amplitude of the wave: if $\omega_i > 0$ our wave is amplified and if $\omega_i < 0$ it is damped. The evaluation of the terms in (VII.9) for the ICP conditions is very difficult, as it requires a knowledge of not only the absolute rates of plasma processes but also their exact dependencies on plasma parameters. However, we shall present such an attempt.

The most troublesome part of this analysis is the evaluation of the energy input terms. In § V we could avoid this problem by assuming some steady state solution. Here we need *absolute* values of $\phi$, so they can be compared with *absolute* values of J (also not well known). However, we have to use this method here again, being aware that the results should not be fully trusted. Contrariwise, it is to be expected that the sign of $\omega_i$ will depend critically on the values of J, $\phi$ and their derivatives. This is due to a demand, that two large terms in (VII.3) should cancel, leaving only a small rest term.

First we note that $\phi_n$ and $\phi_t$ are negative. The fact that $\phi_n < 0$ is to be expected, as the collisional loss term is approximately quadratic with $n_e$, while the energy input is practically $n_e$ independent. The latter fact ($\phi_t < 0$) has been said in § V to be a necessary criterion for stability of energy input. The quantities $J_n$ and $J_t$ are positive. Therefore the first term in (VII.9) is always negative provided $J_n T_{e0}$ is large enough so it can dominate the others. This is, however, not true. Hereby we give some estimates of the terms in (VII.9) for the assumed steady state conditions $n_e = 10^{21}$ m$^{-3}$, $T_e = 1$ eV, $\gamma = 1.3$ (like in § V). Thus we have:

$$J_n = 2\times 10^4 \text{ s}^{-1}$$
$$J_t = 2.7\times 10^{26} \text{ m}^{-3} \text{ s}^{-1} \text{ eV}^{-1}$$
$$\phi_n = - 2.5\times 10^5 \text{ eV s}^{-1}$$
$$\phi_t = - 10^{26} \text{ m}^{-3} \text{ s}^{-1} \qquad \text{VII.11}$$

The evaluation of $J_n$, $J_t$ is based on the following formula for the collective ionization constant ([BEN.90]; see also [WIL.83]):

$$\ln(\kappa_{ion}) = aT_{e0}^4 + bT_{e0}^3 + cT_{e0}^2 + dT_{e0} + e,$$

In the above formula $\kappa_{ion}$ is given in $m^3/s$, $T_{e0}$ in K. a = - 2.69983×$10^{-15}$, b = 1.21373×$10^{-10}$, c = - 2.1524×$10^{-6}$, d = 1.89074×$10^{-2}$, e = -114.838. Remembering that $J(n_{e0},T_{e0}) = \kappa_{ion}\, n_a n_{e0} - \kappa_{rec}\, n_{e0}^3$, we can calculate:

$$J_n = \kappa_{ion} n_a - 3\kappa_{rec} n_{e0}^2$$
$$J_t = \partial\kappa_{ion}/\partial T_{e0}\; n_a n_{e0} - \partial\kappa_{rec}/\partial T_{e0}\; n_{e0}^3$$

The numerical values (VII.11) are obtained from these formulae. For evaluation we keep $n_a$ constant with $n_e$ and $T_e$, calculated from the total pressure: $n_a = p/kT_h$. This is justified in a strongly ionizing plasma, with a low ionization degree. This leads to $J_n > 0$, $J_t > 0$. If our steady state plasma were not ionizing, but close to Saha, $J_n$ would be negative, as it is required by stability condition.

In order to evaluate $\delta$ we assume that the drift velocity of the gas changes from 0 to 10 m/s over 1 cm (see § IV). Thus $\delta = 10/10^{-2}\ s^{-1} = 10^3\ s^{-1}$. Note that $\delta$ calculated in this way is already overestimated.

Now we have to compare magnitudes of the components in (VII.9). For the assumed conditions:

$$J_t T_{e0} - J_n n_{e0} \simeq 10^{26}$$
$$8/3\; n_{e0}\delta \simeq 10^{25}$$
$$-2/3\; \phi_t \simeq 10^{25} - 10^{26}$$
$$2/3\; E_{ion}\, J_t \simeq 10^{27}$$

The first three terms can be thus neglected. The full expression for $\Delta$ is:

$$\Delta = \{J_t T_{e0} - J_n n_{e0} + 8/3\; n_{e0}\delta - 2/3\; \phi_t + 2/3\; E_{ion}\, J_t\}^2$$
$$- 4n_{e0}\{5/3\; \delta\,(J_t T_{e0} - J_n n_{e0}) + 2/3\,(J_n\phi_t - J_t\phi_n) + 5/3\; n_{e0}\delta^2 - 2/3\; \phi_t\delta$$
$$+ 2/3\; E_{ion} J_t \delta\}$$

The leading term in the first part is $(2/3\; E_{ion}\, J_t)^2 \simeq 10^{54}$, in the second part $8/3\; n_{e0}\,(J_n\phi_t - J_t\phi_n) \simeq 10^{53}$, but $2/3\; \phi_t\delta$ and $2/3\; E_{ion}J_t\delta$ can be also large ($10^{52}$). Normally they do not exceed the first term, so $\Delta > 0$. This provides that P is purely imaginary (see (VII.9)) and the group velocity of the disturbance equals the drift velocity of gas. There are two solutions for P. One of them has always Im(P) > 0. This one will always describe a damped wave (see (VII.10b)) with a damping factor in the order of $10^6\ s^{-1}$ and therefore it is not interesting. The other solution can give Im(P) < 0, if the two large terms in (VII.9) cancel. The sign of $J_n\phi_t - J_t\phi_n$ will determine the sign of Im(P) for this solution. When the conditions given above are assumed, $J_n\phi_t - J_t\phi_n > 0$, which would give a damped wave (with a damping factor in the order of $10^4\ s^{-1}$). Typically, we see that the collisional loss term is too large with respect to the energy input term. This causes the absolute value of $\phi_n$ to be too large and $\phi_t$ too small. This problem has been already encountered i

n § V. Therefore in reality one cannot state that the wave is always damped. Here if we "artificially" reduce the loss term by introducing a low electron density at relatively high temperature: $n_e = 10^{20}$ $m^{-3}$, $T_e = 0.8$ eV, $\gamma = 1.2$, we obtain the following values: $J_n = 1.7\times10^3$, $J_t = 3.4\times10^{24}$, $\phi_n = -2.5\times10^4$, $\phi_t = -7.3\times10^{25}$. Immediately we see that the wave becomes amplified with an amplification factor $10^3$ $s^{-1}$. Generally we may state that it is very risky to compare such large numbers, which absolute values are not well known and which should cancel leaving a small term. Therefore we conclude that based on this analysis one cannot decide whether the wave should be damped or amplified. From the experiment it follows that the disturbance is amplified and the calculations do not contradict it.

From the above calculations we can obtain some information about the phase shift between the electron density and temperature. Considering the last equation in (VII.7) it can be found that:

$$\Delta n_e/\Delta T_e \equiv A/B = -\alpha_{22}/\alpha_{21} = J_t/(iP - J_n)$$

Since iP is real the phase shift is either 0 or $\pi$. For a magnified wave Im(P) < 0. Therefore for iP = $|P| > 0$. If $|P| < J_n$ the disturbances of $n_e$ and $T_e$ will be in counterphase. Experimentally $|P| \simeq 10^3$ $s^{-1}$, which is probably smaller than $J_n$.

The linear approach presented above describes a disturbance in the energy and ionization balance for electrons, which propagates as a wave with the drift velocity of the plasma. It is a possible mechanism of creation and propagation of the disturbance, observed in the ICP. The data about the rates of fundamental plasma processes in not sufficient to describe fully this wave. Moreover, within this approximation it is impossible to predict its actual shape and frequency. These parameters must be obtained from the nonlinear theory, possibly taking into account all the kinetic equations. We are also aware, that in many cases using of the linear equations is not justified (the disturbance need not be so small). For large disturbances the assumption, that the heavy particle parameters do not change is not valid anymore. Therefore one should not demand that the theoretical data fit strictly with the experimental ones.

In the following experimental section the data concerning the wave like delayed response will be presented.

## VII.3 EXPERIMENTAL DATA

In Fig. VII.1 the delayed responses of several lines are shown. They are clearly separated in two groups. Ar, H, N and the continuum (at $\lambda$ = 700 - 800 nm) give relatively large responses (typically about 50 - 100% of the steady state intensity), whereas the responses of the analytes are smaller and less regular. Furthermore there is a phase shift of 180 degrees between the two categories. Both have the same period $\tau$ = 1 - 1.2 ms. The shift of the response of continuum is

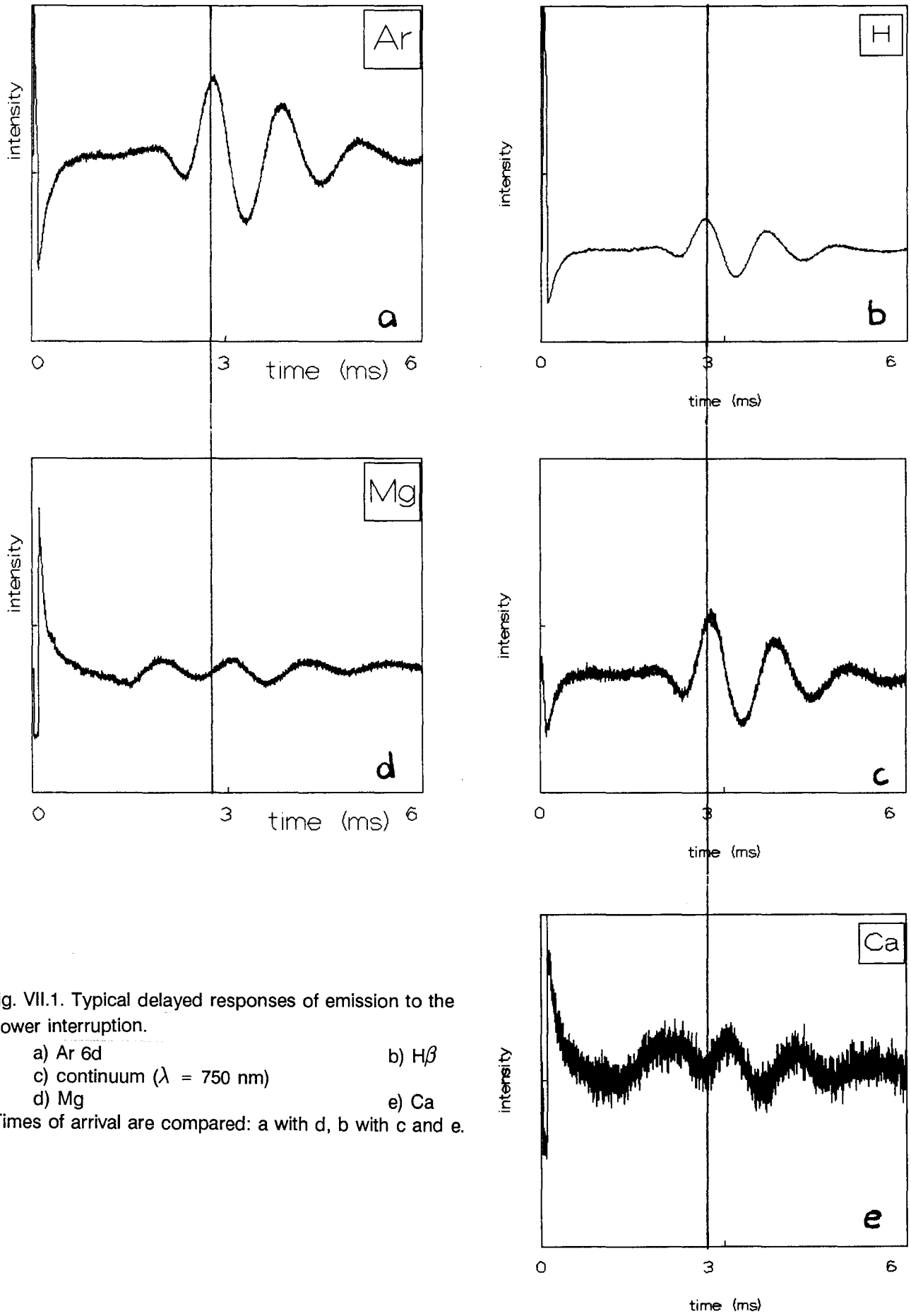


Fig. VII.1. Typical delayed responses of emission to the power interruption.

a) Ar 6d b) H$\beta$
c) continuum ($\lambda$ = 750 nm)
d) Mg e) Ca

Times of arrival are compared: a with d, b with c and e.

wavelength dependent and it will be discussed later.

The phase shift is explained by assuming that the first category of states is governed by the Saha balance and the second one by a Boltzmann like or ESB balance (see § II and [STO.91/3]). The reaction of these states to changing $n_e$ and $T_e$ is different. Suppose that when $n_e$ higher than $n_{e0}$ (steady state), $T_e$ is lower than $T_{e0}$. For a Saha governed level $n(p) \sim n_e^2\, T_e^{-3/2} \exp(E_{ion}/kT_e)$, so a lower $T_e$ and a higher $n_e$ magnify the amplitude doubly. A Boltzmann or ESB governed state does not react to changing $n_e$. Its density changes with temperature according to $n \sim \exp(-E/kT_e)$, so it decreases with decreasing temperature and therefore is in counterphase with a Saha governed state. In [STO.91/3] it is shown, that the transition between the Saha like and Boltzmann like behavior is possible. Fig. VII.2 shows delayed responses of Li for several flows. It is clear that if the transition occurs, the phase shift between the two responses appears. The irregular shape of the responses for analytes is not understood, but it might be related to the large influence of fast diffusion due to the droplets in which analytes are introduced in the plasma.

The disturbance is travelling through the plasma with a velocity close to the drift velocity of argon (see § IV). Knowing the velocity and the time of arrival a place from where the disturbance originates can be found. This place is typically 5 mm underneath the load coil, but it might vary depending on how far the plasma extends below the coils. Fig. VII.3 shows how the disturbance is formed in this area. As soon as it reaches the coil it is amplified and it gets its usual shape. Further

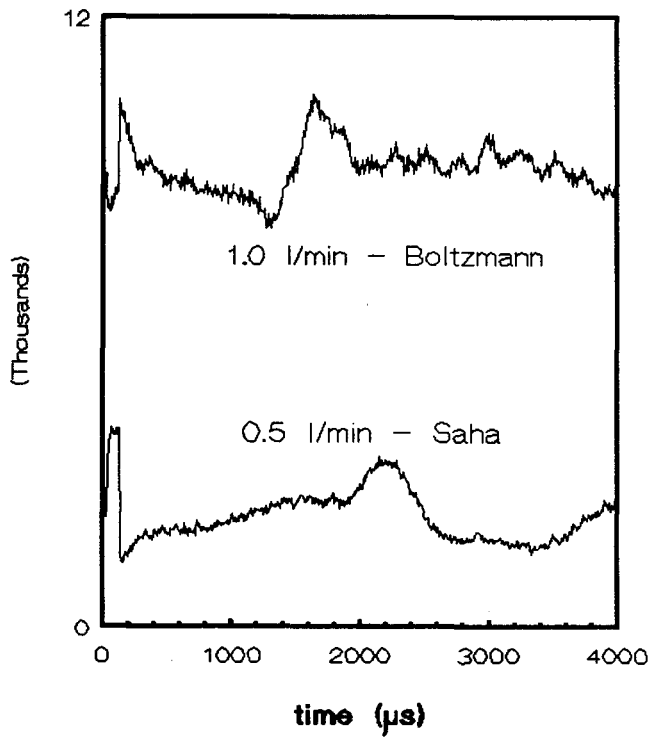


Fig. VII.2. Delayed responses of Li 2p - 2s line for two different central flows. The instantaneous responses are opposite and delayed responses are phase shifted.

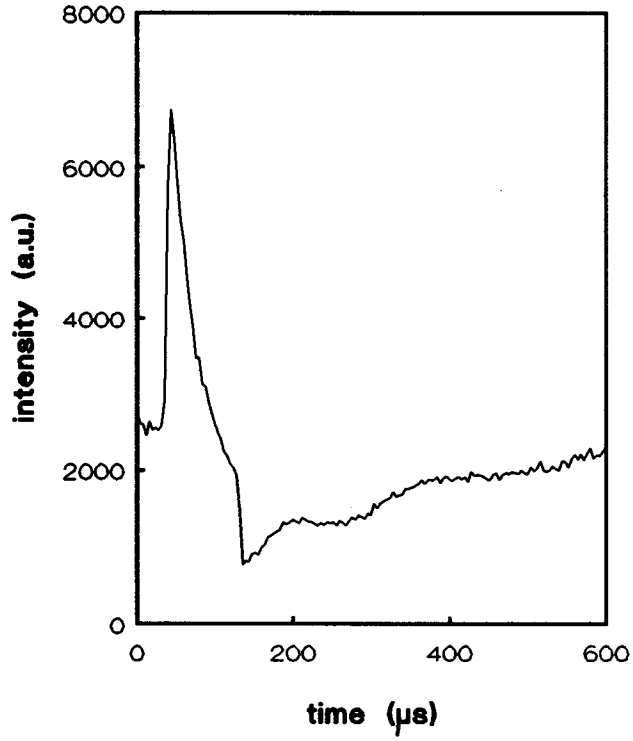


Fig. VII.3. A typical response of Ar 6s line measured 3 mm below the load coil (BLC). The delayed response has a very small amplitude and it follows immediately the instantaneous response.

it is still amplified and transported up through the plasma. When it arrives at c.a. 1 cm above the load coils, its amplitude does not increase anymore and higher it is fast damped. The Fig. VII.4 shows the amplitude of the traveling disturbance dependent on the distance from the place in the plasma, where it was created. The measurement is performed for Ar 549.7 nm line. The increase in amplitude of intensity in time can be approximated by:

$$\Delta I/I = 3.9 \exp(1.05\times 10^2\ x) \qquad \text{(x in meters) or}$$

$$\Delta I/I = 3.9 \exp(1.3\times 10^3\ t) \qquad \text{(t in seconds)}$$

(assuming velocity of gas 12 m/s).

Using the Saha equation and assuming that $n_e$ and $T_e$ are in counterphase with the same relative amplitudes: $\Delta n_e/n_{e0} \approx -\Delta T_e/T_{e0}$ (it will be justified later) we can relate this to the disturbance of $n_e$:

$$\Delta I/I = (2 + 3/2 + E_{ion}/T_{e0})\ \Delta n_e/n_{e0}$$

where $E_{ion}$ = 0.428 eV. Assuming flat profiles of $n_e$ and $T_e$ along the plasma (the actual ones are not very well known) we see that the experimental amplification factor $\omega_i$ is in the order of $10^3$ $s^{-1}$.

Fig. VII.4. Amplitude of the delayed response as a function of the height in the plasma. Dashed lines indicate the coils. Here the amplitude is defined in % of the steady state intensity (I), i.e. $(I_{max} - I)/I \times 100\%$, $I_{max}$ always refers to the first (largest) maximum.

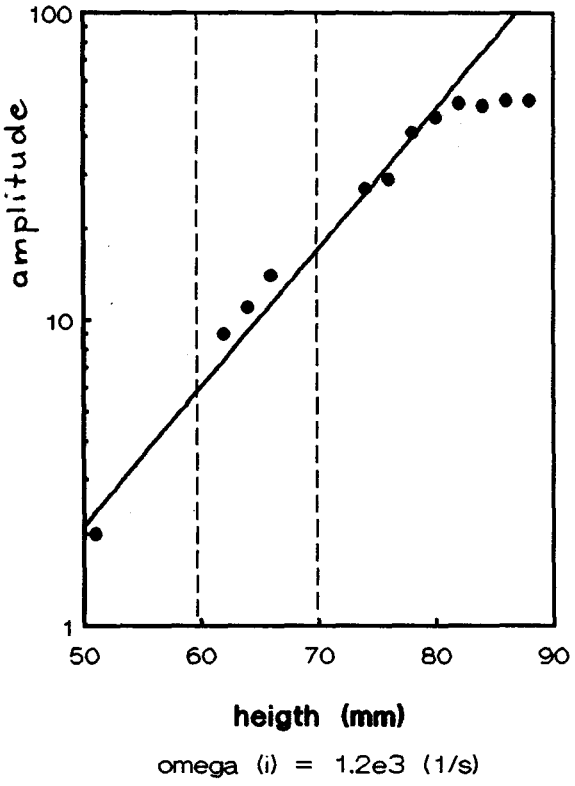


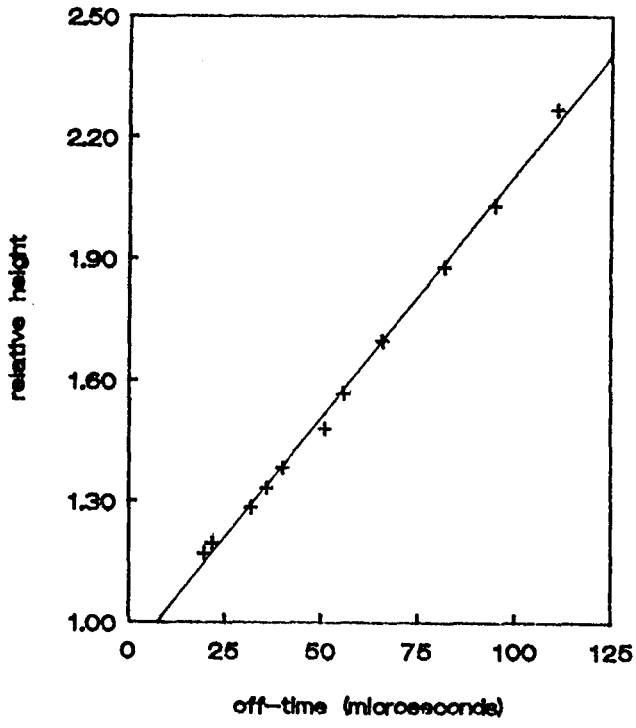


Fig. VII.5. Relative height of the disturbance ($I_{max}/I$) as a function of the off-time ($\mu$s).

The height of the disturbance depends linearly on the off time of the generator (Fig. VII.5). The increase can be understood, as the long off period causes large disturbances of electron temperature and density at the moment of switching the generator on. However, if we remember, that the electron density decay with time obeys:

$$n_e \sim \exp(-at) \quad \text{or} \quad n_e^{-1} \sim b + ct$$

(see § V), we can predict the magnitude of the disturbance in $T_e$. The relation between the peak $T_e^p$ after the heating and the electron density after $t = \tau_{off}$, derived in § V can be approximated as $n_e T_e^p \sim$ const. Therefore $T_e^p \sim \exp(a\tau_{off})$ or $b + c\tau_{off}$, so the deviation of temperature above the steady state value grows linearly with the off time. Since emission intensity does not depend linearly on $T_e$ we cannot explain the linear increase of the amplitude in intensity.

In Fig. VII.6 the radial dependence of the relative height of the disturbance is given for Ar 6s (703 nm) line. This profile is obtained from Abel inverted data of a lateral scan with 25 points (the one used in § IV and V). It is clear that the delayed response is mainly a skin effect. It can be expected, as the disturbance is assumed to originate from the deviation of electron temperature and

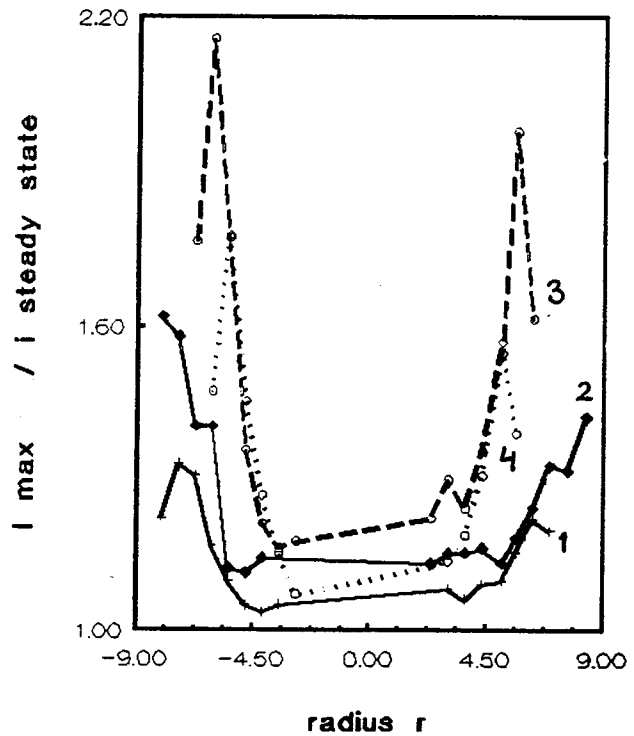


Fig. VII.6. Radially resolved height of the disturbance for 6s Ar line for several plasma conditions:
1 dry plasma, flows: 12/0/0.7 l/min,
power input: V = 3 kV, I = 0.4 A (normal)
2 dry plasma, flows: 12/0/0.7 l/min,
power input: 3.5 kV, 0.45 A (higher)
3 $H_2O$ injection, flows 12/0/0.7 l/min
power input: V = 3.2 kV, 0.37 A
4 0.05 l/min $H_2$ in the central flow, flows:
12/0/0.7 l/min, power input:
3.3 kV, 0.35 3.5 kV, 0.45 A
These data are obtained from Abel inverted lateral scan, used also in § IV and V.

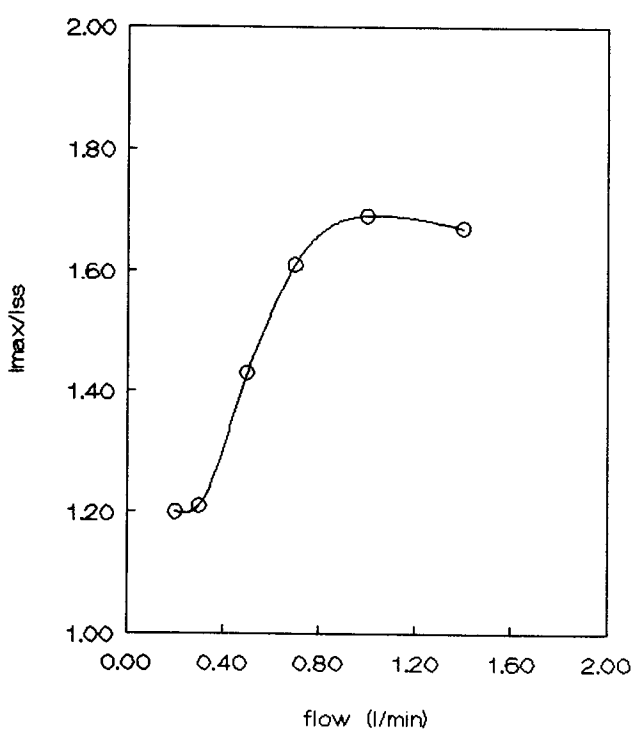


Fig. VII.7. Dependence of the height of the disturbance ($I_{max}/I_{ss}$) on the central flow.

density at the moment of switching on the generator. This disturbance is largest in the skin (see § V), as most of the EM field energy is coupled there.

The amplitude of the disturbance is slightly increasing with increasing power. The injection of hydrogen and especially water amplify it significantly (Fig. VII.6). This also can be understood, as hydrogen and water substantially cool the plasma underneath the coils (evaporation of $H_2O$ and dissociation of $H_2$ and $H_2O$ consumes energy). This results in larger gradients in the expansion zone, and eventually in propagation of larger disturbances. Consequently, the amplitude of the delayed response increases with increasing amount of water injected into the plasma (i.e. increasing central flow, Fig. VII.7).

Fig. VII.8 shows the radial time of arrival at a height of 5 mm ALC for several plasma conditions. It can be immediately seen that the time of arrival is smaller in the wet plasma. This is probably not related to the differences in drift velocities between the dry and wet plasma. Typically the dry plasma extends more below the load coil, so the place in which the disturbance is created is more distant. In a wet plasma changing the central flow in the region 0.5 - 1.0 l/min causes only a small decrease in the time of arrival (about 50 $\mu$s), so once water is introduced, the size of wet plasma stays approximately constant.

For a dry plasma a Poiseuille like profile is found with a maximum velocity in the middle and a smooth falling off to the sides. As expected the velocity in the plasma with a higher power input is larger. For a plasma with hydrogen or water injection the profile is flat. The sloped profile across the plasma is due to the coil geometry. The energy incoupling is larger at one side of the plasma and consequently the gas velocity is slightly higher. The velocity profile can be considered uniform over all the plasma cross section. This is a typical feature of a turbulent flow. The flow is not expected to be turbulent as the Reynolds number:

$$R = w \Lambda / \eta = 1000, \text{ [JON.91]}$$

where $\Lambda$ is the characteristic length, $\eta$ - viscosity.

The theory predicts a laminary flow for $R < 2000$. However, the calculations from which the value of R is obtained were carried out for pure argon plasma,so the possible influence of water and other additives to the plasma was neglected. Therefore turbulency might occur in the plasma. It has a major influence on the modeling of the plasma as the diffusion can become much more dominant. The behavior of analytes [STO.91/3] in the interruption experiment might be also related to this effect.

In Fig. VII.9 the logarithm of the height of the disturbance as a function of the ionization energy of several Ar levels is plotted. Assuming that the disturbance is caused by a fluctuation of $n_e$ and $T_e$ and applying Saha's law (see § III and IV), the electron temperature and density in the maximum or minimum of the disturbance can be found. Assuming Saha equilibrium for the excited states one can derive that the parameters of the line in Fig. VII.9 equal:

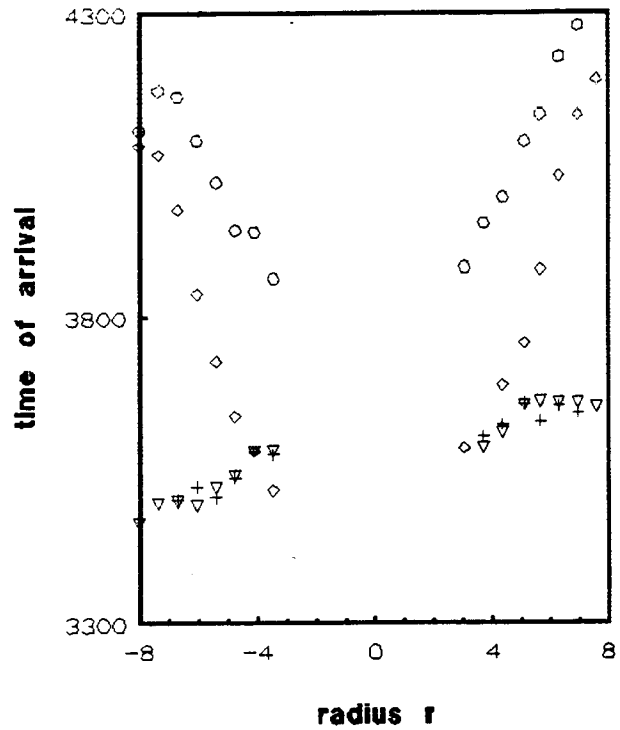


Fig. VII.8. Radially resolved time of arrival of the first maximum of the disturbance. Conditions are the same as in Fig. VII.6.

- o normal power
- ◇ high power
- + $H_2O$ injection
- ▽ $H_2$ injection

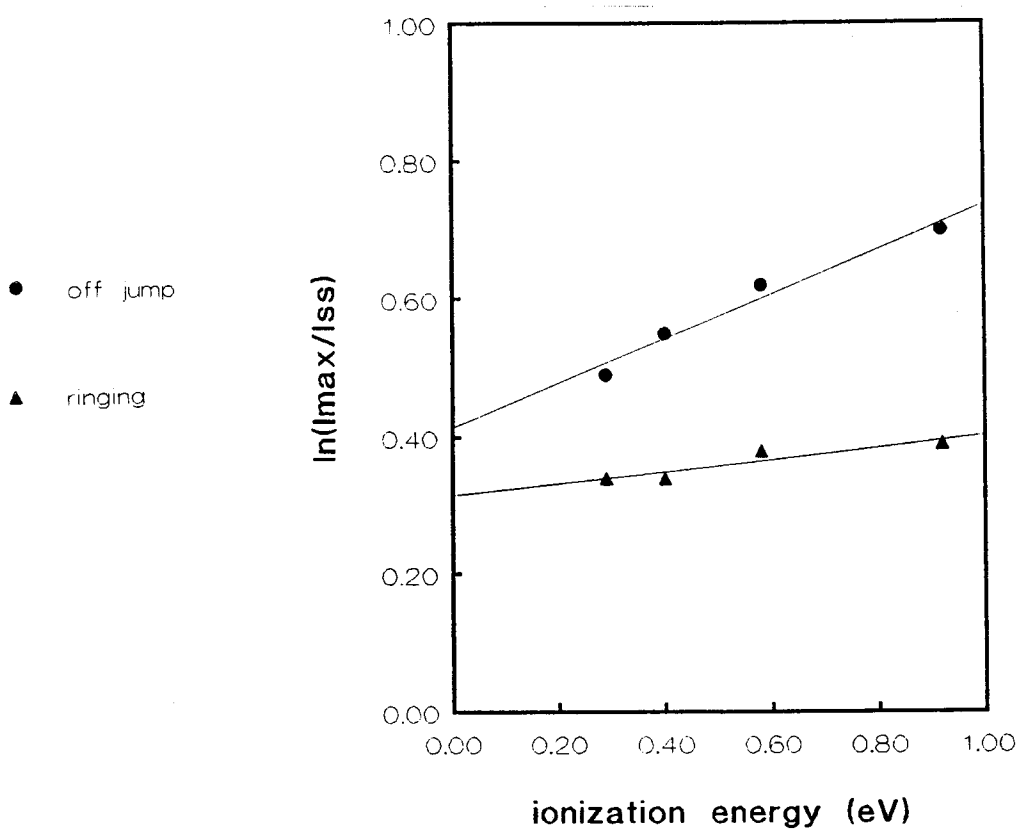


Fig. VII.9. Relative height of the delayed response (ringing) as a function of ionization energy for several Ar levels. In the same picture the cooling jumps of the instantaneous response are plotted. The conditions are: 5 mm ALC, r = 4 mm, flows: 12/0/0.7 l/min, with water injection. The cooling jumps give $\gamma$ = 1.32, $T_e$ = 0.98 eV. The heigth of delayed response gives $T_e^*/T_e$ = 0.92, $n_e^*/n_e$ = 1.10.

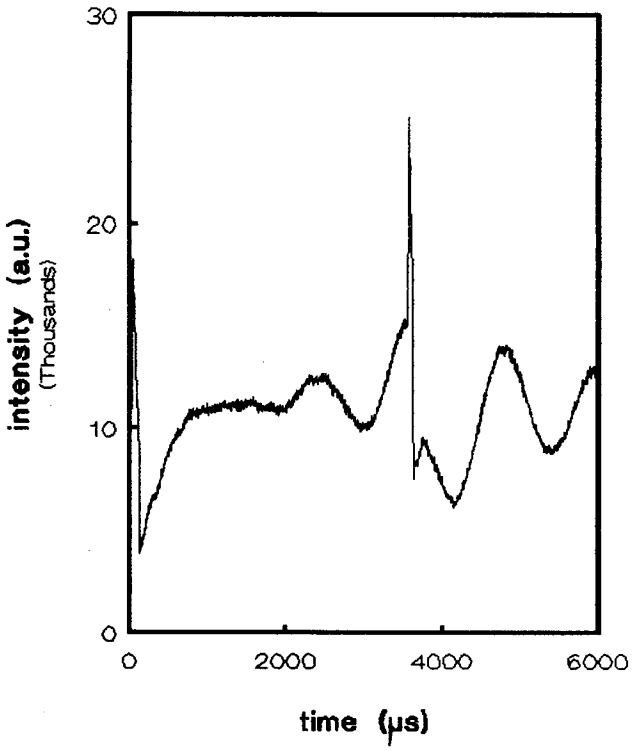


Fig. VII.10. A typical time behavior of Ar line emission in the "double interruption experiment". The time delay between pulses can be regulated. Here the second pulse is applied when the 1st maximum of the delayed response passes the observation zone.

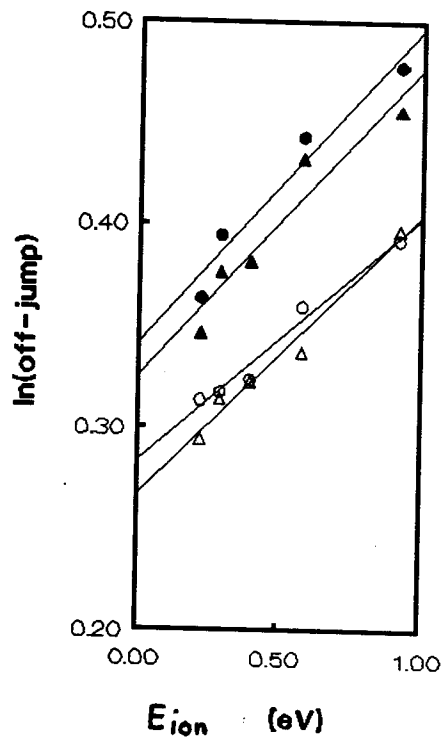


Fig. VII.11. The results of the "double interruption" for two central flows. The other conditions are like in Fig. VII.9. The temperatures determined from these data are:

- o flow 0.2 l/min: $\gamma$ = 1.21, $T_e$ = 1.74 eV for the first pulse,
- Δ flow 0.2 l/min: $\gamma$ = 1.19, $T_e$ = 1.41 eV for the second pulse.
- • flow 1.0 l/min: $\gamma$ = 1.26, $T_e$ = 1.63 eV for the first pulse,
- ▲ flow 1.0 l/min: $\gamma$ = 1.24, $T_e$ = 1.55 eV for the second pulse.

For high flow (more water in the plasma) all jumps are higher, but also data show much more scatter.

$$a_1 = (T_{e0}/T_e^* - 1)/T_{e0},$$
$$a_0 = 2 \ln (n_e^*/n_{e0}) - 3/2 \ln (T_e^*/T_{e0}),$$

where $T_e^*$, $n_e^*$ refer to the maximum or minimum of the disturbance. At the same picture the cooling jumps are plotted for the same experimental data. They give the steady state temperature $T_{e0}$ of 0.98 eV. From this data it can be found that:

$$T_{e0}/T_e^* = 1.09$$
$$n_e^*/n_{e0} = 1.10$$

so the electron density and temperature might be in counterphase. It has been also found that at the minimum of the disturbance $T_e$ is higher and $n_e$ lower that in the steady state. At the top of the disturbance they satisfy $\Delta n_e/n_{e0} \approx - \Delta T_e/T_{e0}$ with a good accuracy. Unfortunately, these data are not very well reproducible. However, the amplitude of the disturbance always tends to increase with ionization energy and gives the deviation of $T_e$ typically between 10 and 30%. The amplitude of the disturbance for 4p level is smaller than it should be according to Saha. In § VI (Absorption measurements) it has been shown that the amplitude for 4s deviates even more. This suggests that the disturbance is essentially an electron temperature effect (like the cooling jump).

A similar conclusion can be drawn from so called "double interruption" experiment. For this purpose the experimental setup has been adapted to make it possible to give a second power interruption at the moment the delayed response passes the observation zone. In Fig. VII.10 the response of an Ar line during this experiment is shown. The first power interruption response, the start of the delayed response and the second power interruption response are visible. In Fig. VII.11 the cooling jumps of the first and second response are given for several argon lines. From this it follows that $\gamma$ found from the second pulse is lower than this in the steady state. However, remembering that the accuracy of the method is poor, we cannot decide whether $T_h$ changes significantly. In Fig. VII.12a the cooling jump of the second power interruption for several time delays between the interruptions, as shown in Fig. VII.12b, is given for Ar 6s (703 nm). The jump is small in the maximum of the disturbance and large in the minimum. This is in agreement with the assumption of fluctuating $T_e$ and $n_e$ at a constant $T_h$, though it is not the final verification of it.

The double interruption experiment can also be used to let two delayed responses interfere with each other. This is shown in Fig. VII.13. It can be seen that the resulting response is not a linear superposition of such two delayed responses, so the non linear effects are important. In order to describe the interference, the full nonlinear equations must be solved.

An interesting indication of the actual phase shift between electron temperature and density is the response of the continuum. In Fig. VII.14 the time of arrival of the delayed disturbance of the continuum is presented as a function of wavelength. The relative height is independent of the wavelength. The wavelength dependence of the time of arrival matches the wavelength dependence

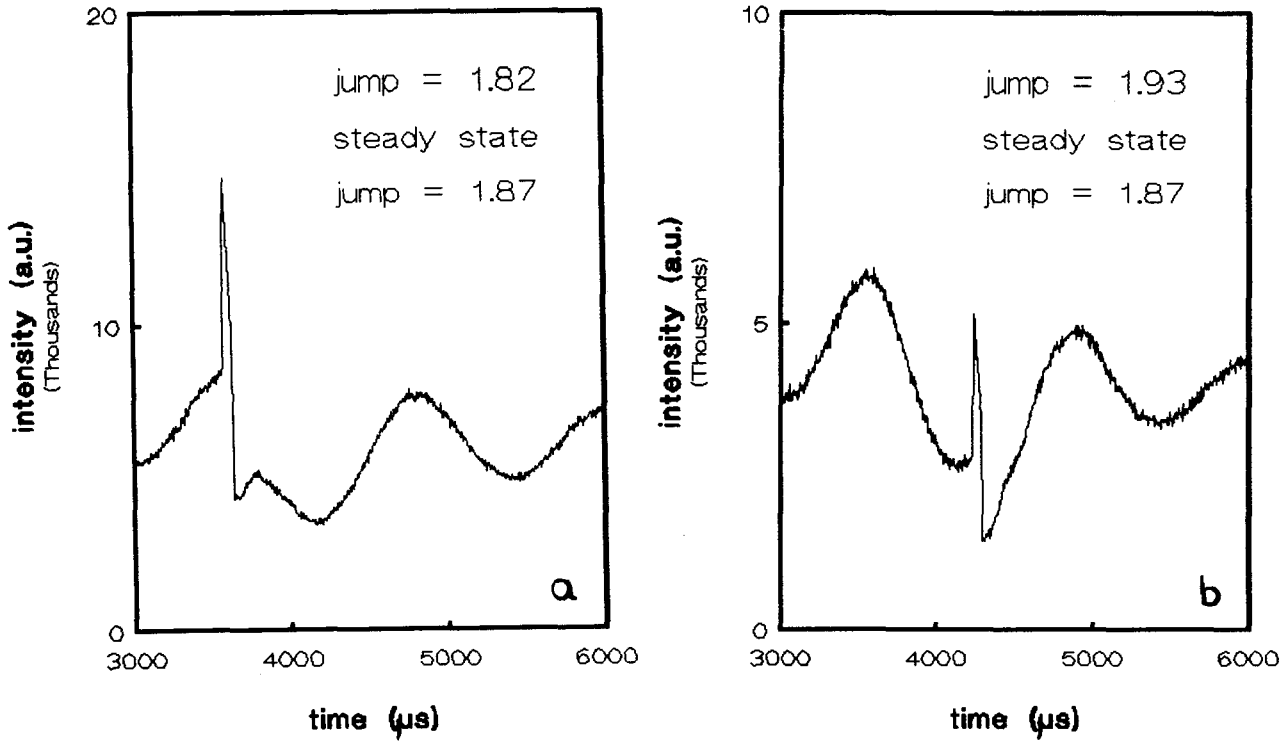


Fig. VII.12. The second pulse is applied
a) in the maximum of the delayed response. Jump = 1.82
b) in the minimum of the delayed response. Jump = 1.93
for 6s Ar line. Steady state jump is 1.87. If $\gamma$ were constant, we would expect the jump in maximum to be higher in the minimum (due to $(\gamma\text{-}1)/kT_e$), since $T_e$ in the maximum is lower than $T_e$ in the minimum. Therefore it can be concluded that $\gamma$ in the maximum is lower than in the minimum. This supports the assumption of fluctuating $T_e$ at constant $T_h$.

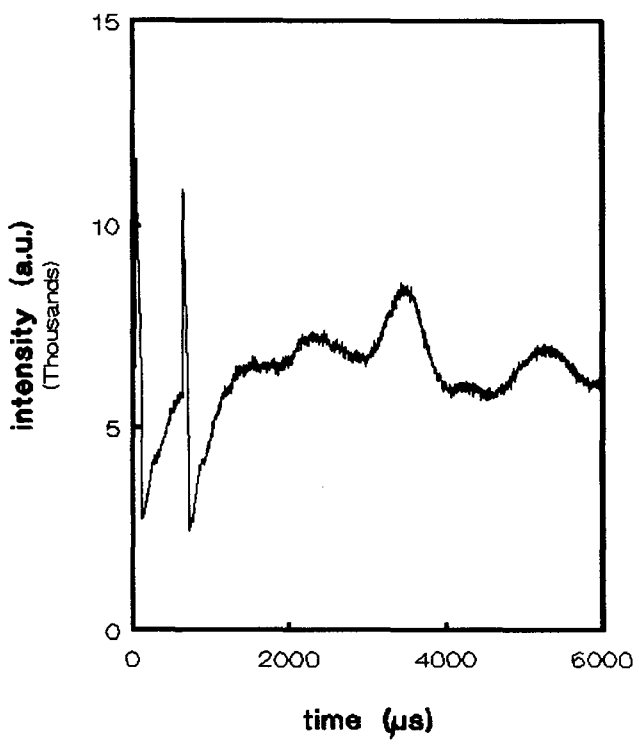


Fig. VII.13. Interference of two delayed responses for Ar 6s line. The delay between two pulses is 600 $\mu$s, which is a half of the period. If the responses superposed linearly, they should cancel.

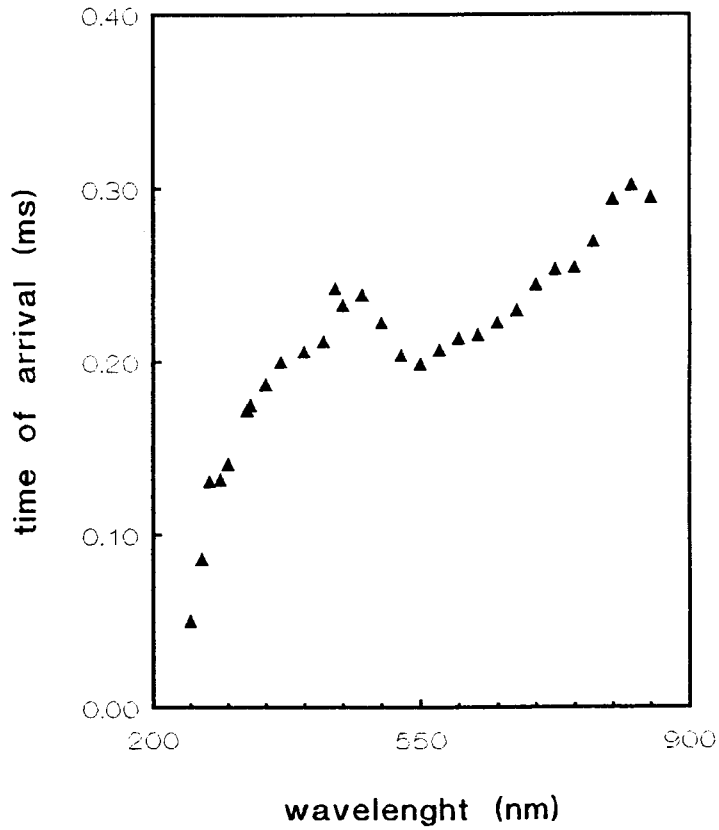


Fig. VII.14. The differences in time of arrival of the disturbance in continuum. The conditions are standard with water injection.

of the heating jump [STO.91/3]. The difference in time of arrival can be interpreted as a phase shift. The dependence of the continuum intensity of $n_e$ and $T_e$ is the following:

$$I \sim n_e^2 \, T_e^{-1/2} \, (1 - \exp(- h\nu/kT_e)) \, \xi \, (n_e, T_e)$$

where $\xi$ is the Bibermann factor. The actual dependence on $T_e$ does not strictly follow the theoretical one [STO.91/3]. It has been verified in the power interruption experiment that the continuum emission intensity is $T_e$ independent at $\lambda \geq 750$ nm. For other wavelengths $T_e$ competes with $n_e$ and eventually for $\lambda < 300$ nm $T_e$ becomes dominant. The phase shift obtained this way is about 300 $\mu$s, so is is smaller than 500 - 600 $\mu$s required for $n_e$ and $T_e$ to be in counterphase. Therefore there is possibly another phase shift, not described by this simplified theory. This shift might have some implications in velocity of the disturbance. From (VII.11) we can see that the existence of a "real" phase shift (not 0 or $\pi$) implies that P is not purely imaginary. Then from (VII.10a) it follows that velocity of the disturbance will not equal drift velocity of plasma. However, in § IV we have compared its velocity with w determined using other methods. As the values are very close, the real part of P should not be large.

The delayed response described above always follows the interruption experiment. However, for some torches we have observed a similar shaped but smaller response. Its amplitude is about 2-3 % of the steady state intensity. It has a period of 440 - 500 $\mu$s and occurs before the delayed response described above. It appears always at the same time, independent of the place in the plasma. In a special torch, 5 cm longer then the others, this 500 $\mu$s response is very large everywhere in the plasma (Fig. VII.15) except from the place far below the load coil. The plasma in this torch is longer and narrower so the comparison is troublesome. In opposition to the axially traveling responses, this response might be caused by radial oscillations, occurring in every place after switching on the ICP power.

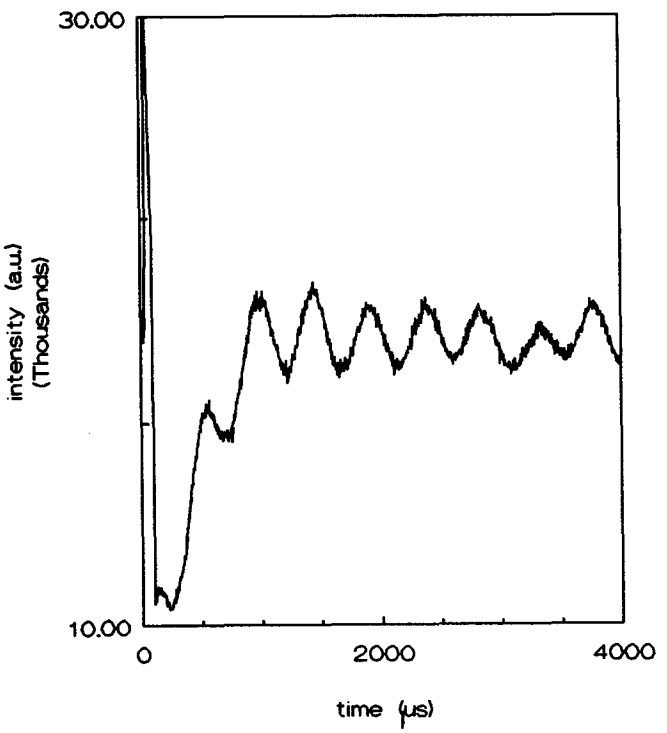


Fig. VII.15. The instantaneous oscillation with a period of 500 $\mu$s, observed in a long ICP torch. Recorded for Ar 6s line.

Fig. VII.16. The spontaneous disturbance created in the steady state. The conditions are standard with water injection. The period of this disturbance is approximately 1 ms.

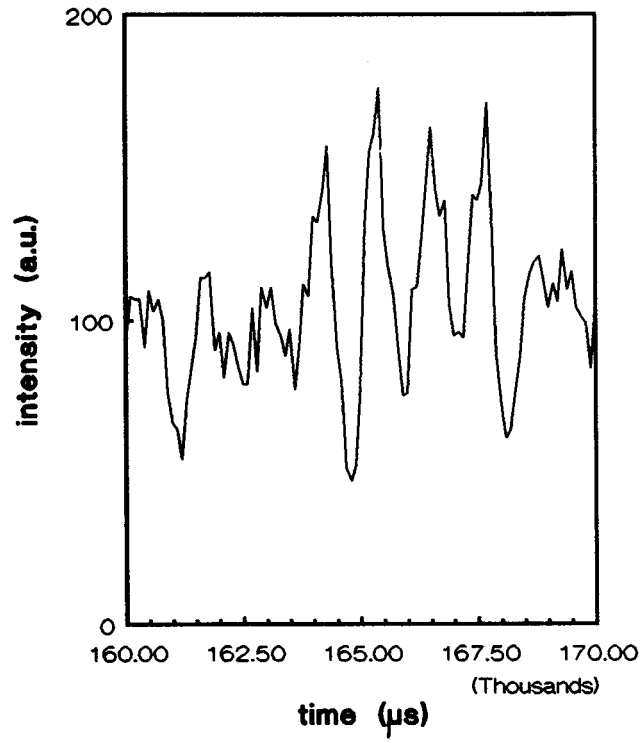


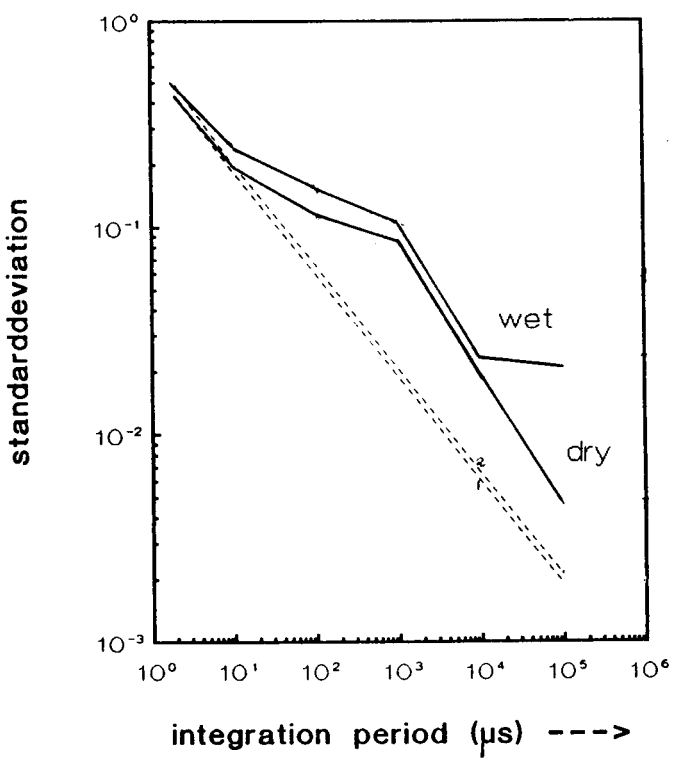


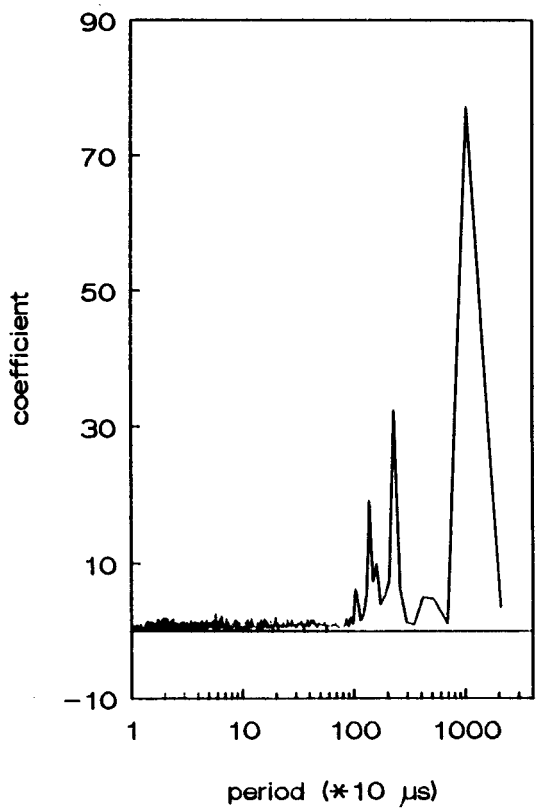


Fig. VII.18. The frequency spectrum correspondir to Fig. VII.17 in presence of water.

Fig. VII.17. Standard deviation as a function of the integration period. The dashed lines represent the standard deviation in case of only shot noise. The real behavior of the noise is described by the solid lines. The deviation at 1 ms is due to the spontaneous disturbance in the plasma. The deviation at 0.1 s in case of water injection is due to the peristaltic pump (10 Hz).

## VII.4 SPONTANEOUS DISTURBANCES

From the derivation presented in the theoretical part it follows that any deviation of $n_e$ and Te can be transported through the plasma. Therefore these disturbances are expected also to occur during the steady state. Indeed, in a measurement with a long integration time (Fig. VII.16) some periodic structures with a period of approximately 1 ms are found. In Fig. VII.17 the standard deviation of the measured signal is given as a function of integration time. The dotted line indicates the theoretical shot noise given by $\sigma = N^{-1/2}$, where N is the number of counts. For small integration times the noise behaves like shot noise and follows the theoretical line. When the integration period is in the order of the period of the disturbance a clear deviation is visible. For a plasma in which water is injected the deviation is larger, which is in agreement with the observed dependence of the magnitude of the delayed response. In Fig. VII.18 a frequency spectrum of the signal, obtained from Fourier analysis is shown. For the frequencies around 1000 Hz, related with $\tau$ = 1 ms there is a maximum. All three pictures indicate that the line emission from the ICP contains a systematic periodic behavior with a time constant of 1 ms. The interruption technique only serves to trigger a dynamic plasma phenomenon. The power interruption gives larger disturbances, so the amplitude of responses are larger. This is not the only method. Another possibility would be resonant ionization of plasma species performed in a short laser pulse.

## VII.5 CONCLUSION

From the continuity and energy equations it follows that a small disturbance of $n_e$ and $T_e$ underneath the load coil can propagate through the plasma, frozen in the flow. Such a disturbance allows to study the plasma velocity profile. These disturbances occur always in the plasma and have a period of c.a. 1 ms. Power interruption causes not only an instantaneous response but also a triggers a $n_e$ - $T_e$ disturbance, which can be observed as a delayed response. The magnitude of the disturbance is dependent on plasma parameters like power and the presence of water or hydrogen. Further study is strongly recommended, as the phenomenon is far from being fully understood.

# VIII. CONCLUSIONS AND RECOMMENDATIONS

## VII.1 CONCLUSIONS

* The power interruption experiment is a very powerful tool to study both global physical properties of the plasma (like energy flows, velocities, temperatures) as well as the interactions on the particle scale (elementary balances, chemical processes).

* We have shown that in our conditions the deviations of our system from LTE are substantial. The main source of deviation is the particles flow, which causes a decoupling of the ground state from Saha equilibrium. As it has appeared, the deviation extends also on the excited states. This makes the spectroscopical methods of temperature determination not reliable.

* The only experimentally determined parameters which value can be trusted is the ratio $\gamma = T_e/T_h$ and electron density.

* Considering the local energy balance for a given $\gamma$ and $n_e$ brings an estimation of temperatures. This is due to the fact that the energy input and losses must be balanced. A lower limit for $T_e$ has been found. This estimation is always valid, whether the plasma is in LTE or not.

* The recombination mechanisms have been discussed. Some indications about the actual mechanism has been found from the experimental data. The influence of additives on the plasma has been discussed.

* The absorption measurement on partially optically thick Ar 4p - 4s lines has been shown to be a good method to study the departures from Saha equilibrium.

* A disturbance in emission from the ICP has been found, both in the steady state and following the power interruption. It has been attributed to a disturbance in the energy balance. It has been proven to be fundamental plasma process, always present in the plasma. We have developed a linear theory that provides the propagation mechanism of this disturbance.

## VII.2 RECOMMENDATIONS

Particular recommendations have been already included in every chapter. Generally we may say, that a good reference technique to determine the plasma parameters is needed. This would allow to avoid many ambiguities in interpretation of the observed effects. Most of the discussed phenomena need further studies, both experimental and theoretical.

## IX REFERENCES


[BEN.90] D.A. Benoy, 'A computer model for the relation between source terms and transport in inductively coupled plasmas, IVO TUE (1990) ISBN 90-5282-094-5.

[BEN.91] D.A. Benoy, J.A.M. van der Mullen, B. van der Sijde and D.C. Schram, accepted for publication in QSRT, (1991).

[BOU.82] P.W.J.M. Boumans and M. ch. Lux-Steiner, Spectrochim. Acta 37B, 97 (1982).

[BRA.90] D.D.B. van Bragt, internal report (1990).

[BYD.88] a: E.L. Bydder and G.P. Miller, Spectrochim. Acta 43B, 819 (1988). b: E.L. Bydder and G.P. Miller, Spectrochim. Acta 43B, 1431 (1988).

[CAU.84] B.L. Caughlin and M.W. Blades, Spectrochim. Acta 39B, 1583 (1984).

[CAU.85] B.L. Caughlin and M.W. Blades, Spectrochim. Acta 40B, 987 (1985).

[FAR.85] P.B. Farnsworth, Appl. Spectrosc., 39, 1078 (1985).

[FEY.90] a:F.H.A.G Fey, W.W. Stoffels, P. van der Linden and J.A.M. van der Mullen, b: F.H.A.G. Fey, W.W. Stoffels. J.A.M. van der Mullen and D.C. schram, contributions to ESCAMPIG, Orleans, France, june 1990.

[FEY.91/1] F.H.A.G. Fey, W.W. Stoffels, J.A.M. van der Mullen, B. van der sijde and D.C. Schram, Sprctrochim. Acta 46B, 885, (1991).

[FEY.91/2] F.H.A.G Fey, W.W. Stoffels, E. Stoffels, J.A.M. van der Mullen, B. van der Sijde and D.C. Schram, contribution to ISPC 10, Bochum, Germany (August 1991).

[FEY.91/3] F.H.A.G. Fey, unpublished data.

[GRI.63] H. Griem, Phys. Rev. 13, 1170 (1963).

[GUR.63] D.B. Gurevich, I.V. Podmoshenskii, Opt. Spectrosc. 15, 319 (1963).

[JON.91] E.C.J.N. de Jong, internal report (1991).

[KAR.75] V.I. Karpman, 'Non-linear waves in dispersive media', Pergamon Press (1975)

[LAN.87] L.D. Landau, E.M. Lifshitz, Fluid Mechanics, 2nd edition, Pergamon Books Ltd. (1987)

[MIL.90] G.P. Miller, Spectrochim. Acta 45B, 329 (1990)

[MUL.87] J.A.M. van der Mullen, I.J.M.M. Raaijmakers, A.C.A.P. van Lammeren, D.C. Schram , B. van der Sijde and H.J.W. Schenkelaars, Spectrochim. Acta 42B, 1039 (1987).

[MUL.86] J.A.M. van der Mullen, PhD Thesis, indhoven University of Technology (1986).

[MUL.90] J.A.M. van der Mullen, Physics Reports 191, 109 (1990).

[NOW.88] S. Nowak, J.A.M. van der Mullen and D.C. Schram, Spectrochim. Acta 43B, 1235 (1988).

[NOW.89] S. Nowak, J.A.M. van der Mullen, A.C.A.P. van Lammeren and D.C. Schram, Spectrochim. Acta 44B, 411 (1989).

[OHL.87] K.D. Ohls, D.W. Golightly, A. Montaser in 'Inductively Coupled Plasmas in analytical atomic spectrometry', edited by A. Montaser and D.W. Golightly, VCH Publishers, (1987).

[OLE.87] J.W. Olesik and K.R. Bradley, Spectrochim. Acta 42B, 377 (1987).

[OTO.91] D.K. Otorbaev, private communication to the author.

[RAA.83] I.J.M.M. Raaijmakers, P.W.J.M. Boumans, B. van der Sijde and D.C. Schram, Spectrochim. Acta 38B, 697 (1983).

[SAN.91] M.C.M. van der Sanden, R. van den Bercken, J.J. van Broeckhoven and D.C. Schram, contribution to plasma symposium Lunteren, March 1991.

[SIJ.90] B. van der Sijde and J.A.M. van der Mullen, J.Quant. Spectrosc. Radiat. Transfer 44, 39 (1990).

[STO.90] W.W. Stoffels, internal report (1990).

[STO.91/1] E. Stoffels, W.W. Stoffels, D.A. Benoy, F.H.A.G. Fey and J.A.M. van der Mullen, contribution to PISE, Toulouse, France (June 1991).

[STO.91/2] W.W. Stoffels, E. Stoffels, F.H.A.G. Fey, J.A.M. van der Mullen, controbution to ISPC - 10, Bochum, Germany (August 1991).

[STO.91/3] W.W. Stoffels, internal report to be published in August 1991.

[WIE.69] W.L. Wiese, M.W. Smith and B.M. Miles, 'Atomic Transition Probabilities', NBS, (1969).

[WIL.91] A.T.M. Wilberts, PhD thesis, Eindhoven University of Technology (1991).

[WIL.83] B. Willems, internal report (1983).